UNIVERSITY OF CALIFORNIA
SANTA CRUZ

THE EVOLUTION OF NORTH PACIFIC CLIMATE SINCE THE LATE MIOCENE

A dissertation submitted in partial satisfaction
of the requirements for the degree of

DOCTOR OF PHILOSOPHY

in

OCEAN SCIENCES

by

Jonathan P. LaRiviere

March 2013

The Dissertation of Jonathan LaRiviere is approved:

_____
Professor Ana Christina Ravelo, chair

_____
Associate Professor Matthew McCarthy

_____
Professor Christopher Edwards

_____
Assistant Research Professor at Lamont-Doherty Earth Observatory Pratigya Polissar

_____
Tyrus Miller
Vice Provost and Dean of Graduate Studies

Table of Contents

List of Figures

List of Tables

Abstract

Jonathan P. LaRiviere

The evolution of North Pacific climate since the late Miocene

A lack of paleo-proxy data has made it difficult to determine the mechanisms responsible for the warm climates of the late Miocene and early Pliocene. Though modeling work suggests that the global distribution of sea surface temperatures (SSTs) and the depth of the global thermocline may have been important to maintaining past warm climates, paleoceanographic data is needed to test these ideas. This dissertation uses geochemical proxy reconstructions of SST, thermocline depth, and precipitation from North Pacific sediments to test the role that the oceans played in shaping late Miocene and Pliocene climates. Chapter 2 uses alkenone paleothermometry and $\delta^{18}O$ of planktonic foraminifera to show that the SSTs of the mid-latitude North Pacific ~13-5 Ma were decoupled from atmospheric pCO_2, possibly due to a deeper-than-modern global thermocline. The data indicates that thermocline shoaling after ~5 Ma, possibly related to changes in ocean basin shape, led to a stronger coupling between SSTs and atmospheric pCO_2 in more recent epochs. Chapter 3 uses new alkenone and Mg/Ca SSTs with published SST estimates to test the importance of SST gradients in the warm late Miocene and early Pliocene. Kriging of SST data was used to construct maps of late Miocene, Pliocene, and Pleistocene time-slices. The results, which show that basin-wide SST gradients were weak (relative to modern) in the early Pliocene but even weaker during the late

Miocene, support the hypothesis that weak SST gradients contributed to warm global temperatures. Chapter 4 assesses the utility of the $\delta D_{n\text{-alkanes}}$ in marine sediments as a proxy of precipitation on the continents. Ground-truthing of California Margin core tops indicated that $\delta D_{n\text{-alkanes}}$ from southern California Margin sediments are suitable for down-core reconstructions of past precipitation. Additionally, a low-resolution $\delta D_{n\text{-alkane}}$ record generated for this study showed that the establishment of the modern mediterranean climate in southern California might have resulted from the SST changes described in Chapters 2 and 3. Overall, this dissertation shows that reconstructions of past oceanographic and climate conditions of the North Pacific support the hypothesis that SST gradients played a major role in shaping the warm climates of the early Pliocene and late Miocene.

To my wife,

Ingrid,

the best teammate that I could ever have,

and my parents,

Paul and Kathryn.

Acknowledgements

There are so many people to thank.

My advisor, Christina Ravelo, has been a friend and scientific mentor throughout my PhD. She not only gave me the opportunity and encouragement to work on the projects in this dissertation, but she also gave me the opportunity to dive in a submersible, dredge for fossil corals in Hawaii, and present our work at international meetings in San Francisco, France, and China. Christina has always encouraged me to do my best work and to do good science. Christina is an exceptional scientist and I am lucky to have been able to work with her.

I would also like to thank my dissertation reading committee: Pratigya Polissar, Chris Edwards, and Matt McCarthy. Pratigya has been a great friend and role model and has put considerable effort into teaching me how to become an organic geochemist. I can't thank him enough for his support both scientifically and emotionally during my PhD. Chris Edwards and Matt McCarthy have both given me helpful feedback on my dissertation and I believe that their suggestions have helped me to improve my dissertation substantially during the writing process.

The work that went into my dissertation would not have been possible without the support of the talented scientists at UCSC. My friends Dyke Andreasen and Rob

Franks have both provided invaluable technical advisement and support and have also spent countless hours listening to me talk about whatever is on my mind. Linda Anderson has been a wonderful friend who has given me helpful scientific feedback on days that I was excited about research and she listened patiently on the days when I was not. Paul Koch and Jim Zachos have taught me a great deal about paleoclimate and gave me very helpful feedback on early drafts of my first manuscript.

I would like to thank Darren Ficklin for helping me with GIS work in Chapter 3 and for being a great friend. I would also like to thank Linda Heusser for pollen analysis and help with interpretations in Chapter 4.

Christina Ravelo's lab group has been my primary scientific support network while working on my research. I greatly appreciate the scientific discussions, joking, and emotional support from everyone who has been a part of the lab during my time at UCSC. While I was working on dissertation research Heather Ford, Petra Dekens, Karla Knudson, Fabian Batista, Kelsey Dyez, Shiloh Schlung, Sarah White, Mea Cook, and Dave Field have all helped me in countless ways. Max Aung, Joey Hermosillo, Paul Talmage, and Leah Lajoie have all helped me with sample preparation and analysis; I cannot thank them enough. It has also been my pleasure to work with many of the other undergraduates in the lab over the past six and a half years.

I would also like to thank the other graduate students at Earth and Marine Sciences. The paleoclimate research group at UCSC is comprised of some of the brightest and coolest young scientists that I can imagine. My fifth floor officemates have been great friends and a tremendous support through the years. My surfing partners were invaluable during my time at UCSC: Evan, Matt, Fabian, and Ryan — thank you.

Most of all, I'd like to thank my family. My parents, Ingrid's parents, Brad, Amanda, Katie and Jason have all helped me get through my PhD; they have celebrated with me during happy times and comforted me when I felt beaten down by this work. Thank you. Finally, Ingrid, thank you for your unconditional love, inspiration, positive attitude, and un-ending support over the past 11 years. You have had faith in me when I have not. I couldn't have done this without you.

The majority of my financial support during graduate school was from Christina Ravelo's National Science Foundation funding. Her grants funded analyses, conference presentations, publication fees, and during many quarters, my tuition and research stipends. I also received research funding in 2008 from the Dr. Earl H. Myers and Ethel M. Myers Oceanographic and Marine Biology Trust and in 2009 from a Friends of Long Marine Lab Student Research and Education Award. A UCSC Chancellor's Dissertation-Year Fellowship supported my 2011-2012 academic

year. The UCSC Graduate Student Association supported travel for several conferences.

The Integrated Ocean Drilling Program, the Oregon State University Marine Geology Repository, and the United States Geological Survey provided samples used in my research.

The text of this dissertation includes a reprint of the following previously published material: LaRiviere, J. P., A. C. Ravelo, A. Crimmins, P. S. Dekens, H. L. Ford, M. Lyle, and M. W. Wara (2012), Late Miocene decoupling of oceanic warmth and atmospheric carbon dioxide forcing, *Nature*, *486*(7401), 97-100. The co-authors listed in this publication directed and supervised the research which forms the basis for the dissertation. J.P.L. and A.C.R. did the primary data analysis and wrote the paper with intellectual feedback from all authors. J.P.L. generated alkenone temperature reconstructions; J.P.L., P.S.D., H.L.F., A.C. and M.W.W. analyzed foraminifera $\delta^{18}O$.

Chapter 1. Introduction

This dissertation focuses on the past ~13 million years (myrs) of North Pacific climate, a time interval that spans a large range of climate states, from the warmer-than-modern intervals of the late Miocene and early Pliocene to the glacial/interglacial climates of the Pleistocene [*Zachos et al.*, 2001]. This interval provides an opportunity to examine the Earth's climate response to variations in atmospheric greenhouse gasses, ocean circulation, and tectonics. Specifically, the late Miocene and early Pliocene enable investigations of the role that the oceans play in maintaining warm global and regional climates, which is the primary aim of this dissertation.

In the early Pliocene, ~4.3-4 Ma, atmospheric pCO_2 was only slightly higher than modern levels (by <50ppmv [*M. Pagani et al.*, 2010; *Seki et al.*, 2010]) but the global mean temperature was ~4° warmer than the modern global mean [*Brierley and Fedorov*, 2010]. Thus, a major question for paleoceanographers is why the early Pliocene, with near-modern pCO_2, was so much warmer than modern. One hypothesis is that much of the early Pliocene warmth, relative to modern, can be attributed to weaker-than-modern basin-wide sea surface temperature (SST) gradients [*Brierley et al.*, 2009].

Using idealized models of early Pliocene SSTs *Brierley et al.* [2009] and *Brierley and Fedorov* [2010] demonstrated that meridional SST gradients help to determine the

strength and dimensions of Hadley circulation, poleward heat transport, global temperatures, and precipitation patterns. The models suggest that weaker-than-modern SST gradients, a deeper-than-modern global thermocline, and associated cloud and water-vapor feedbacks resulted in mean global temperatures that were 3-4°C warmer-than-modern. The model results also demonstrated that a long-term shoaling of the thermocline and strengthening of SST gradients could have helped to enable the emergence of large Northern Hemisphere ice sheets in the Pleistocene [*Brierley and Fedorov*, 2010]. However, the modeling efforts that uncovered this potential oceanic mechanism of late Neogene and Quaternary climate change used paleo-proxy data from disparate regions to guide their sensitivity studies of weaker-than-modern SST gradients and the idealized SST gradients in the models were not specific to one geologic time interval [*Brierley et al.*, 2009]. Thus, because this work has highlighted the major role that SST distributions may have played in the global climate system, it has become critical that paleoceanographers use proxy-data to test whether weaker-than-modern SST gradients and a deeper-than-modern global thermocline were predominant features of the warm early Pliocene.

An additional test of this oceanic mechanism for maintaining warm global climates can be found in the climate of the late Miocene, ~12-5 Ma. The late Miocene is characterized by global conditions that were both warmer- and wetter-than-modern [*Pound et al.*, 2011] and by a lack of large Northern Hemisphere ice sheets [*Zachos et al.,* 2001]. The reasons for the lack of large Northern Hemisphere ice sheets and

global warmth in the late Miocene are not well understood [*Ruddiman*, 2010]. This is in part because in the late Miocene atmospheric pCO_2 was likely near pre-industrial levels [*Pagani et al.*, 1999]. *Ruddiman* [2010] pointed out that it is possible that the proxy-based pCO_2 estimates for the late Miocene are incorrect. However, the balance of data from multiple proxies agree that late Miocene pCO_2 was relatively low [*LaRiviere et al.*, 2012 SI] and recent multi-proxy studies have shown that by ~13Ma, following the middle Miocene Climatic Optimum (MMCO), atmospheric carbon dioxide concentrations had already dropped to ~300ppmv [*Foster et al.*, 2012; *Badger et al., in press*]. Thus, the late Miocene provides us with an opportunity to evaluate the role that the oceans played in maintaining global and regional climates during low pCO_2 conditions.

In this dissertation we have used geochemical proxies to reconstruct SSTs and thermocline depth in the North Pacific and have tested the role that oceanic conditions played in shaping the global climates of the late Miocene, Pliocene, and Pleistocene. In addition to generating new data, we have compiled all of the available published SST data and generated synoptic maps of global SSTs during the late Neogene and Quaternary. We use these maps to further constrain past SST gradient changes. Finally, we have begun to investigate the regional manifestations of terrestrial climate change that may be associated with long-term changes in basin-wide SST gradients with a study of leaf-wax isotopic composition in California Margin sediments.

In chapter 2, "Late Miocene decoupling of oceanic warmth and atmospheric carbon dioxide forcing" [*LaRiviere et al.*, 2012] we generated the first late Miocene geochemical SST estimates from the North Pacific and tested the hypothesis that the late Miocene oceanic conditions played a role in maintaining warm global conditions when atmospheric pCO_2 concentrations were relatively low. We used alkenone paleothermometry to generate SST reconstructions for several Ocean Drilling Program (ODP) sites in the North Pacific that span the past ~13 myrs. The results showed that the temperatures of the mid-latitude North Pacific ~13-5 myrs ago were substantially warmer-than-modern and decoupled from atmospheric carbon dioxide concentrations, a surprising finding given the strong coupling between global climate and atmospheric carbon dioxide in modern times. We also used the difference in oxygen isotopic composition of subsurface-dwelling and surface-dwelling planktonic foraminifera to assess changes in the depth of the tropical thermocline over this time interval. The thermocline and SST data were consistent with existing climate model sensitivity studies of the early Pliocene, which was characterized by weak meridional SST gradients, and indicated that the long-term shoaling of the thermocline after ~5 Ma, which may be related to tectonic changes in oceanic gateways such as the closing of the Central American Seaway, may be able to explain the stronger coupling between atmospheric carbon dioxide, SSTs, and climate that is characteristic of the Pliocene and Pleistocene epochs.

In Chapter 3, "Basin-wide sea surface temperature distributions of the Pleistocene, Pliocene, and late Miocene," we further tested the hypothesis that relatively weak SST gradients could explain the past warm climates of the late Miocene and early Pliocene. To fully investigate the role of the oceans in shaping North Pacific climate since the late Miocene it is critical to have firm constraints on the basin-wide SST distributions. We reconstructed the spatial distribution of SSTs for five time-slices in the late Neogene and Quaternary using new alkenone and Mg/Ca-based SST estimates and previously published SST data. We used a variogram and kriging approach to construct high fidelity global maps of SSTs from each time-slice and to reconstruct the meridional temperature gradient in the western Pacific. The maps show heterogeneous regional cooling since the late Miocene that resulted in long-term strengthening of basin-wide meridional and zonal SST gradients, dramatic cooling in eastern boundary current and high-latitude regions, and relatively constant temperatures in the western tropical Pacific. Our work indicates that the relatively weak meridional SST gradient of the late Miocene may have contributed to the global warmth of the late Miocene despite near-preindustrial pCO_2 concentrations.

In chapter 4, "The utility of leaf-wax δD as a proxy for precipitation in coastal western North America: a core-top transect and down-core pilot study," we assessed the effectiveness of the hydrogen isotopic composition (δD) of terrestrial leaf wax compounds (*n*-alkanes) in marine sediments as a proxy for precipitation in coastal western North America. This work was motivated by the ultimate goal of testing the

hypothesis that the emergence of the summer-dry mediterranean climate in coastal western North America resulted from changes in SSTs since the late Miocene [*Lyle et al.*, 2008]. However, because the reliability of $\delta D_{n\text{-alkanes}}$ as a recorder of precipitation in coastal western North America was uncertain, we first needed to ground-truth the proxy.

We tested the relationship between the $\delta D_{n\text{-alkanes}}$ preserved in marine sediments and the $\delta D_{precipitation}$ on land using a North-South transect of core-tops from the California Margin. Our core-top results showed that in the southern region of the California Margin (~29-36°N) the $\delta D_{n\text{-alkanes}}$ faithfully records the proximal $\delta D_{precipitation}$. In the central region of the California Margin (~37-39°N) the $\delta D_{precipitation}$ is also recorded by sedimentary *n*-alkanes, but the *n*-alkane source is from the interior Central Valley watershed of California. The $\delta D_{n\text{-alkanes}}$ north of ~39°N do not seem to effectively record $\delta D_{precipitation}$. In this region the $\delta D_{n\text{-alkane}}$ signal is complicated by uncertainties in vegetation source waters, water-shed extent, *n*-alkane ages, and $\delta D_{precipitation}$ in northern California.

In chapter 4 we also constructed a low-resolution down-core record of $\delta D_{n\text{-alkanes}}$ from ODP Site 1010 in the southern California Margin. The record spans the past ~10.5 myrs. The down-core record exhibits a shift to relatively low $\delta D_{n\text{-alkane}}$ values that began after the early Pliocene and continued through the late Pleistocene. This isotopic trend may have resulted from a reduction of summer precipitation in southern

California during the late Pliocene and Pleistocene and could reflect precipitation changes associated with the strengthening of basin-wide SST gradients during these times.

The projects in this dissertation aim to provide needed constraints on the evolution of North Pacific climate since the late Miocene. Chapters 2 and 3 show that the late Miocene North Pacific had warmer SSTs, smaller equator-to-pole SST gradients, and a deeper thermocline than the early Pliocene ocean, and that climate feedbacks associated with these late Miocene oceanic conditions could have played a major role in maintaining global warmth during relatively low atmospheric pCO_2 conditions [*LaRiviere et al.*, 2012]. Chapter 4 focuses on assessing the utility of $\delta D_{n\text{-alkanes}}$ from marine sediments in the California Margin as a proxy of terrestrial precipitation since the late Miocene. The low-resolution down-core record indicated that the establishment of the mediterranean climate in southern California might have resulted from the SST changes that were outlined in chapters 2 and 3. Overall, it seems that the late Miocene, which, at this point, has not received much attention from the paleoclimate community, was a more extreme example of a warmer-than-modern climate than the much-studied Pliocene; a finding that dramatically highlights the role that the ocean plays in determining global climate.

References

Badger, M.P.S., C.H. Lear, R.D. Pancost, G.L. Foster, T.R. Bailey, M.J. Leng, and H.J. Abels (*in press*), CO_2 drawdown following the middle Miocene expansion of the Antarctic Ice Sheet, *Paleoceanography* .

Brierley, C. M., and A. V. Fedorov (2010), Relative importance of meridional and zonal sea surface temperature gradients for the onset of the ice ages and Pliocene-Pleistocene climate evolution, *Paleoceanography*, *25*, 16.

Brierley, C. M., A. V. Fedorov, Z. H. Liu, T. D. Herbert, K. T. Lawrence, and J. P. LaRiviere (2009), Greatly expanded tropical warm pool and weakened Hadley circulation in the early Pliocene, *Science*, *323*(5922), 1714-1718.

Foster, G.L., C.H. Lear, and J.W.B. Rae (2012), The evolution of pCO_2, ice volume and climate during the middle Miocene, *Earth and Planetary Science Letters*, 341-344, 243-254.

LaRiviere, J. P., A. C. Ravelo, A. Crimmins, P. S. Dekens, H. L. Ford, M. Lyle, and M. W. Wara (2012), Late Miocene decoupling of oceanic warmth and atmospheric carbon dioxide forcing, *Nature*, *486*(7401), 97-100.

Lyle, M., J. Barron, T. J. Bralower, M. Huber, A. Olivarez-Lyle, A. C. Ravelo, D. K. Rea, and P. A. Wilson (2008), Pacific Ocean and Cenozoic evolution of climate, *Reviews of Geophysics*, *46*(2002), 47.

Pagani, M., K. H. Freeman, and M. A. Arthur (1999), Late Miocene atmospheric CO_2 concentrations and the expansion of C4 Grasses, *Science*, *285*, 876-879.

Pagani, M., Z. H. Liu, J. LaRiviere, and A. C. Ravelo (2010), High Earth-system climate sensitivity determined from Pliocene carbon dioxide concentrations, *Nature Geoscience*, *3*(1), 27-30.

Pound, M. J., A. M. Haywood, U. Salzmann, J. B. Riding, D. J. Lunt, and S. J. Hunter (2011), A Tortonian (Late Miocene, 11.61-7.25 Ma) global vegetation reconstruction, *Palaeogeography Palaeoclimatology Palaeoecology*, *300*(1-4), 29-45.

Ruddiman, W. F. (2010), A Paleoclimatic Enigma?, *Science*, *328*(5980), 838-839.

Seki, O., G. L. Foster, D. N. Schmidt, A. Mackensen, K. Kawamura, and R. D. Pancost (2010), Alkenone and boron-based Pliocene pCO_2 records, *Earth and Planetary Science Letters*, *292*(1-2), 201-211.

Zachos, J., M. Pagani, L. Sloan, E. Thomas, and K. Billups (2001), Trends, rhythms, and aberrations in global climate 65 Ma to present, *Science*, *292*(5517), 686-693.

LETTER

doi:10.1038/nature11200

Late Miocene decoupling of oceanic warmth and atmospheric carbon dioxide forcing

Jonathan P. LaRiviere[1], A. Christina Ravelo[1], Allison Crimmins[1]†, Petra S. Dekens[1]†, Heather L. Ford[1], Mitch Lyle[2] & Michael W. Wara[1]†

Deep-time palaeoclimate studies are vitally important for developing a complete understanding of climate responses to changes in the atmospheric carbon dioxide concentration (that is, the atmospheric partial pressure of CO_2, p_{CO_2})[1]. Although past studies have explored these responses during portions of the Cenozoic era (the most recent 65.5 million years (Myr) of Earth history), comparatively little is known about the climate of the late Miocene (~12–5 Myr ago), an interval with p_{CO_2} values of only 200–350 parts per million by volume but nearly ice-free conditions in the Northern Hemisphere[2,3] and warmer-than-modern temperatures on the continents[4]. Here we present quantitative geochemical sea surface temperature estimates from the Miocene mid-latitude North Pacific Ocean, and show that oceanic warmth persisted throughout the interval of low p_{CO_2} ~12–5 Myr ago. We also present new stable isotope measurements from the western equatorial Pacific that, in conjunction with previously published data[5–10], reveal a long-term trend of thermocline shoaling in the equatorial Pacific since ~13 Myr ago. We propose that a relatively deep global thermocline, reductions in low-latitude gradients in sea surface temperature, and cloud and water vapour feedbacks may help to explain the warmth of the late Miocene. Additional shoaling of the thermocline after 5 Myr ago probably explains the stronger coupling between p_{CO_2}, sea surface temperatures and climate that is characteristic of the more recent Pliocene and Pleistocene epochs[11,12].

High-latitude climate reconstructions from the oxygen isotopic composition ($\delta^{18}O$) of benthic foraminifera[3] reveal a long-term cooling trend over the past ~50 Myr that occurred in conjunction with decreasing p_{CO_2} (ref. 2). However, although CO_2 levels were near pre-industrial values (280 p.p.m.v.) during the late Miocene (even the highest end of both the alkenone and leaf stomata estimates of CO_2 indicate that late Miocene CO_2 levels were less than the modern values of ~390 p.p.m.v.), high-latitude climate was too warm to support the growth of large Northern Hemisphere ice sheets[2,3] (Fig. 1a, f and Supplementary Information).

Climate modellers have tested whether external boundary conditions, such as the reduced topography of mountainous regions during the late Miocene[13], could have lowered the p_{CO_2} threshold for glaciation[14–16]; however, these tests focused on regional ice sheet growth rather than global temperatures and have not accounted for climate conditions outside the high latitudes. Palaeoclimate estimates from vegetation reconstructions suggest that warmer-than-modern conditions existed not just in the high latitudes but were globally widespread ~12–7 Myr ago[4] (Supplementary Information). Vegetation probably acted as a strong warming feedback in the late Miocene[17]; however, the boundary conditions that underlie such a vegetation distribution are not well constrained. Ocean circulation would have been integral to the global climate system of the late Miocene, but very little quantitative data exist to constrain surface circulation. For this reason, we reconstructed changes in sea surface temperature (SST) in the mid-latitude North Pacific Ocean and monitored the depth of the western tropical Pacific thermocline (the boundary between the warm surface ocean layer and the subsurface cold deep ocean) for the past ~13 Myr.

The SST estimates are derived from sediments collected at three Ocean Drilling Program (ODP) sites: Site 1010 (30° N, 118° W) in the subtropical east Pacific; Site 1021(39° N, 128° W) in the northeast Pacific at the seaward side of the northern edge of the California Current; and Site 1208 (36° N, 158° E) in the northwest Pacific at the transition zone between the subtropical and subarctic gyres (Fig. 2). SST estimates are based on the alkenone unsaturation proxy ($U^{k'}_{37}$) using the calibration of ref. 18. The 1010 and 1021 SST reconstructions are continuous since ~13 Myr before present. The SST reconstruction from Site 1208 is continuous since ~10 Myr before present.

The warmest SSTs occurred at the beginning of the late Miocene with subsequent cooling over the length of all three records. At subtropical east Pacific Site 1010, SSTs cooled by 5 °C between 9 and 5.8 Myr ago, and cooled an additional ~8 °C from the early Pliocene warm period, about 3.7 Myr ago, into the recent Pleistocene ice ages (Fig. 1e). A similar pattern of SST cooling was observed at northeast Pacific Site 1021; SSTs cooled by ~5 °C by 5.8 Myr ago and, after a ~3 °C increase from ~5.8 to 4.5 Myr ago, subsequently cooled an additional ~8.5 °C into the ice ages (Fig. 1e). At the northwest Pacific Site 1208, SSTs decreased by ~3 °C by 5.8 Myr ago, and continued to cool by an additional ~4 °C from 2.7 Myr ago and into the ice ages (Fig. 1d). Overall, when compared to SST estimates from the western Pacific warm pool[5], our new records of warm subtropical SSTs reveal that late Miocene meridional SST gradients were reduced relative to those of the Pliocene. Site movement by plate tectonics from one ocean temperature regime to another can explain no more than ~2 °C of the SST trend since 13 Myr ago (Supplementary Information).

Our SST records provide, despite some regional variability, the first documentation that late Miocene SSTs across a broad swathe of the North Pacific were significantly warmer than present (by 5–8 °C), and that there was nearly unidirectional cooling over the past 13 Myr. Furthermore, our records are consistent with other palaeodata[4,13,19], including bottom-water temperature estimates[19] (Fig. 1b), which indicate that the climate was warmer during the late Miocene than during the early Pliocene warm period. Thus, the preponderance of data, including our new records, indicates that global temperatures of the late Miocene, with relatively low p_{CO_2} of $<$350 p.p.m.v., exceeded that of the early Pliocene warm period, with relatively high p_{CO_2} of $>$350 p.p.m.v. (Fig. 1f). This decoupling between temperature and atmospheric p_{CO_2} trends requires an explanation. One possibility is that changes in boundary conditions (for example, continental topography, ocean basin shape) played a major role in determining the sensitivity of Earth's climate to CO_2 forcing.

During the late Miocene, the Central American Seaway (CAS) was open, the Indonesian Seaway was wider than at present, and the Bering

[1]Ocean Sciences Department, University of California, Santa Cruz, California 95064, USA. [2]Department of Oceanography, Texas A&M University, College Station, Texas 77843, USA. †Present addresses: US Environmental Protection Agency, Climate Change Division, Washington DC 20460, USA (A.C.); Department of Geosciences, San Francisco State University, San Francisco, California 94132, USA (P.S.D.); Freeman Spogli Institute for International Studies, Stanford Law School, Stanford, California 94305, USA (M.W.W.).

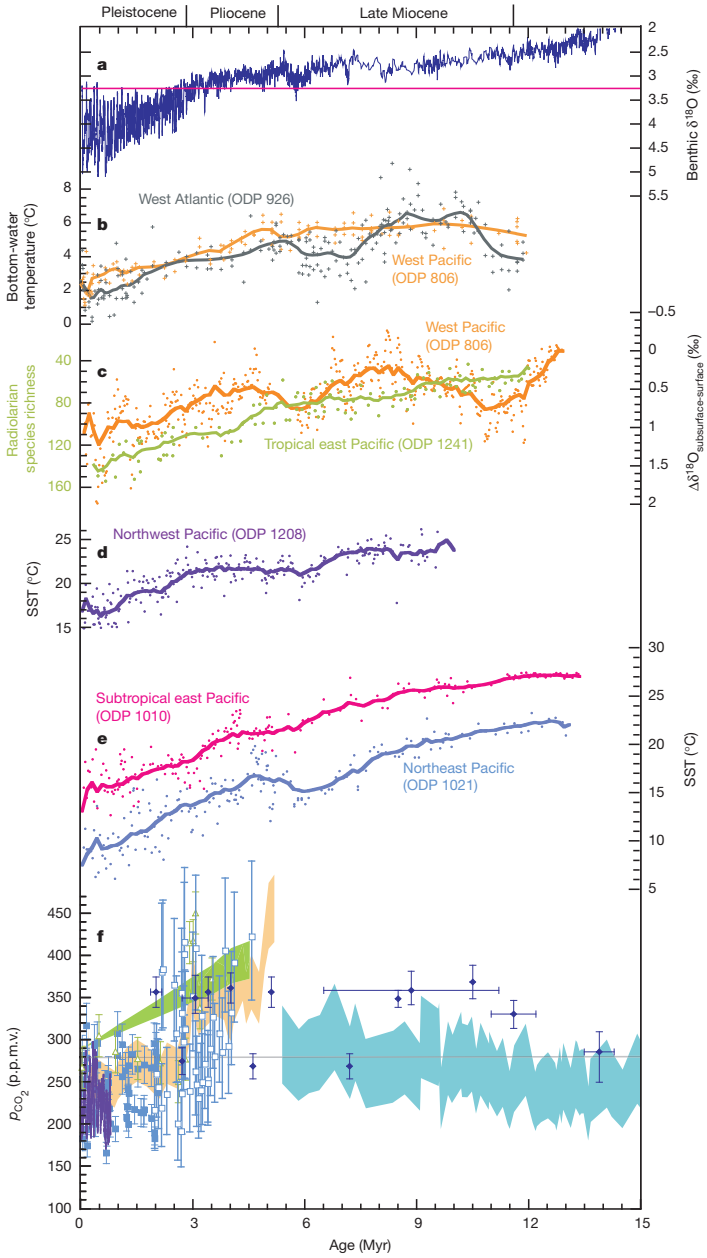

Figure 1 | Late Neogene oceanic conditions and atmospheric p_{CO_2}. **a**, Benthic foraminifera $\delta^{18}O$ record of high-latitude climate change[3,30]. Pink line denotes modern $\delta^{18}O$. **b**, Mg/Ca-derived bottom-water temperatures from ODP Sites 806 and 926 (ref. 19). **c**, Oxygen isotopic difference between thermocline and surface foraminifera from Site 806 (orange curve, right-hand vertical axis) is inversely related to thermocline depth[5–7]. Radiolarian species richness from Site 1241[10] (green curve, left-hand vertical axis) is a reflection of thermocline depth. **d**, Alkenone SST estimates from Site 1208. **e**, Alkenone SST estimates from Sites 1021 and 1010. **f**, Estimates of atmospheric p_{CO_2} from ice cores (purple line), boron isotopes (open squares, filled squares and triangles), alkenones (green[11], gold and blue shading), and leaf stomata (diamonds). Grey line marks pre-industrial p_{CO_2} concentrations (280 p.p.m.v.). Vertical error bars represent reported uncertainty in boron isotope and leaf stomata p_{CO_2} estimates. Reported age uncertainties for leaf stomata estimates are denoted with horizontal bars. Green, gold and blue shading indicates the range between published maximum and minimum alkenone p_{CO_2} estimates. See Supplementary Information for p_{CO_2} data sources. Heavy lines in **b**–**e** represent Stineman smoothing curves applied in KaleidaGraph software (v4.1.3; http://www.synergy.com/).

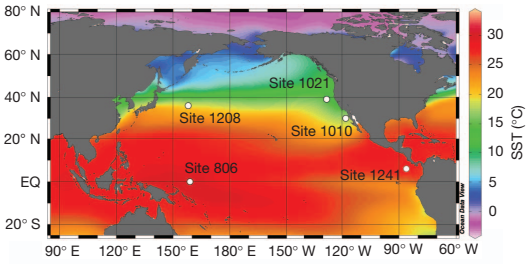

Figure 2 | Sites used in this study. ODP Sites 1208 (36° N, 158° E), 1021 (39° N, 128° W), 1010 (30° N, 118° W), 806 (0° N, 159° E) and 1241 (6° N, 86° W) overlaid on a map of mean annual SSTs[31]. EQ, Equator.

Strait was closed[13]; however, by the end of the early Pliocene the CAS was closed, the geography of the Indonesian Seaway was more similar to its modern configuration, and the Bering Strait was open[13]. Although none of the existing modelling sensitivity studies indicate that these tectonic changes could directly explain the warm, mid-latitude North Pacific temperatures observed in our reconstructions[20,21], modelling of the early Pliocene climate (5–3 Myr ago) does suggest that the CAS may have played a role in determining the depth of the thermocline. Results from general circulation models indicate that when the CAS was open, the modelled tropical thermocline was deeper[22,23], consistent with observations of the tropical Pacific thermocline[5–10,22]. Such a change in thermocline depth is important, because the ventilated thermocline maintains the balance between high-latitude oceanic heat loss and low-latitude heat gain[24]; a change in thermocline depth implies changes in surface ocean conditions that determine cloud, atmospheric water vapour and SST distributions[25]. Thus, changes in thermocline depth may be driven by internal dynamics or by changes in external boundary conditions, such as oceanic gateways, and could help to explain the climate of the late Miocene.

To assess changes in the shallow, wind-driven circulation of the ventilated thermocline, we monitored relative changes in thermocline depth at west Pacific ODP Site 806 (0° N, 159° E) (Fig. 2) using the $\delta^{18}O$ values of shells from surface-dwelling and subsurface-dwelling planktonic foraminifera. We made new stable isotopic measurements of *Globorotalia tumida* for the interval of ~4.8–0 Myr ago, which, in conjunction with previously published data[5–7] on this and other species, provides records of the $\delta^{18}O$ of *Globigerinoides sacculifer*, a surface dweller, and of *G. tumida*/*Globorotalia menardii*/*Globorotalia fohsi*, subsurface dwellers, for the past ~13 Myr. The difference between these species, $\Delta\delta^{18}O_{subsurface\text{-}surface}$, reflects thermocline depth[5–7], with low values indicating a thick mixed layer and deep thermocline, and high values indicating a thinner mixed layer and shallower thermocline. Whereas the previously published data showed two pronounced intervals of a relatively thin mixed layer ~13–11 and ~7–5.8 Myr ago, the additional isotopic data in our study reveal a long-term trend in $\Delta\delta^{18}O_{subsurface\text{-}surface}$ and indicate that the western equatorial Pacific thermocline has gradually shoaled since ~13 Myr ago (Supplementary Information). Evidence for thermocline changes in the eastern tropical Pacific comes from radiolarian species richness (ODP 1241; 6° N, 86° W), which shows a monotonic increase since ~12 Myr ago[10], and is consistent with a long-term increase in the number of ecological niches available as the thermocline became shallower (Fig. 1c). In addition, the authors of ref. 10 interpreted the radiolarian assemblage changes since ~4.2 Myr ago to indicate the shoaling of the eastern tropical Pacific thermocline from a relatively deep configuration that existed for the majority, if not all, of the late Miocene. Furthermore, foraminifera faunal reconstructions throughout the tropical Pacific show that the thermocline has generally shoaled from a relatively deep position in the middle Miocene to a shallower depth by the end of the late Miocene[8,9].

Overall, our data indicate that the oceanic state of the late Miocene was similar to that of the early Pliocene warm period, though more extreme (with warmer SSTs, smaller SST gradients and a deeper thermocline). Modelling of the early Pliocene conditions demonstrates that a tight coupling between the deep thermocline, expanded tropical warmth, and the reduction in meridional and zonal SST gradients resulted in mean global temperatures 3–4 °C warmer than today and the suppression of Northern Hemisphere glaciation[26]. The models, which are constrained by Pliocene proxy data, show that the expanded tropical warmth results in enhanced subtropical evaporation, greenhouse warming from water vapour, and warming from an increase in subtropical high 'greenhouse clouds'. These processes form a feedback loop that further facilitates maintenance of a deep thermocline and a warm climate with expanded tropical warmth[27]. Applying this idea to the Miocene provides a framework to understand our new SST and thermocline observations, all of which are consistent with warmer-than-modern global temperatures, as is the case in the early Pliocene. Furthermore, when applied to the Miocene, the Pliocene body of work suggests that, in the absence of large changes in p_{CO_2}, a tectonically driven change in upper ocean structure and tropical warm pool expanse could have, by itself, affected global temperatures through changes in atmospheric water vapour (a greenhouse gas) concentrations and in planetary albedo (through cloud type and distribution).

Changes in thermocline depth could explain the differences between late Miocene and Pliocene climate responses to atmospheric p_{CO_2} forcing. The shoaling of the thermocline has been directly linked to intensification of tropical SST gradients[22,28] and the strength of Walker and Hadley atmospheric circulation. However, when the thermocline is sufficiently deep (as it was in the tropical Pacific during the late Miocene), its movement is not coupled with SSTs. An increase in coupling appears to occur when the thermocline is shallow enough to pass some threshold depth. This threshold can explain why the thermocline depth variation in the western equatorial Pacific—a region where the thermocline is currently deeper than the surface Ekman layer of wind-driven mixing—did not appear to be coupled to SSTs until the thermocline in the eastern tropical Pacific shoaled adequately; such shoaling happened in the early Pliocene or, at the earliest, during the conclusion of the late Miocene. Once the thermocline became sufficiently shallow to affect SSTs, the climate system seems to have become sensitive to climate perturbations that had previously been inconsequential, including those driven by changes in p_{CO_2}. For example, with a shallow thermocline any small change (for example, in winds or in upwelling strength) that affected the low-latitude SSTs would be accompanied by strong positive feedbacks; changes in surface pressure gradients could reinforce initial changes in winds and in atmospheric water vapour and cloud formation[26] that amplify global temperature change. A shallower thermocline and accompanying enhanced climate sensitivity could explain why the Northern Hemisphere ice ages began in the Pliocene, rather than in the Miocene at comparable p_{CO_2} levels, and why a close coupling between glacial–interglacial climate cycles and p_{CO_2} developed after ~2.7 Myr ago[29].

Differences in the oceanic gateway boundary conditions of the late Miocene and Pliocene may have been the ultimate cause of the increase in climate sensitivity to p_{CO_2} forcing; the ocean basin configuration of the Pliocene, rather than the configuration that existed for the majority of the late Miocene, enabled the thermocline to shoal past a depth that was critical for coupling the thermocline and SSTs. However, although the closing of the CAS is the best candidate for forcing major upper-ocean structure changes in the earliest Pliocene, much work is needed to verify this idea and to test the effects of other ocean gateways on thermocline depth. Future work should aim to increase the geographic coverage of the surface and subsurface oceanographic reconstructions

with an emphasis on ocean gateway regions (for example, the CAS, Indonesian Seaway and Bering Strait). Such evidence would help to constrain the timing and the nature of ocean circulation change, and therefore climate change, associated with tectonic events in the late Miocene and early Pliocene.

METHODS SUMMARY

Lipids were extracted from 0.5–5 g of crushed sediment with either a 3:1 dichloromethane:methanol mix or pure dichloromethane using a Dionex ASE200 accelerated solvent extractor. The total lipid extract was evaporated to dryness under N_2 and redissolved in 100–200 µl of toluene with hexatriacontane and heptatriacontane internal standards. Separation of organic compounds was carried out on an HP6890 gas chromatograph equipped with a flame ionization detector. Long-term reproducibility of liquid standard replicates included in each gas chromatography run was within ± 0.007 $U^{k'}_{37}$ units, which is equivalent to ± 0.2 °C (s.d., $n = 139$). We monitored the long-term precision of the entire method by processing a sediment standard with each batch of samples. Reproducibility for the sediment standards used for the 1208, 1021 and 1010 sites was ± 0.016 (s.d., $n = 25$), ± 0.013 (s.d., $n = 27$) and ± 0.015 (s.d., $n = 9$) $U^{k'}_{37}$ units, respectively. The standard error of the estimate for the global SST calibration of ref. 18 is ± 1.5 °C.

Fossil shells of *G. tumida* were analysed for oxygen isotopic composition ($\delta^{18}O$) using a Fisons Prism III dual inlet isotope ratio mass spectrometer. The precision of NBS-19 (NIST-8544) and of an in-house Carrera Marble standard was better than 0.08‰ for $\delta^{18}O$. Measurements of $\delta^{18}O$ are reported relative to Vienna-Pee Dee Belemnite (V-PDB).

Received 15 November 2011; accepted 2 May 2012.

1. Hansen, J. *et al.* Target atmospheric CO_2: where should humanity aim? *Open Atmos. Sci. J.* **2,** 217–231 (2008).
2. Ruddiman, W. F. A paleoclimatic enigma? *Science* **328,** 838–839 (2010).
3. Zachos, J., Pagani, M., Sloan, L., Thomas, E. & Billups, K. Trends, rhythms, and aberrations in global climate 65 Ma to present. *Science* **292,** 686–693 (2001).
4. Pound, M. J. *et al.* A Tortonian (Late Miocene, 11.61–7.25 Ma) global vegetation reconstruction. *Palaeogeogr. Palaeoclimatol. Palaeoecol.* **300,** 29–45 (2011).
5. Nathan, S. A. & Leckie, R. M. Early history of the Western Pacific Warm Pool during the middle to late Miocene (~13.2–5.8 Ma): role of sea-level change and implications for equatorial circulation. *Palaeogeogr. Palaeoclimatol. Palaeoecol.* **274,** 140–159 (2009).
6. Wara, M. W., Ravelo, A. C. & Delaney, M. L. Permanent El Niño-like conditions during the Pliocene warm period. *Science* **309,** 758–761 (2005).
7. Chaisson, W. P. & Ravelo, A. C. Pliocene development of the east-west hydrographic gradient in the equatorial Pacific. *Paleoceanography* **15,** 497–505 (2000).
8. Keller, G. Depth stratification of planktonic foraminifers in the Miocene ocean. *Geol. Soc. Am.* **163,** 177–195 (1985).
9. Kennett, J. P., Keller, G. & Srinivasan, M. S. Miocene planktonic foraminiferal biogeography and paleoceanographic development of the Indo-Pacific region. *Geol. Soc. Am.* **163,** 197–236 (1985).
10. Kamikuri, S., Motoyama, I., Nishi, H. & Iwai, M. Evolution of Eastern Pacific Warm Pool and upwelling processes since the middle Miocene based on analysis of radiolarian assemblages: Response to Indonesian and Central American Seaways. *Palaeogeogr. Palaeoclimatol. Palaeoecol.* **280,** 469–479 (2009).
11. Pagani, M., Liu, Z. H., LaRiviere, J. & Ravelo, A. C. High Earth-system climate sensitivity determined from Pliocene carbon dioxide concentrations. *Nature Geosci.* **3,** 27–30 (2010).
12. Siegenthaler, U. *et al.* Stable carbon cycle-climate relationship during the late Pleistocene. *Science* **310,** 1313–1317 (2005).
13. Lyle, M. *et al.* Pacific Ocean and Cenozoic evolution of climate. *Rev. Geophys.* **46,** RG2002 (2008).
14. DeConto, R. M. *et al.* Thresholds for Cenozoic bipolar glaciation. *Nature* **455,** 652–656 (2008).
15. Foster, G., Lunt, D. & Parrish, R. Mountain uplift and the glaciation of North America — a sensitivity study. *Clim. Past* **6,** 707–717 (2010).
16. Lunt, D., Foster, G., Haywood, A. & Stone, E. Late Pliocene Greenland glaciation controlled by a decline in atmospheric CO_2 levels. *Nature* **454,** 1102–1105 (2008).
17. Knorr, G., Butzin, M., Micheels, A. & Lohmann, G. A warm Miocene climate at low atmospheric CO_2 levels. *Geophys. Res. Lett.* **38,** L20701, http://dx.doi.org/10.1029/2011GL048873 (2011).
18. Müller, P. J., Kirst, G., Ruhland, G., von Storch, I. & Rosell-Melé, A. Calibration of the alkenone paleotemperature index $U^{K'}_{37}$ based on core-tops from the eastern South Atlantic and the global ocean (60°N-60°S). *Geochim. Cosmochim. Acta* **62,** 1757–1772 (1998).
19. Lear, C. H., Rosenthal, Y. & Wright, J. D. The closing of a seaway: ocean water masses and global climate change. *Earth Planet. Sci. Lett.* **210,** 425–436 (2003).
20. Lunt, D. J., Valdes, P. J., Haywood, A. & Rutt, I. C. Closure of the Panama Seaway during the Pliocene: implications for climate and Northern Hemisphere glaciation. *Clim. Dyn.* **30,** 1–18 (2007).
21. Schneider, B. & Schmittner, A. Simulating the impact of the Panamanian seaway closure on ocean circulation, marine productivity and nutrient cycling. *Earth Planet. Sci. Lett.* **246,** 367–380 (2006).
22. Steph, S. *et al.* Early Pliocene increase in thermohaline overturning: a precondition for the development of the modern equatorial Pacific cold tongue. *Paleoceanography* **25,** PA2202, http://dx.doi.org/10.1029/2008PA001645 (2010).
23. Zhang, X. *et al.* Changes in equatorial Pacific thermocline depth in response to Panamanian seaway closure: insights from a multi-model study. *Earth Planet. Sci. Lett.* **317–318,** 76–84 (2012).
24. Boccaletti, G., Pacanowski, R. C., Philander, S. G. H. & Fedorov, A. V. The thermal structure of the upper ocean. *J. Phys. Oceanogr.* **34,** 888–902 (2004).
25. Philander, S. G. & Fedorov, A. V. Role of tropics in changing the response to Milankovich forcing some three million years ago. *Paleoceanography* **18,** 1045, http://dx.doi.org/10.1029/2002PA000837 (2003).
26. Brierley, C. M. & Fedorov, A. V. Relative importance of meridional and zonal sea surface temperature gradients for the onset of the ice ages and Pliocene-Pleistocene climate evolution. *Paleoceanography* **25,** PA2214, http://dx.doi.org/10.1029/2009PA001809 (2010).
27. Fedorov, A., Brierley, C. & Emanuel, K. Tropical cyclones and permanent El Niño in the early Pliocene epoch. *Nature* **463,** 1066–1070 (2010).
28. Fedorov, A. V. *et al.* The Pliocene paradox (mechanisms for a permanent El Niño). *Science* **312,** 1485–1489 (2006).
29. Herbert, T., Peterson, L., Lawrence, K. & Liu, Z. Tropical ocean temperatures over the past 3.5 million years. *Science* **328,** 1530–1534 (2010).
30. Lisiecki, L. E. & Raymo, M. E. A. Pliocene-Pleistocene stack of 57 globally distributed benthic delta $\delta^{18}O$ records. *Paleoceanography* **20,** PA1003, http://dx.doi.org/10.1029/2004PA001071 (2005).
31. Locarnini, R. A., Mishonov, A. V., Antonov, J. I., Boyer, T. P. & Garcia, H. E. in *World Ocean Atlas 2005, NOAA Atlas NESDIS 61* Vol. 1 (ed. Levitus, S.) 182 (US Government Printing Office, 2006).

Supplementary Information is linked to the online version of the paper at www.nature.com/nature.

Acknowledgements We thank the Ravelo laboratory group for discussions. We also thank J. Zachos and P. Koch for comments on the manuscript. L. Lajoie, P. Talmage and T. M. Aung assisted in sample preparation and analysis. D. Andreasen and R. Franks provided analytical support. This research used samples and/or data provided by the Integrated Ocean Drilling Program (IODP). Funding for this research was provided by NSF grant OCE0902047.

Author Contributions J.P.L. and A.C.R. did the primary data analysis and wrote the paper with intellectual feedback from all authors. J.P.L. generated alkenone temperature reconstructions; J.P.L., P.S.D., H.L.F., A.C. and M.W.W. analysed foraminifera $\delta^{18}O$.

Author Information Reprints and permissions information is available at www.nature.com/reprints. The authors declare no competing financial interests. Readers are welcome to comment on the online version of this article at www.nature.com/nature. Correspondence and requests for materials should be addressed to J.P.L. (jlarivie@ucsc.edu).

doi:10.1038/nature11200

Records of atmospheric pCO_2

Numerous proxies of past pCO_2 have been used to reconstruct the variation in atmospheric carbon dioxide over the last 15 myrs (Figure SI 1). The compiled proxy records generally show that atmospheric CO_2 levels during the late Miocene (~12-5 myrs ago) were near pre-industrial values. All but three data points (~8, 11, and 12 myrs ago) indicate that throughout the late Miocene the high end of pCO_2 levels was less than modern values of ~390ppmv. However, despite the good agreement between the various pCO_2 estimates for the late Miocene, we suggest that based on the current state of understanding of the geochemical proxies, four previously published records within the 15 myr composite are unreliable. First, Raymo et al.'s[1] pCO_2 estimates, based on the bulk carbon isotopes of sedimentary organic matter, were susceptible to contamination from non-marine sources, an issue that has been addressed with the advancement of compound specific isotope measurements[2]. Second, the pCO_2 estimates of Freeman and Hayes (1992) were based on the carbon isotopes of sedimentary porphyrins[3]. The source uncertainties associated with porphyrins have since been addressed through the development of the alkenone pCO_2 proxy[2]. Third, since the boron isotope estimates of Pearson and Palmer[4], there has been substantial advancement in the understanding of boron isotope fractionation factors, the evolution of seawater $\delta^{11}B$, diagenetic effects[5], and analytical methodology[6]. Fourth, because more work is needed to fully understand planktonic foraminifera B/Ca dependency on [CO_3^{2-}], temperature, and growth rate[7,8], we consider it premature to apply

the B/Ca to long (myr) reconstructions of past pCO_2, as Tripati et al.[9] did. For these reasons, we have excluded the abovementioned records from Figure 1.

A recent compilation of ancient pCO_2 estimates also included data from paleosols[10,11] as well as two additional leaf stomata estimates[12] in the 15 myr long reconstruction[13]. However, the uncertainties associated with these estimates are too large to constrain the pCO_2 changes of the past 15 myrs. For this reason we have excluded these estimates from Figure SI 1 and Figure 1.

Global warmth during the late Miocene

In contrast to the paucity of temperature estimates available from the late Miocene oceans, there is an abundance of paleobotanical and paleoecological data from the continents. Pound et al.[14] recently compiled the available plant and vertebrate fossil data into a 240-site paleoecological database for the Tortonian (11.61-7.25 myrs ago). The fossil assemblage database then allowed the authors to use coexistance[15] and CLAMP[15-19] techniques to make climate estimates for the late Miocene. The vegetation reconstruction exhibited a warmer and wetter world than modern with data coverage in the Western US, Europe, India, southeast Asia, western South America, Alaska, central Africa, parts of northern Asia, and southern Australia. The authors subsequently filled gaps in the data coverage by driving a vegetation model (BIOME 4) with the HadAM3 AGCM model. This modeling effort indicated that global temperatures 11.61-7.25 myrs ago may have been as much as 4.5°C warmer than modern.

Age models

Age models are based on shipboard age models for ODP Sites 1010 and 1021[20], revised foraminiferal and magnetostratigraphy for ODP Site 1208[21], and isotope stratigraphy as well as

biostratigraphy for ODP Site 806[22]. The 1010 and 1021 SST reconstructions have an average sample interval of ~70 kyrs. The SST reconstruction from Site 1208 has an average sample interval of ~40 kyrs.

Site movement

Because tectonic movement of the Pacific plate resulted in poleward movement of the sites used in our study, it was necessary to consider the impact of site movement on each of the SST reconstructions. For this reason, we estimated the paleolocations of Site 1208 based on Pacific Plate movement[23] and used published estimates of paleolocations for Sites 1010 and 1021[24] to examine the temperature change that can be attributed to site migration relative to the modern mean annual SST field[25]. The following table shows mean annual SSTs from the modern site locations compared to the modern mean annual SSTs at the backtracked site locations corresponding to the oldest part of each record in our study:

Site	**Mean annual SST at present site location (°C)**	**Modern mean annual SST at Site's 10myr paleolocation (°C)**	**Modern mean annual SST at Site's 13myr paleolocation (°C)**	**SST difference (paleolocation-modern location)** (°C)
1208	18.8	20.7		1.9
1021	14.3		15.1	0.8
1010	17.2		18.6	1.4

This analyses shows that over the last 10 myrs, not more than 1.9° of cooling recorded in the ODP Site 1208 data could be attributed to the northward site movement. Even less cooling recorded in the ODP Sites 1021 and 1010 could be attributed to northward movement of those sites.

$\Delta\delta^{18}O_{subsurface\text{-}surface}$ at ODP Site 806

The following table shows the average $\Delta\delta^{18}O_{subsurface\text{-}surface}$ values for several intervals of the past ~13 myrs. Average values 13-6 myrs ago more than doubled by 2-0 myrs ago.

Interval (myrs ago)	Average $\Delta\delta^{18}O_{subsurface\text{-}surface}$ (‰)
13-6	0.43083
5-3	0.57270
2-0	1.07286

References

1 Raymo, M. E., Grant, B., Horowitz, M. & Rau, G. H. Mid-Pliocene warmth: Stronger greenhouse and stronger conveyor. *Marine Micropaleontology* **27**, 313-326 (1996).

2 Pagani, M., Arthur, M. A. & Freeman, K. H. Miocene evolution of atmospheric carbon dioxide. *Paleoceanography* **14**, 273-292 (1999).

3 Freeman, K. H. & Hayes, J. M. Fractionation of carbon isotopes by phytoplankton and estimates of ancient CO_2 levels. *Global Biogeochemical Cycles* **6**, 185-198 (1992).

4 Pearson, P. N. & Palmer, M. R. Atmospheric carbon dioxide concentrations over the past 60 million years. *Nature* **406**, 695-699 (2000).

5 Pagani, M., Lemarchand, D., Spivack, A. & Gaillardet, J. A critical evaluation of the boron isotope-pH proxy: The accuracy of ancient ocean pH estimates. *Geochimica Et Cosmochimica Acta* **69**, 953-961 (2005).

6 Foster, G. L. Seawater pH, pCO_2 and CO_3^{2-} variations in the Caribbean Sea over the last 130 kyr: A boron isotope and B/Ca study of planktic forminifera. *Earth and Planetary Science Letters* **271**, 254-266 (2008).

7 Seki, O. *et al*. Alkenone and boron-based Pliocene pCO_2 records. *Earth and Planetary Science Letters* **292**, 201-211 (2010).

8 Yu, J. M., Elderfield, H. & Hönisch, B. B/Ca in planktonic foraminifera as a proxy for surface seawater pH. *Paleoceanography* **22**, PA2202 (2007).

9 Tripati, A. K., Roberts, C. D. & Eagle, R. A. Coupling of CO_2 and ice sheet stability over major climate transitions of the last 20 million years. *Science* **326**, 1394-1397 (2009).

10 Ekart, D. D., Cerling, T. E., Montanez, I. P. & Tabor, N. J. A 400 million year carbon isotope record of pedogenic carbonate: Implications for paleoatmospheric carbon dioxide. *American Journal of Science* **299**, 805-827 (1999).

11 Retallack, G. J. Refining a pedogenic-carbonate CO_2 paleobarometer to quantify a middle Miocene greenhouse spike. *Palaeogeography, Palaeoclimatology, Palaeoecology* **281**, 57-65 (2009).

12 Retallack, G. J. Greenhouse crises of the past 300 million years. *Geological Society of America Bulletin* **121**, 1441-1455 (2009).

13 Beerling, D. J. & Royer, D. L. Convergent Cenozoic CO_2 history. *Nature Geoscience* **4**, 418-420 (2011).

14 Pound, M. J. *et al*. A Tortonian (Late Miocene, 11.61-7.25 Ma) global vegetation reconstruction. *Palaeogeography, Palaeoclimatology, Palaeoecology* **300**, 29-45 (2011).

15 Mosbrugger, V. & Utescher, T. The coexistence approach - a method for quantitative reconstructions of Tertiary terrestrial palaeoclimate data using plant fossils. *Palaeogeography, Palaeoclimatology, Palaeoecology* **134**, 61-86 (1997).

16 Wolfe, J. Temperature parameters of humid to mesic forests of eastern Asia and relation for forests of other regions of the northern Hemisphere and Australasia. *U.S. Geol. Surv. Prof. Paper* **11061106**, 1-37 (1979).

17 Wolfe, J. A. A method of obtaining climatic parameters from leaf assemblages. *U.S. Geological Survey Bulletins* **2040**, 1-71 (1993).

18 Spicer, R. A. Recent and future developments of CLAMP: Building on the legacy of Jack A. Wolfe. *Courier Forschungsinstitut Senckenberg* **258**, 109-118 (2007).

19 Spicer, R. A. *et al*. New developments in CLAMP: Calibration using global gridded meteorological data. *Palaeogeography, Palaeoclimatology, Palaeoecology* **283**, 91-98 (2009).

20 Lyle, M., Koizumi, I., Richter, C. & Leg 167 Shipboard Scientific Party. *Proceedings of the Ocean Drilling Program, Initial Reports* **167** (1997).

21 Venti, N. *Revised late Neogene mid-latitude planktic foraminiferal biostratigraphy for the northwest Pacific (Shatsky Rise), ODP leg 198* Master of Science thesis, University of Massachusetts, (2006).

22 Mayer, A.L., Jansen, E., Backman, J., Takayama, T. Climatic cyclicity at site 806: the GRAPE record. *Proceedings of the Ocean Drilling Program, Scientific Results* **130**, 623-639 (1993).

23 Pares, J. M. & Moore, T. C. New evidence for the Hawaiian hotspot plume motion since the Eocene. *Earth and Planetary Science Letters* **237**, 951-959 (2005).

24 Lyle, M. Reconstructed geographic positions and water depths for Leg 167 drill sites. *Proceedings of the Ocean Drilling Program, Initial Reports* **167**, 41-46 (1997).

25 Locarnini, R. A., Mishonov, A. V., Antonov, J. I., Boyer, T. P. & Garcia, H. E. Temperature. *World Ocean Atlas 2005, NOAA Atlas NESDIS 61* Volume 1 (ed S. Levitus) 182 (U.S. Government Printing Office, 2006).

26 Petit, J. R. *et al*. Climate and atmospheric history of the past 420,000 years from the Vostok ice core, Antarctica. *Nature* **399**, 429-436 (1999).

27 Pepin, L., Raynaud, D., Barnola, J. M. & Loutre, M. F. Hemispheric roles of climate forcings during glacial-interglacial transitions as deduced from the Vostok record and LLN-2D model experiments. *Journal of Geophysical Research-Atmospheres* **106**, 31885-31892 (2001).

28 Raynaud, D. *et al*. Palaeoclimatology - The record for marine isotopic stage 11. *Nature* **436**, 39-40 (2005).

29 Siegenthaler, U. *et al*. Stable carbon cycle-climate relationship during the late Pleistocene. *Science* **310**, 1313-1317 (2005).

30 Monnin, E. *et al*. Atmospheric CO_2 concentrations over the last glacial termination. *Science* **291**, 112-114 (2001).

31 Indermuhle, A., Monnin, E., Stauffer, B., Stocker, T. F. & Wahlen, M. Atmospheric CO_2 concentration from 60 to 20 kyr BP from the Taylor Dome ice core, Antarctica. *Geophysical Research Letters* **27**, 735-738 (2000).

32 Luthi, D. *et al*. High-resolution carbon dioxide concentration record 650,000-800,000 years before present. *Nature* **453**, 379-382 (2008).

33 Hönisch, B., Hemming, N. G., Archer, D., Siddall, M. & McManus, J. F. Atmospheric carbon dioxide concentration across the Mid-Pleistocene Transition. *Science* **324**, 1551-1554 (2009).

34 Bartoli, G., Hönisch, B. & Zeebe, R. Atmospheric CO_2 decline during the Pliocene intensification of Northern Hemisphere Glaciations. *Paleoceanography* **26**, PA4213 (2011).

35 Kürschner, W. M. & Kvacek, Z. Oligocene-Miocene CO_2 fluctuations, climatic and palaeofloristic trends inferred from fossil plant assemblages in central Europe. *Bulletin of Geosciences* **84**, 189-202 (2009).

36 Kürschner, W. M., Van Der Burgh, J., Visscher, H. & Dilcher, D. L. Oak leaves as biosensors of late Neogene and early Pleistocene paleoatmospheric CO_2 concentrations. *Marine Micropaleontology* **27**, 299-312 (1996).

37 Van Der Burgh, J., Visscher, H., Dilcher, D. L. & Kürschner, W. M. Paleoatmospheric signatures in Neogene fossil leaves. *Science* **260**, 1788-1790 (1993).

38 Stults, D. Z., Wagner-Cremer, F. & Axsmith, B. J. Atmospheric paleo-CO_2 estimates based on Taxodium distichum (Cupressaceae) fossils from the Miocene and Pliocene of Eastern North America. *Palaeogeography, Palaeoclimatology, Palaeoecology* **309**, 327-332 (2011).

39 Beerling, D. J., Fox, A. & Anderson, C. W. Quantitative uncertainty analyses of ancient atmospheric CO_2 estimates from fossil leaves. *American Journal of Science* **309**, 775-787 (2009).

40 Pagani, M., Liu, Z. H., LaRiviere, J. & Ravelo, A. C. High Earth-system climate sensitivity determined from Pliocene carbon dioxide concentrations. *Nature Geoscience* **3**, 27-30 (2010).

41 Pagani, M., Freeman, K. H. & Arthur, M. A. Late Miocene atmospheric CO_2 concentrations and the expansion of C4 Grasses. *Science* **285**, 876-879 (1999).

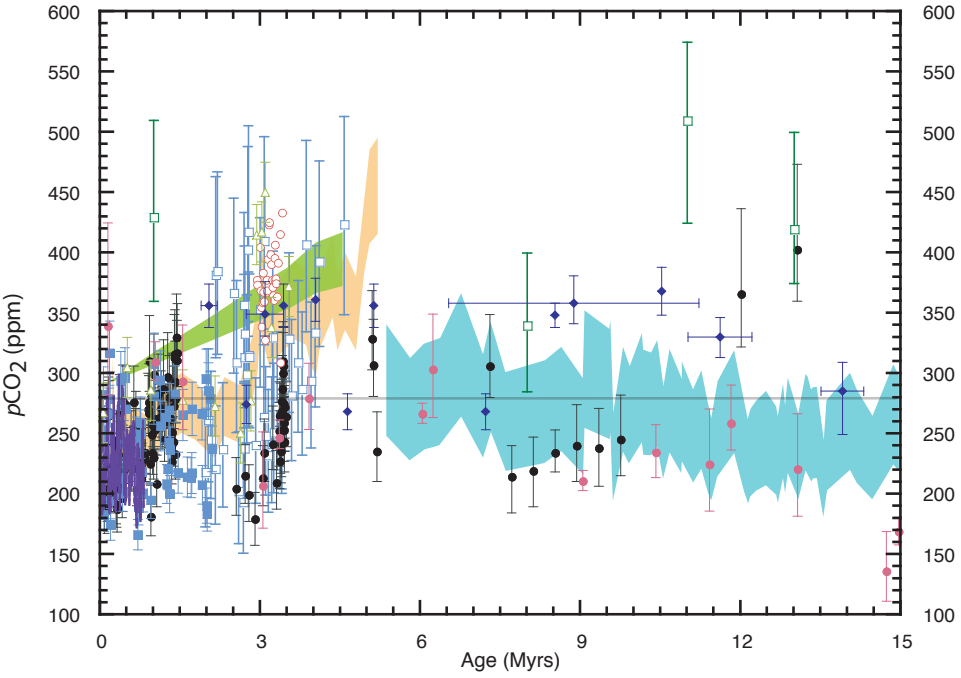

Figure SI 1. Estimates of atmospheric pCO_2. Estimates from ice cores (purple line[26-32]), boron isotopes (pink filled circles[4], blue filled squares[33], blue open squares[34], green open triangles[7]), boron/calcium ratios of planktonic foraminifera (black circles[9]), plant stomata (blue diamonds[35-39]), carbon isotopes of bulk sedimentary organic C (red open circles[1]), carbon isotopes of sedimentary porphyrins (green open squares[3]), and alkenones (green[40], gold[7], and blue shading[41]). Gray line marks pre-industrial pCO_2 concentrations (280ppmv). Vertical error bars represent reported uncertainty in pCO_2 estimates. Reported age uncertainties are denoted with horizontal bars. Shading indicates the range between published maximum and minimum alkenone pCO_2 estimates[7,40,41].

Chapter 3. Basin-wide sea surface temperature distributions of the Pleistocene, Pliocene, and late Miocene

Abstract

A lack of Neogene sea surface temperature (SST) data has made it difficult to determine the role that basin-wide temperature distributions played in shaping the climates both before and following the onset of widespread Northern Hemisphere glaciation (NHG). To better characterize the basin-wide distribution of SSTs, we used new geochemical SST estimates, as well as previously published data, to map global SSTs for two time slices from before the onset of NHG, centered at ~4.15, and 9 Ma, and three time slices after the onset of NHG, centered at 2.55, 1.45, and ~0.55 Ma. The basin-wide SST patterns of the earliest time slices are distinctly different from the time slices that follow the onset of glaciation ~2.7myrs ago. The late Miocene and early Pliocene time slices show the presence of warm subtropical eastern boundary current (EBC) regions, zonally uniform SSTs in the tropics and mid-latitudes, poleward expansion of tropical warmth, and poleward offsets of the subarctic/subtropical transition zones prior to the onset of NHG. The time slice for 2.7-2.4 Ma shows a meridional temperature gradient in the western Pacific that is similar to the gradient of the early Pliocene, though the EBCs were cooler relative to the early Pliocene. The two most recent time slices show EBCs with SSTs that were similar-to or cooler than modern SSTs and meridional temperature gradients in the western pacific that are steeper than those of the Miocene and Pliocene. The maps,

combined with SST time series comparisons, reveal heterogeneous regional SST changes that resulted in long-term strengthening in basin-wide gradients. The observed strengthening of Pacific SST gradients since the late Miocene supports the hypothesis that changes in basin-wide SST distributions were instrumental in maintaining the warmth and suppression of Northern Hemisphere Glaciation in the low pCO_2 conditions of the late Miocene.

3.1 Introduction

The spatial distribution of sea surface temperatures (SST) on basin-wide scales plays a critical role in coupling oceanic conditions with the global climate system. For instance, the spatial distribution of SSTs in the tropical Pacific (cold tongue in the eastern equatorial Pacific (EEP), warm pool in the western equatorial Pacific) comprises the foundation for Walker circulation. Changes in this SST distribution determine the extra-tropical teleconnections that affect climate on a global scale (e.g. ENSO, the largest source of interannual global climate variability) [*Chiang*, 2009]. Modeling studies also indicate that both the location of SST maxima and the structure of meridional SST gradients drive the large-scale atmospheric convection that determines the position and strength of Hadley circulation cells [*Clement*, 2006]. Thus, changes in basin-wide temperature gradients and the spatial distribution of SSTs have the potential to impact the global climate system. For this reason, reconstructions of past SST distributions and changes in large-scale temperature gradients can provide valuable information in ongoing efforts to

understand long-term trends in the Earth's climate.

Climate model sensitivity studies that used proxy-data constraints of past SSTs have suggested that the strengthening of both meridional and zonal SST gradients may have played a major role in the evolution of Neogene climates prior to and following the onset of Northern Hemisphere glaciation [*Brierley and Fedorov*, 2010; *Brierley et al.*, 2009]. The modeling showed that as basin-wide SST gradients became more pronounced, conditions favoring northern Hemisphere glaciation developed and persisted. However, these modeling efforts used paleo-temperature proxy data that was too sparse to adequately constrain the SST distributions of any particular geologic interval and, because the proxy-data came from disparate regions around the globe, the meridional gradients that represented the early Pliocene and Pleistocene could only be estimated under the assumption that it was possible to correct for the regionality of a particular proxy record. In other words, these efforts were sensitivity studies forced by crude and idealized changes in SST gradients. To model the mechanisms of climate change during past geologic intervals, an improved picture of the trends in basin-wide SST distributions is needed.

The reconstruction of SSTs from a single oceanographic site cannot adequately resolve basin-wide trends; rather records from a single site are suited to resolve regional climate signals. Several studies aimed at understanding the onset of Northern Hemisphere glaciation have assessed change in zonal and meridional SST gradients by reconstructing Plio/Pleistocene SSTs from multiple regions [*Etourneau et al.*, 2010; *Martinez-Garcia et al.*, 2010; *Wara et al.*, 2005]. However, over the past

17 years the efforts of paleoceanographers to generate high-quality geochemical records of late Neogene climates has produced an even greater array of sites from around the globe that can be used to develop a synoptic understanding of SSTs since the late Miocene.

Here we use a combination of time series comparisons and mapping to constrain the development of SST gradients in the Pacific basin since the late Miocene. We generated new data to resolve the evolution of meridional SST gradients in the west Pacific (at ~165°E), and combined it with published geochemical SST time series data to provide a complete compilation of available data. To control for the various geochemical approaches used by researchers in the original publications, we applied a uniform dissolution correction to the raw Mg/Ca temperature estimates and used consistent SST calibrations between data sets. We used statistical significance tests to compare paleo temperature estimates to modern conditions and then used a variogram and kriging approach to develop gridded fields of paleo-proxy data between sites for five time slices of the late Neogene and Quaternary periods. The results are synoptic, though simplified, snapshots of the major features of the global SST distributions at ~0.7-0.4, 1.6-1.3, 2.7-2.4, 4.3-4.0 and 9.25-8.75 Ma. These maps of SST allow us to identify major global trends in basin-wide SST distributions, resolve the meridional SST profile from 37°S to 54°N along 165°E in the western Pacific, and quantitatively evaluate uncertainties in our estimates of basin-wide conditions. In addition, we use time series data from the mid-latitude and tropical Pacific to investigate the evolution of Pacific basin SST

gradients. By using the maps and time series together we test the idea that weak zonal and meridional SST gradients were a prevalent feature of the early Pliocene and late Miocene, and thus can help to explain why these geological periods were warmer than modern climates.

3.2 Methods

For this study we generated new SST records from six sites in the Pacific. This new data includes alkenone SST estimates from DSDP Sites 173 and 207 and ODP Sites 1207 and 1340, and Mg/Ca SST estimates from DSDP Site 208 and ODP Site 873. We then used this new data as well as published alkenone and Mg/Ca SST estimates to reconstruct the evolution of SST patterns over the past 13myrs (Table 1; Figure 1).

Sea surface temperature estimates from alkenones

We reconstructed past surface water temperatures using the alkenone paleothermometer at sites with adequate alkenone concentrations in the sediment and mean modern annual SSTs that were markedly lower than the upper limit of the alkenone proxy. This proxy is derived from the $U^{k'}_{37}$ index; the measure of $C_{37:2}$ alkenones to the sum of $C_{37:2}$ and $C_{37:3}$ alkenones that are produced, in the modern ocean, by the coccolithophorid algae *Gephyrocapsa oceanica* and *Emiliania huxleyi* [*Prahl and Wakeham*, 1987]. Higher values of $U^{k'}_{37}$ reflect higher growth temperatures of the alkenone producing algae [*Prahl et al.*, 1988]. We applied the global calibration of *Müller* [1998] to convert $U^{k'}_{37}$ into SST where $U^{k'}_{37} = 0.033T + 0.044$ [*Muller et al.*, 1998].

Lipids were extracted from .5-5g of crushed dry sediment with either a 3:1 dichloromethane:methanol mix or pure dichloromethane using a Dionex Accelerated Solvent Extractor (ASE200). The total lipid extract was evaporated under a stream of N_2 (Zymark Turbovap, water bath at 35°C) and redissolved in 100-200µl of toluene spiked with hexatriacontane and heptatriacontane as internal standards. 1µl of sample was injected into a HP6890 GC-FID with a cool-on-column inlet. Separation of organic compounds was carried out on a DB-1 GC column (60m x .32mm x 0.1µm film thickness, Agilent) with either an integrated fused-silica guard column (1-10m x .32mm, Duraguard) or a separate fused silica guard column attached to the main column using an Agilent ultimate union (1-10m x .32mm, Restek). The initial GC oven temperature was 90°C. The GC oven temperature was increased by 25°C/min until reaching 250°C, 1°C/min until reaching 303°C, and 20°C/min until reaching 325°C, where it was held constant for 20 min. ~8cm of the guard column was cut off prior to each run in order to maintain good chromatography. We used Agilent Chemstation software to manually integrate the alkenone peak areas required for determination of $U^{k'}_{37}$ values. Long-term reproducibility of liquid standard replicates included in each GC run was within $\pm$ 0.007 $U^{k'}_{37}$ units, which is equivalent to $\pm$ 0.2°C.

Sea surface temperature estimates from foraminiferal Mg/Ca

For sites 208 and 873 we used the Mg/Ca of planktonic foraminifera shells to reconstruct past SSTs. At Site 873 the modern SST is above the upper limit of the alkenone paleothermometer making Mg/Ca an especially suitable proxy for SST at

the site. This proxy is derived from the temperature dependent substitution of magnesium into calcium carbonate shells; sediment trap, culture, and core-top studies have shown that the Mg/Ca follows a temperature dependence that can be described with a logarithmic equation [*Anand et al.*, 2003; *Barker et al.*, 2005; *Dekens et al.*, 2002]. In this study we used the dissolution correction of *Regenberg et al.* [2006] and the calibration of *Anand et al.* [2003] to reconstruct past temperatures.

Sediments were soaked in DI water for 24hrs, washed and sieved at 63μm, and picked for *G. sacculifer* (w/o sac, 355-425 μm size fraction). Approximately 25 shells from each sample were crushed under glass plates, with an emphasis on only cracking the shell chambers, as opposed to powdering the shells. Crushed samples were then cleaned using the "modified Boyle" protocol described in *Ford et al.* [2012], which includes a methanol rinse to remove clays, oxidative and reductive cleaning steps, and a weak acid leach. Samples were run for minor element ratios on a PerkinElmer Optima 8300 inductively coupled plasma optical emission spectrometer (ICP-OES). Foram and liquid standards were included in each batch of samples to evaluate analytical precision. Long-term reproducibility was $\pm$0.028 (n=317) and $\pm$0.256mmol/mol (n=77) for the liquid and foram standards, respectively.

Mapping SSTs

We constructed maps of SSTs for time slices before and after the onset of Northern Hemisphere glaciation using the published age models for each site. We used biostratigraphic age models for DSDP 208, 209 [*Hills and Thierstein*, 1989], and

ODP 873 [*Rack et al.*, 1995], a magnetostratigraphic age model for ODP 1207 [*Evans et al.*, 2005], the Shipboard age model for IODP U1340 [*Expedition 323 Scientists,* 2011], and a combination of magnetostratigraphic and biostratigraphic age models for DSDP 173 [*Expedition 18 Scientists*, 1973; *Heinrichs*, 1973]. Four of the time slices were 300kyr long (spanning 0.7-0.4, 1.6-1.3, 2.7-2.4, and 4.3-4.0Ma) and one time slice was 500kyrs long (spanning 9.25-8.75Ma) (Figure 1).

Because the data coverage for the time slices in our study is spatially sparse, it is unlikely that the defining currents and major features of each ocean could be reproduced using the absolute temperature estimates and site distribution of the paleo data alone. In an effort to account for these circulation features, we added an interpolated anomaly surface grid to the modern mean annual SST grid. To do this we first estimated the modern mean annual SSTs for each site using the gridded World Ocean Atlas modern mean annual SST dataset and the 2D estimation tool in Ocean Data View software [*Locarnini et al.*, 2010; *Schlitzer*, 2012]. We then compared the modern SSTs and the proxy-based paleo SST estimates (Table 2) to determine a paleo SST anomaly at each site:

$$\text{paleo anomaly} = SST_{\text{timeslice}} - SST_{\text{modern mean annual}}$$

We gridded the paleo SST anomalies using the variogram and kriging tools in ArcMap9.3 GIS software (Figure 2). This gridding method uses the spatial distribution of samples to perform a weighted-average interpolation between data [*Schafer-Neth et al.*, 2005] and provides an associated map of standard error in the interpolated surface inherent to the kriging model (Figure 3). We used an ordinary

cokriging approach to facilitate gridding; paleo anomalies were cokriged with the modern World Ocean Atlas mean annual SST dataset using a spherical kriging model [*Locarnini et al.*, 2010]. This approach is suitable for gridding paleo data because the heterogeneous spatial distribution of sites requires an interpolation method that can resolve the small-scale variability in a densely sampled region while also using large-scale variability to inform the gridding of data in regions that are sparsely sampled [*Schafer-Neth et al.*, 2005]. Cokriging allowed the high-coverage data of the World Ocean Atlas to aid the kriging of the sparsely sampled paleo time slices. To estimate the basin-wide distributions of absolute SSTs we added the gridded anomaly maps of each time slice to the modern World Ocean Atlas gridded data set (Figure 4).

We used cross-validation in ArcMap9.3 to determine how well the kriging model predicted values in regions without data. Cross-validation involves omitting a site from the kriged dataset, predicting the value at that location using the degraded dataset, and then comparing the predicted value with the actual value of the omitted site [*Krivoruchko*, 2011]. This comparison of predicted and actual data was repeated for all sites and allowed us to evaluate cross-validation errors for each time slice. Generally, our kriging technique resulted in cross-validation root-mean-square errors of ~2°C (Table 3). These relatively high root-mean-square errors may be the result of sparse sampling of the global ocean, proxy error, and/or the heterogeneous SST distributions of past intervals.

Some uncertainty in the paleo-reconstruction maps results from our use of the World Ocean Atlas SST data [*Locarnini et al.*, 2010] as both a co-kriging reference

dataset and as a base-map for the paleo-map reconstructions. Specifically, uncertainty arises because the correlation length scales of past SSTs are unknown. In each of the time slices the ocean basin shape, large-scale atmospheric wind patterns, and regional climatology all would have played a role in determining the appropriate SST correlation length scales. Though it is beyond the scope of this study, we note that the sensitivity of our gridded paleo-anomaly maps to cokriging with the global World Ocean Atlas could be assessed by cokriging paleo-SSTs with a regional modern SST dataset and comparing the two anomaly maps.

With our kriging approach the difference in the geochemical proxy value vs. kriged surface temperatures at each site was typically <0.4°C. In the prediction standard error maps of the kriged surfaces, the regions that have paleo-proxy data exhibit relatively low error; error generally increases in regions farther from sites (Figure 3). The relatively low-error regions comprise the focus of our discussion.

3.3 Complications of synthesizing SST records

The temperature records that we compiled for this study were generated over the past 17 years by many different research groups often using different methodologies for estimating SSTs. As a result, to construct a synthesis of the available temperature estimates we needed to make the data internally consistent. While there could have been issues in comparing temperature estimates of different proxies or comparing SST estimates based on different temperature calibrations within the same proxy, the area that required the most adjustment in order to achieve internal consistency with the data was accounting for the effect of dissolution in

Mg/Ca records. Previous work has shown that temperature calibrations of alkenones are generally consistent [*Lawrence et al.*, 2007] and the core-top, culture, and sediment trap calibrations of *G. sacculifer* and *G. ruber* Mg/Ca with temperature are generally consistent [*Barker et al.*, 2005]. Furthermore, work in the EEP indicates that alkenones and Mg/Ca generally agree on long time scales [*Dekens et al.*, 2008]. Accounting for a dissolution bias in Mg/Ca records, however, remains a topic of some debate and the methods of dealing with this varied from study to study.

Dissolution of foraminiferal carbonate by corrosive waters preferentially dissolves Mg and as a result lowers the Mg/Ca ratio of the carbonate [*Barker et al.*, 2005]. This lowering of the original Mg/Ca ratio results in proxy-based estimates that underestimate water temperatures; in other words, dissolution results in a bias towards cooler values. Dissolution corrections based on shell mass [*Rosenthal and Lohmann*, 2002], water depth [*Dekens et al.*, 2002], or $\Delta[CO_3^{2-}]$, where $\Delta[CO_3^{2-}]$ is the difference between in situ carbonate ion concentration ($[CO_3^{2-}]$) and carbonate ion concentration at saturation [*Dekens et al.*, 2002; *Regenberg et al.*, 2006], have all been used to estimate and correct for the effects of dissolution on paleo temperature reconstructions [*Dekens et al.*, 2008; *Karas et al.*, 2011a; *Nathan and Leckie*, 2009; *Wara et al.*, 2005]. However, in many cases, often based on the modern conditions at each particular site (e.g. shallow water depth, good foraminifera preservation), authors decided that dissolution corrections were unnecessary [*de Garidel-Thoron et al.*, 2005; *Groeneveld*, 2005; *Groeneveld et al.*, 2006; *Karas et al.*, 2011b; *Karas et*

al., 2009; *Nurnberg and Groeneveld*, 2006; *Rackebrandt et al.*, 2011; *Russon et al.*, 2010; *Steinke et al.*, 2010].

There is evidence that dissolution affects preservation of the paleo-temperature signal when $\Delta[CO_3^{2-}]$ is < ~18-26μmol/kg [*Dekens et al.*, 2002; *Regenberg et al.*, 2006] and that the susceptibility to dissolution is species specific [*Regenberg et al.*, 2006]. To address these issues we corrected the raw Mg/Ca values of the previously published records with species-specific dissolution corrections for *G. sacculifer* and *G. ruber* [Regenberg et al., 2006]. We estimated $\Delta[CO_3^{2-}]$ at each site by merging the gridded GLODAP ocean carbon dataset [*Key et al.*, 2004] with the gridded World Ocean Atlas temperature dataset [*Locarnini et al.*, 2010] and used Ocean Data View software to derive $\Delta[CO_3^{2-}]$ at each site (in regions not covered by the GLODAP gridded data we used $\Delta[CO_3^{2-}]$ estimates of *Goyet et al.* [2000]). We applied species-specific Mg/Ca corrections when $\Delta[CO_3^{2-}]$ was less than 22.10μmol/kg for *G. sacculifer* and 25.28umol/kg for *G. ruber* [*Regenberg et al.*, 2006]. We then calculated SSTs using the *Anand et al.* [2003] multispecies calibration of Mg/Ca=0.38exp0.090T. The SST record from ODP1172 was based on the Mg/Ca of *G. bulloides* and could not be corrected for dissolution. SSTs for this site were calculated using the calibration of *Mashiotta et al.* [1999].

Our approach of using a species-specific correction for dissolution based on $\Delta[CO_3^{2-}]$ at each site is an attempt to correct for dissolution effects in a uniform way among all of the Mg/Ca datasets. This correction aims to directly account for the cause of dissolution; low $\Delta[CO_3^{2-}]$. However, we found that at Site 806 the $\Delta[CO_3^{2-}]$

corrected temperature estimates from Holocene *G. sacculifer* underestimated modern mean annual SSTs by 1.1°C, while Holocene *G. ruber* Mg/Ca overestimated modern mean annual SSTs by 0.4°C. Since Site 806 is in a location where there is good constraint on modern $\Delta[CO_3^{2-}]$ (GLODAP bottle observations at 164°E, 3°N show $\Delta[CO_3^{2-}]$ = 4.067umol/kg at 2269m depth, we estimated nearby site 806 $\Delta[CO_3^{2-}]$ = 5.692umol/kg) and has both *G. sacculifer* and *G. ruber* data from the Holocene as well as older intervals, we chose to anchor all of the Mg/Ca records in our data synthesis to the Holocene temperature estimates at Site 806. We added 1.1°C to all temperature estimates based on *G. sacculifer* and subtracted 0.4°C from all temperature estimates based on *G. ruber*. This adjustment allows all Mg/Ca temperature estimates to be compared to the Mg/Ca-based temperature estimates of Site 806, which were relatively stable since the late Miocene.

Each data set included in our synthesis had a unique sampling resolution with some records resolving orbital scale variability and others providing only a single data point within the bounds of a time slice. We averaged all of the proxy data within a time slice in an attempt to get at the mean conditions of each time slice and to determine the mean paleo anomalies at each site. However, because the climatology in any region is determined by both the mean as well as the standard deviation in temperatures, to best understand the significance of the proxy data within each time slice we used the Wilcoxan-mean-Whitney test to compare median SSTs of each proxy record to the median of monthly SSTs from 1958-2007 at each site [*SODA:Carton and Giese*, 2008] (Figure 2). We compare medians, as opposed to

means, because it is likely that the SSTs within each time slice do not follow a normal distribution. For example, the Pleistocene glacials have become progressively cooler since ~3.5 Ma, while the interglacial SST values have remained relatively steady [*Herbert et al.*, 2010]. This trend towards cooler glacial SSTs enhances the non-normality of SSTs in each time slice after ~3.5 Ma.

3.4 Basin-wide SST distributions

In the following time slice summaries SSTs are reported relative to modern mean annual conditions at each site, unless otherwise stated.

The late Miocene 9.25-8.75 Ma

More than half of the records that comprise the late Miocene dataset are from sites in the mid-latitudes (Figures 2, 4) and much of our understanding of this time slice comes from comparing the late Miocene portion of the records with the early Pliocene portion of the same records. Mean SST estimates indicate that mid-latitude eastern boundary current (EBC) regions of the North Pacific and South Atlantic were ~5-8°C warmer than today. The western North Pacific exhibited mean SSTs ~4-5°C warmer than modern. In the South China Sea mean SSTs were ~2°C warmer than modern. The tropical SSTs of the west Pacific warm pool and the tropical Arabian Sea were similar to modern mean annual SSTs. At each site, the late Miocene temperatures were warmer than those of the early Pliocene portion of the record. This observation led us to construct the late Miocene timeslice map using early Pliocene SST values to anchor regions that did not have late Miocene SST estimates; our main

assumption was that in regions without direct geochemical estimates the climate was at least as warm as that of the early Pliocene. Due to sparse sampling the late Miocene timeslice is the least constrained of all the intervals discussed in this study.

The early Pliocene 4.3-4.0 Ma

The mid-latitude sites that exemplify the warm late Miocene cooled to some extent by the early Pliocene, but the early Pliocene climate was still characteristically warm (Figures 2, 4). EBC SSTs ranged from near-modern values to temperatures ~10°C warmer than modern. This range of EBC SSTs may reflect differences in the local oceanography of each site such as proximity to upwelling regions or local surface currents. Mid-latitude sites from the western North and South Pacific recorded average SSTs ~2-3°C warmer than today's.

Other parts of the globe were also characterized by relatively warm SSTs in the early Pliocene. Mean SSTs of the high-latitude North Pacific and North Atlantic were ~6-8°C warmer-than-modern. The tropics differed from modern conditions the most in the eastern equatorial Pacific upwelling regions; SSTs were warmer than the region's modern waters by as much as ~4°C. In contrast, mean SSTs in the non-upwelling tropical regions (e.g. the west Pacific warm pool, the tropical Indian Ocean, the western tropical Atlantic, and the South China Sea) ranged from just under ~1°C warmer to ~2°C cooler than modern mean annual SSTs. Mean SSTs at Caribbean Site 999 were ~4°C cooler than modern mean annual SSTs.

The Plio-Pleistocene 2.7-2.4 Ma

A transitional state between the warm early Pliocene and the ice age climate

of the Pleistocene is somewhat visible in the Plio-Pleistocene timeslice with cooling relative to the early Pliocene observed in many, though not all, regions (Figures 2, 4). In this timeslice the mean SSTs of the high latitude North Atlantic cooled by ~3°C relative to the early Pliocene; however, mean SSTs in the Bering Sea and sub-Arctic Pacific were still within 1° of the early Pliocene values. Though North Atlantic mid-latitude sites outside of the EBCs were within 1°C of modern values 2.7-2.4myrs ago, the mid-latitude regions outside of the EBCs of the North Pacific and the South Atlantic were ~2-3°C warmer than modern waters.

The EBC regions and the tropics also displayed variability in site-to-site conditions during this timeslice. For example, eastern equatorial upwelling sites were ~1-4°C warmer than modern SSTs while the tropical non-upwelling sites recorded SSTs that ranged from values near modern mean annual SSTs to ~3°C cooler than modern mean annual SSTs. EBC temperatures ranged from ~1°C cooler to ~6°C warmer than modern mean annual SSTs.

The early Pleistocene 1.6-1.3Ma

The mean SSTs of the early Pleistocene timeslice were more similar to modern conditions than during any of the earlier time slices (Figures 2, 4). Non-upwelling tropical regions were near modern values or cooler by no more than ~2°C. Tropical upwelling sites in the eastern equatorial Pacific were less than ~2°C warmer than modern. Mid-latitude regions were ~4°C cooler to ~3°C warmer than modern. Subtropical sites in the Coral Sea were up to ~4°C warmer than modern. High latitude sites in both the North Pacific and North Atlantic were ~5°C and ~3°C

warmer than modern, respectively.

The late Pleistocene 0.7-0.4Ma

The majority of oceanic regions for which we have late Pleistocene data exhibit mean SSTs that were either cooler-than or close-to modern values (Figures 2, 4). Most mid-latitude regions were relatively cool, with mean SSTs that were cooler than modern by ~0.5-5°C. In tropical non-upwelling regions temperatures ranged from ~1°C warmer to ~2° cooler than modern and mean SSTs from tropical upwelling regions ranged from ~2°C warmer to ~1°C cooler than modern.

In contrast to the prevalence of SSTs that were near-modern or cooler-than-modern SSTs, the SSTs from the Coral Sea and the high-latitude sites of the Pacific and North Atlantic were warmer than modern mean annual SSTs. SST estimates from the Bering Sea, the sub-arctic North Pacific, and the subarctic North Atlantic were 2-3°C warmer than modern mean annual SSTs; however, these estimates can be explained by the seasonality of alkenone production. Modern production of alkenones in these regions is limited to the warm seasons which are 3°, 4°, and 3° warmer than modern mean annual SSTs in the Bering Sea, subarctic Pacific, and subarctic Atlantic, respectively [*Harada et al.*, 2003; *Haug et al.*, 2005; *Lawrence et al.*, 2009; *Locarnini et al.*, 2010]. Thus the warm paleo SSTs at these sites are within the modern warm season temperature range. Unless the season of alkenone production was different in this time slice (as well as in the 1.6-1.3 Ma time slice), the proxy SSTs indicate that the past warm season temperatures of the high latitudes were similar to the modern warm season SSTs. In contrast, the warm SSTs at

tropical/subtropical sites in the Coral Sea, which were ~3-4°C warmer than modern mean annual temperatures, are outside of the modern seasonal SST range.

Site GEOB3801-6, in the South Atlantic, exhibits SSTs ~8°C warmer than modern, and appears to be an outlier. One possible explanation for the warm SSTs at this site is that because *Rackebrandt et al.* [2011] attempted to exclude any foraminifera that showed signs of dissolution from geochemical analysis, no dissolution correction was needed at this site. The *Regenberg et al.* [2006] Mg/Ca dissolution correction increased mean SST values by ~8°C relative to SSTs determined from uncorrected Mg/Ca values. If this dissolution correction is not applied, South Atlantic Site GEOB3801-6 exhibits temperatures 0.7-0.4 Ma that are similar to modern SSTs.

Basin-wide SST gradients in the Pacific

The meridional gradient in the west Pacific

The difference in SSTs between the mid-latitude and tropical western Pacific was smallest in the late Miocene and grew progressively larger as the as the mid-latitudes cooled through the Pliocene and Pleistocene (Figure 4, 5a). This meridional SST gradient can be assessed by comparing the SSTs of Site 806 in the western equatorial Pacific (0°N, 160°E) with those of Site 1208 in the mid-latitude northwest Pacific (36°N, 158°N). The modern difference in mean annual SSTs between these sites is ~11°C [*Locarnini et al.*, 2010]. Even after accounting for ~1.5°C of warming that could be attributed to site movement of 1208 [*LaRiviere et al.*, 2012], the SST

gradient between these two regions was reduced by more than 4°C in the 9.5-8.75 Ma time slice. The SST gradient became larger through the Pliocene and Plio/Pleistocene transition but did not reach modern values until after ~2 Ma. In the late Pleistocene the gradient slightly exceeded the modern difference between SSTs at sites 806 and 1208.

In addition to the time series comparison, the transect of sites running N-S in the western Pacific allows us to estimate the shape of the meridional gradient of each time slice. Based on the interpolated map surface along 165°E, the early Pliocene and late Miocene gradients exhibit a relaxed profile, with mid and high-latitude temperatures generally at or exceeding the summer maximum temperatures observed in the modern ocean and near-modern mean annual temperatures in the tropical Pacific (Figure 6). The overall effect of the reduced temperature difference between the tropics, mid, and high-latitudes is a relatively broad zone of tropical warmth and a poleward shift of the subtropical/subarctic transition zones. Of these warm intervals, the late Miocene shows the greatest reduction, relative to modern conditions, in the meridional gradient and the most poleward expansion of low latitude warmth.

In the North Pacific, the poleward extent of warm SSTs decreases through the 1.6-1.3 and 0.7-0.4Ma time slices (Figure 7). By the 1.6-1.3 and 0.7-0.4 Ma intervals the North Pacific temperatures were either near or cooler-than the modern mean annual SSTs along 165°E. Throughout all of the time slices most of the tropical west Pacific SSTs varied from modern SSTs by no more than ~2°C.

In contrast to the Pleistocene SSTs along 165°E in the North Pacific, SSTs

between ~10 and 25°S were warmer than even the maximum temperatures in a typical seasonal range. Because part of this maximum is between sites, and is therefore unconstrained by geochemical data, it is likely that this warm "hump" in the profile is an artifact of the kriging technique.

The zonal gradient in the mid-latitude Pacific

The SST difference across the subtropical pacific was smallest in the late Miocene and subsequently increased through the Pliocene time slice (Figures 4, 5b). During the late Miocene time slice the SST difference between Northern California Site 1021 (39°N) and the Shatsky Rise sites 1207 (38°N) and 1208 (36°N) was ~4°C. By the early Pliocene the SST difference between Site 1021 and Sites 1208/1207 was ~6-7°C. This difference was fairly stable through the Pleistocene with the western mid-latitude Pacific ~6-8°C warmer than the eastern side of the basin.

The eastern tropical and subtropical North Pacific

When compared with temperature records from the tropical Pacific, the Site 1010 (~30°N, in the southern California Current) temperature reconstruction reveals a striking convergence in ocean temperatures of the tropical and eastern subtropical North Pacific during the late Miocene. (Figures 4, 5c). New SST data from EEP Site 1338 indicates that during the 9.25-8.75Ma time slice the EEP SSTs were not significantly different from SSTs in the warm pool [*Rousselle et al.*, 2013], though some SST estimates from Site 1338 are near the upper temperature limit of the alkenone proxy and should be considered a minimum SST estimate. Eastern subtropical North Pacific Site 1010 had temperatures just ~2-3°C cooler than SSTs

throughout the tropical Pacific.

Long-term cooling in the southern California Margin was underway through the latest Miocene and by the early Pliocene the site was ~5-6°C cooler than the tropical Pacific sites. The difference in SSTs at Sites 806 and 846 became larger through the early Pleistocene [*Wara et al.*, 2005] and the southern California margin region continued to cool. By the 1.6-1.3 Ma time slice Site 1010 was 8°C cooler than the eastern equatorial Pacific and ~12°C cooler than the western tropical Pacific. By the latest Pleistocene the regions remained distinct; the southern subtropical site in the California current was cooler than the EEP by ~6°C.

3.5 Discussion

Overall, the basin-wide SST distributions during the late Miocene and early Pliocene resulted in reduced zonal SST gradients in the tropical and mid-latitude North Pacific and reduced meridional SST gradients in the eastern subtropical and western North Pacific. The eventual strengthening of these gradients occurred at different times depending on the region. Generally, global SST distributions and gradients closely resembled modern conditions by the Pleistocene time slices 1.6-1.3 and 0.7-0.4 Ma.

In the case of the North Pacific, SSTs were zonally uniform in the late Miocene and then, because the eastern side of the basin cooled more than the western side of the basin, became warmer in the west than in the east. In the early Pliocene, the difference between SSTs in the west and those in the east became more

pronounced; however, Pliocene East-West temperature differences were still smaller than the across-basin temperature differences in the Quaternary.

In the modern ocean California Current advection of cool subarctic water along the eastern side of the North Pacific subtropical gyre combined with nearshore and offshore upwelling directs subtropical SST isotherms equatorward [*Lyle et al.*, 2000]. As a result, Site 1010, which is at 30°N in the eastern Pacific, has a modern mean annual temperature that is similar to the modern mean annual SSTs at sites 1208 and 1207, which are in the western Pacific at 36°N and 38°N, respectively. In the late Miocene, this SST contrast broke down; Site 1010 SSTs were ~3°C greater than temperatures at the more northern sites of 1207 and 1208 in the western Pacific (1010 was ~4-6°C warmer if all of the records are adjusted for site movement). At the same time, SSTs at Site 1021, which is in the northern California Current at 39°N, were within ~4°C of SSTs at Sites 1208 and 1207 (1021 SSTs were less than ~2° cooler than 1208 and 1207 SSTs when adjusted for site movement) (Figure 5b). Aside from a transient warming event in the Northern California margin ~5.5-4 Ma, there was no major change in the gradient between sites 1021, located in the Northern California Current, and 1010, located in the southern California Current. Such a constant gradient implies that there was no change in the either the relative amount of upwelling between the two sites and/or in the advection of cool waters south in the California Current.

SST reconstructions from Site 1010 indicate that in the late Neogene there was zonal uniformity in SSTs across the lower latitudes of the North Pacific

subtropical gyre. When considered together, the transect data from 165°E, estimates of tropical SSTs from sites 806 [*Nathan and Leckie*, 2009; *Wara et al.*, 2005] and 1338 [*Rousselle et al.*, 2013] and the SST time slice maps suggest that there may have been substantial poleward and eastward broadening of warm pool tropical temperatures in the late Miocene and early Pliocene. Overall, the maps and time series indicate that, in the North Pacific, and possibly globally, temperatures were more zonally uniform in the late Miocene than at any other time in the late Neogene and Quaternary periods.

This synoptic view of late Neogene and Quaternary geochemical SST records shows that the late Miocene was a more extreme example of a warm climate than the warm early Pliocene, a result that is consistent with deep water temperature reconstructions [*Lear et al.*, 2003] and terrestrial climate reconstructions [*Pound et al.*, 2011]. Based on our new data, timeslice maps, and North Pacific time series comparisons, it appears that one major ingredient in the picture of Pliocene warmth, reduced meridional SST gradients, was even more extreme in the late Miocene. In addition, we find that the temperatures across the North Pacific basin were more zonally uniform in the late Miocene. The SST changes since the late Miocene time slice, and possibly even since the early late Miocene, are consistent with the SST trends investigated in model sensitivity experiments of *Brierley and Fedorov* [2010] and *Brierley et al.* [2009]. Though their model simulations were focused on the suppression of Northern Hemisphere ice sheets in the early Pliocene, the results provide some insight to the reasons for late Miocene warmth [*LaRiviere et al.*, 2012].

In the modeling experiments, relaxation of the modern basin-wide meridional and zonal SST gradients resulted in an increase in mean global temperature of ~4°C. The reduced SST gradients led to a weakening, expansion, and Northward displacement of Hadley Circulation cells, increased atmospheric water vapor, an increase in subtropical 'high' greenhouse clouds, and a decrease in low reflective clouds [*Brierley and Fedorov*, 2010; *Brierley et al.*, 2009]. Under these conditions the reduced meridional SST gradient and zonal uniformity of mid-latitude SSTs promoted subduction of warm water into the thermocline and caused a feedback loop in which the thermocline deepened and upwelled water was relatively warm. Due to a deep thermocline, warm upwelling regions helped to maintain the reduced SST gradients and redistribution of clouds. As the basin-wide gradients strengthened, the models indicated that these warming feedbacks were reduced (e.g. the thermocline shoaled, upwelling regions cool, low reflective clouds develop over upwelling regions, Hadley and Walker circulation become stronger) and continental conditions suitable for Northern Hemisphere glaciation developed [*Brierley and Fedorov*, 2010].

An important note is that the thermocline of the tropical Pacific, a key player in this type of circulation-driven warming, was deeper in the late Miocene [*LaRiviere et al.*, 2012]. The relatively deep thermocline can explain some of the heterogeneity in SST changes that we observe in our synoptic study. In subtropical and tropical upwelling regions where thermocline depth and SSTs are now coupled, the water upwelled during the late Miocene and early Pliocene was substantially warmer than modern upwelled waters. Once the thermocline shoaled past some threshold depth,

upwelling processes delivered much cooler sub-thermocline waters to the surface [*Dekens et al.*, 2007]. Though there is still a lack of geochemical SST estimates from the central subtropical North and South Pacific, the interpolated time slice maps imply that the mid-latitude regions in the North Pacific that contribute to the subduction of warm thermocline waters have been cooling since the late Miocene (Figure 4). This trend in the spatial distribution of SSTs is consistent with the shoaling thermocline mechanism; however, SST reconstructions from the subtropical gyre are needed to fully test the accuracy of the interpolated SST estimates in these regions.

3.6 Conclusions

The synoptic reconstruction of late Neogene and Quaternary proxy-based SSTs highlights a heterogeneity of regional SST changes that comprises a long-term trend of strengthening basin-wide sea surface temperature gradients since the late Miocene. The climates of the late Miocene and early Pliocene were characterized by dramatic warmth, relative to modern, in EBC and tropical regions that now exhibit cool upwelling, moderate warming in mid-latitude non-EBC regions, and relatively small temperature changes in tropical non-upwelling regions. Time slice maps, gradient profiles, and time series comparisons exhibit reduced meridional and zonal SST gradients during the warm early Pliocene but even more relaxed gradients in the late Miocene. These basin-wide SST distributions may have been capable of maintaining warmth in the global climate without an increase in atmospheric pCO_2, as the SST distributions of the interpolated maps are consistent with a deep global

thermocline. By the ice age climates of the Pleistocene these SST gradients had strengthened and SST distributions more closely resembled modern configurations.

This type of data compilation highlights the spatial heterogeneity of proxy reconstructions of Neogene and Quaternary SSTs; the data clusters tightly in high sedimentation regions (e.g. high productivity upwelling regions) while low sedimentation rates throughout much of the open ocean make paleo reconstructions difficult. However, synoptic SST reconstructions and kriging, such as in this study, can help to elucidate the basin-wide SST patterns that may be critical to understanding past climates. As more SST reconstructions from Neogene and Quaternary intervals become available, future work should aim to use an advanced kriging approach similar to that of the MARGO project. Such improvements would include kriging ocean basins separately to reflect the different physical processes in each basin, masking land, and weighing available data according to proxy errors/reliability/quality [*Schafer-Neth et al.*, 2005].

References

Anand, P., H. Elderfield, and M. H. Conte (2003), Calibration of Mg/Ca thermometry in planktonic foraminifera from a sediment trap time series, *Paleoceanography*, *18*(2), 28-1 - 28-15.

Barker, S., I. Cacho, H. Benway, and K. Tachikawa (2005), Planktonic foraminiferal Mg/Ca as a proxy for past oceanic temperatures: a methodological overview and data compilation for the Last Glacial Maximum, *Quaternary Science Reviews*, *24*(7-9), 821-834.

Brierley, C. M., and A. V. Fedorov (2010), Relative importance of meridional and zonal sea surface temperature gradients for the onset of the ice ages and Pliocene-Pleistocene climate evolution, *Paleoceanography*, *25*, 16.

Brierley, C. M., A. V. Fedorov, Z. H. Liu, T. D. Herbert, K. T. Lawrence, and J. P. LaRiviere (2009), Greatly expanded tropical warm pool and weakened Hadley circulation in the early Pliocene, *Science*, *323*(5922), 1714-1718.

Carton, J. A., and B. S. Giese (2008), A reanalysis of ocean climate using Simple Ocean Data Assimilation (SODA), *Monthly Weather Review*, *136*(8), 2999-3017.

Chiang, J. C. H. (2009), The Tropics in Paleoclimate, *Annual Review of Earth and Planetary Sciences*, 37, 263-297.

Clement, A. C. (2006), The role of the ocean in the seasonal cycle of the Hadley circulation, *Journal of the Atmospheric Sciences*, *63*(12), 3351-3365.

de Garidel-Thoron, T., Y. Rosenthal, F. Bassinot, and L. Beaufort (2005), Stable sea surface temperatures in the western Pacific warm pool over the past 1.75 million years, *Nature*, *433*(7023), 294-298.

Dekens, P. S., and A. C. Ravelo (*in prep*), Sea surface temperatures from Site 758.

Dekens, P. S., A. C. Ravelo, and M. McCarthy (2007), Warm upwelling regions in the Pliocene warm period, *Paleoceanography*, 22(3),12.

Dekens, P. S., D. W. Lea, D. K. Pak, and H. J. Spero (2002), Core top calibration of Mg/Ca in tropical foraminifera: Refining paleotemperature estimation, *Geochemistry Geophysics Geosystems*, *3*(4), 29.

Dekens, P. S., A. C. Ravelo, M. D. McCarthy, and C. A. Edwards (2008), A 5 million year comparison of Mg/Ca and alkenone paleothermometers, *Geochemistry Geophysics Geosystems*, *9*(10),18.

Etourneau, J., P. Martinez, T. Blanz, and R. Schneider (2009), Pliocene-Pleistocene variability of upwelling activity, productivity, and nutrient cycling in the Benguela region, *Geology*, *37*(10), 871-874.

Etourneau, J., R. Schneider, T. Blanz, and P. Martinez (2010), Intensification of the Walker and Hadley atmospheric circulations during the Pliocene-Pleistocene climate transition, *Earth and Planetary Science Letters*, *297*(1-2), 103-110.

Evans, H. F., J. E. T. Channell, and W. W. Sager (2005), Late Miocene-Holocene magnetic polarity stratigraphy and astrochronology, ODP Leg 198, Shatsky Rise, *Proceedings of the Ocean Drilling Program, Scientific Results*, *198*, 39.

Expedition 18 Scientists (1973), Site 173, *Initial Reports of the Deep Sea Drilling Program,* XVII, 31-96.

Expedition 323 Scientsits (2011), Site U1340, *Proceedings of the Integrated Ocean Drilling Program*, 323, 1-81.

Ford, H. L., A. C. Ravelo, and S. Hovan (2012), A deep Eastern Equatorial Pacific thermocline during the early Pliocene warm period, *Earth and Planetary Science Letters*, *355-356*, 152-161.

Goyet, C., R. J. Healy, and J. P. Ryan (2000), Global distribution of total inorganic carbon and total alkalinity below the deepest winter mixed layer depths, edited by O. R. N. L. Carbon Dioxide Information Analysis Center, U.S. Department of Energy, Oak Ridge, Tennessee, 40.

Groeneveld, J. (2005), Effect of the Pliocene closure of the Panamanian Gateway on Caribbean and East Pacific sea surface temperatures and salinities by applying combined Mg/Ca and $\delta^{18}O$ measurements (5.6–2.2 Ma), PhD thesis, University of Kiel, Kiel, Germany.

Groeneveld, J., S. Steph, R. Tiedemann, D. Garbe-Schonberg, D. Nurnberg, and A. Sturm (2006), Pliocene mixed-layer oceanogrpahy for Site 1241 using combined Mg/Ca and $\delta^{18}O$ analyses of *Globigerinoides sacculifer*, *Proceedings of the Ocean Drilling Program Scientific Results*, *202,* 27.

Harada, N., K. H. Shin, A. Murata, M. Uchida, and T. Nakatani (2003), Characteristics of alkenones synthesized by a bloom of Emiliania huxleyi in the Bering Sea, *Geochimica Et Cosmochimica Acta*, *67*(8), 1507-1519.

Haug, G. (1995), Zur Paläo-Ozeanographie und Sedimentationsgeschichte im Nordwest-Pazifik während der letzten 6 Millionen Jahre (ODP-Site 882), PhD thesis, Institute for Geosciences, Christian Albrechts University, Kiel, Germany.

Haug, G. H., et al. (2005), North Pacific seasonality and the glaciation of North America 2.7 million years ago, *Nature*, *433*(7028), 821-825.

Heinrichs, D.F. (1973), Paleomagnetic studies of sediments from DSDP Site 173, *Initial Reports of the Deep Sea Drilling Program*, XVII, 843-846.

Herbert, T. D., and J. D. Schuffert (1998), Alkenone unsaturation estimates of late Miocene through late Pliocene sea-surface temperatures at Site 958, *Proceedings of the Ocean Drilling Program, Scientific Results*, *159T,* 17-21.

Herbert, T. D., L. C. Peterson, K. T. Lawrence, and Z. H. Liu (2010), Tropical Ocean Temperatures Over the Past 3.5 Million Years, *Science*, *328*(5985), 1530-1534.

Hills, S. J., and H. R. Thierstein (1989), Plio-pleistocene calcareous plankton biochronology, *Marine Micropaleontology*, *14*(1-3), 67-96.

Huang, Y., S. C. Clemens, W. Liu, Y. Wang, and W. L. Prell (2007), Large-scale hydrological change drove the late Miocene C4 plant expansion in the Himalayan foreland and Arabian Peninsula, *Geology*, *35*(6), 531-534.

Jia, G., F. Chen, and P. A. Peng (2008), Sea surface temperature differences between the western equatorial Pacific and northern South China Sea since the Pliocene and their paleoclimatic implications, *Geophys. Res. Lett.*, *35*, 1-5.

Karas, C., D. Nürnberg, R. Tiedemann, and D. Garbe-Schonberg (2011a), Pliocene Indonesian Throughflow and Leeuwin Current dynamics: Implications for Indian Ocean polar heat flux, *Paleoceanography*, *26*, 1-9.

Karas, C., D. Nürnberg, R. Tiedemann, and D. Garbe-Schonberg (2011b), Pliocene climate change of the Southwest Pacific and the impact of ocean gateways, *Earth and Planetary Science Letters*, *301*(1-2), 117-124.

Karas, C., D. Nürnberg, A. K. Gupta, R. Tiedemann, K. Mohan, and T. Bickert (2009), Mid-Pliocene climate change amplified by a switch in Indonesian subsurface throughflow, *Nature Geoscience*, *2*(6), 433-437.

Key, R. M., A. Kozyr, C. L. Sabine, K. Lee, R. Wanninkhof, J. L. Bullister, R. A. Feely, F. J. Millero, C. Mordy, and T. H. Peng (2004), A global ocean carbon climatology: Results from Global Data Analysis Project (GLODAP), *Global Biogeochemical Cycles*, *18*(4), 1-23.

Krivoruchko, K. (2011), *Spatial Statistical Data Analysis for GIS Users*, Esri Press, Redlands, California, 928.

LaRiviere, J. P., A. C. Ravelo, A. Crimmins, P. S. Dekens, H. L. Ford, M. Lyle, and M. W. Wara (2012), Late Miocene decoupling of oceanic warmth and atmospheric carbon dioxide forcing, *Nature*, *486*(7401), 97-100.

Lawrence, K. T., and T. D. Herbert (2005), Late quaternary sea-surface temperatures in the western Coral Sea: Implications for the growth of the Australian Great Barrier Reef, *Geology*, *33*(8), 677-680.

Lawrence, K. T., Z. H. Liu, and T. D. Herbert (2006), Evolution of the eastern tropical Pacific through Plio-Pleistocene glaciation, *Science*, *312*(5770), 79-83.

Lawrence, K. T., T. D. Herbert, P. S. Dekens, and A. C. Ravelo (2007), The application of the alkenone organic proxy to the study of Plio-Pleistocene climate, in *Deep-Time Perspectives on Climate Change: Marrying the Signal from Computer Models and Biological Proxies*, edited by M. Williams, A. M. Haywood, F. J. Gregory and D. N. Schmidt, pp. 539-562, The Geological Society, London.

Lawrence, K. T., S. Sosdian, H. E. White, and Y. Rosenthal (2010), North Atlantic climate evolution through the Plio-Pleistocene climate transitions, *Earth and Planetary Science Letters*, *300*(3-4), 329-342.

Lawrence, K. T., T. Herbert, C. Brown, M. Raymo, and A. Haywood (2009), High-amplitude variations in North Atlantic sea surface temperature during the early Pliocene warm period, *Paleoceanography*, *24*, 1-15.

Lear, C. H., Y. Rosenthal, and J. D. Wright (2003), The closing of a seaway: ocean water masses and global climate change, *Earth and Planetary Science Letters*, *210*(3-4), 425-436.

Li, L., Q. Y. Li, J. Tian, P. X. Wang, H. Wang, and Z. H. Liu (2011), A 4-Ma record of thermal evolution in the tropical western Pacific and its implications on climate change, *Earth and Planetary Science Letters*, *309*(1-2), 10-20.

Locarnini, R. A., A. V. Mishonov, J. I. Antonov, T. P. Boyer, H. E. Garcia, O. K. Baranova, M. M. Zweng, and D. R. Johnson (2010), World Ocean Atlas 2009 Volume 1: Temperature, edited by S. Levitus, *NOAA Atlas NESDIS 68*, U.S. Government Printing Office, Washington, D.C.

Lyle, M., I. Koizumi, M. L. Delaney, and J. A. Barron (2000), Sedimentary record of the California Current system, middle Miocene to Holocene: A synthesis of Leg 167 results, *Proceedings of the Ocean Drilling Program, Scientific Results*, 167, 341-376.

Marlow, J. R., C. B. Lange, G. Wefer, and A. Rosell-Melé (2000), Upwelling intensification as part of the Pliocene-Pleistocene climate transition, *Science*, *290*(5500), 2288-2291.

Martínez-Garcia, A., A. Rosell-Melé, E. L. McClymont, R. Gersonde, and G. H. Haug (2010), Subpolar Link to the Emergence of the Modern Equatorial Pacific Cold Tongue, *Science*, *328*(5985), 1550-1553.

Mashiotta, T. A., D. W. Lea, and H. J. Spero (1999), Glacial-interglacial changes in Subantarctic sea surface temperature and δ^{18}O-water using foraminiferal Mg, *Earth and Planetary Science Letters*, *170*(4), 417-432.

McClymont, E. L., and A. Rosell-Melé (2005), Links between the onset of modern Walker circulation and the mid-Pleistocene climate transition, *Geology*, *33*(5), 389-392.

McClymont, E. L., A. Rosell-Melé, J. Giraudeau, C. Pierre, and J. M. Lloyd (2005), Alkenone and coccolith records of the mid-Pleistocene in the south-east Atlantic: Implications for the $U^{k'}_{37}$ index and South African climate, *Quaternary Science Reviews*, *24*(14-15), 1559-1572.

Müller, P. J., G. Kirst, G. Ruhland, I. von Storch, and A. Rosell-Melé (1998), Calibration of the alkenone paleotemperature index $U^{k'}_{37}$ based on core-tops from the eastern South Atlantic and the global ocean (60°N-60°S), *Geochimica et Cosmochimica Acta*, *62*(10), 1757-1772.

Naafs, B. D. A., R. Stein, J. Hefter, N. Khelifi, S. De Schepper, and G. H. Haug (2010), Late Pliocene changes in the North Atlantic Current, *Earth and Planetary Science Letters*, *298*(3-4), 434-442.

Nathan, S. A., and R. M. Leckie (2009), Early history of the Western Pacific Warm Pool during the middle to late Miocene (~13.2-5.8 Ma): Role of sea-level change and implications for equatorial circulation, *Palaeogeography Palaeoclimatology Palaeoecology*, *274*(3-4), 140-159.

Nürnberg, D., and J. Groeneveld (2006), Pleistocene variability of the Subtropical Convergence at East Tasman Plateau: Evidence from planktonic foraminiferal Mg/Ca (ODP Site 1172A), *Geochemistry Geophysics Geosystems*, *7*(4), 1-18.

Pagani, M., Z. H. Liu, J. LaRiviere, and A. C. Ravelo (2010), High Earth-system climate sensitivity determined from Pliocene carbon dioxide concentrations, *Nature Geoscience*, *3*(1), 27-30.

Pound, M. J., A. M. Haywood, U. Salzmann, J. B. Riding, D. J. Lunt, and S. J. Hunter (2011), A Tortonian (Late Miocene, 11.61-7.25 Ma) global vegetation reconstruction, *Palaeogeography, Palaeoclimatology, Palaeoecology*, *300*, 29-45.

Prahl, F. G., and S. G. Wakeham (1987), Calibration of unsaturation patterns in long-chain ketone compositions for paleotemperature assessment, *Nature*, *330*(6146), 367-369.

Prahl, F. G., L. A. Muehlhausen, and D. L. Zahnle (1988), Further evaluation of long-chain alkenones as indicators of paleoceanographic conditions, *Geochimica Et Cosmochimica Acta*, *52*(9), 2303-2310.

Rack, F. R., T. R. Janecek, E. Erba, J. Fenner, and J. S. Gee (1995), Synthesis of terrigenous accumulation rates and biostratigraphic studies at sites in the northwestern Pacific Ocean, with comparisons to adjacent regions of the Pacific Gyre, *Proceedings of the Ocean Drilling Program. Scientific results*, *144*, 691-736.

Rackebrandt, N., H. Kuhnert, J. Groeneveld, and T. Bickert (2011), Persisting maximum Agulhas leakage during MIS 14 indicated by massive Ethmodiscus oozes in the subtropical South Atlantic, *Paleoceanography*, *26*, 1-13.

Regenberg, M., D. Nurnberg, S. Steph, J. Groeneveld, D. Garbe-Schonberg, R. Tiedemann, and W. C. Dullo (2006), Assessing the effect of dissolution on planktonic foraminiferal Mg/Ca ratios: Evidence from Caribbean core tops, *Geochemistry Geophysics Geosystems*, *7*(7), 1-23.

Rincón-Martinez, D., F. Lamy, S. Contreras, G. Leduc, E. Bard, C. Saukel, T. Blanz, A. Mackensen, and R. Tiedemann (2010), More humid interglacials in Ecuador during the past 500 kyr linked to latitudinal shifts of the equatorial front and the Intertropical Convergence Zone in the eastern tropical Pacific, *Paleoceanography*, *25*, 1-15.

Rodrigues, T., A. H. L. Voelker, J. O. Grimalt, F. Abrantes, and F. Naughton (2011), Iberian Margin sea surface temperature during MIS 15 to 9 (580-300 ka): Glacial suborbital variability versus interglacial stability, *Paleoceanography*, *26*, 1-16.

Rommerskirchen, F., T. Condon, G. Mollenhauer, L. Dupont, and E. Schefuss (2011), Miocene to Pliocene development of surface and subsurface temperatures in the Benguela Current system, *Paleoceanography*, *26*, 1-15.

Rosenthal, Y., and G. P. Lohmann (2002), Accurate estimation of sea surface temperatures using dissolution-corrected calibrations for Mg/Ca paleothermometry, *Paleoceanography*, *17*(3), 16-1-16-6.

Rousselle, G., C. Beltran, M.-A. Sicre, I. Raffi, and M. De Rafelis (2013), Changes in sea-surface conditions in the Equatorial Pacific during the middle Miocene-Pliocene as inferred from coccolith geochemistry, *Earth and Planetary Science Letters*, *361*, 412-421.

Russon, T., M. Elliot, A. Sadekov, G. Cabioch, T. Correge, and P. De Deckker (2010), Inter-hemispheric asymmetry in the early Pleistocene Pacific warm pool, *Geophysical Research Letters*, *37*, 1-5.

Schafer-Neth, C., A. Paul, and S. Mulitza (2005), Perspectives on mapping the MARGO reconstructions by variogram analysis/kriging and objective analysis, *Quaternary Science Reviews*, *24*(7-9), 1083-1093.

Schefuss, E., J. S. S. Damste, and J. H. F. Jansen (2004), Forcing of tropical Atlantic sea surface temperatures during the mid-Pleistocene transition, *Paleoceanography*, *19*(4), 1-12.

Schlitzer, R. (2012), Ocean Data View, http://odv.awi.de.

Steinke, S., J. Groeneveld, H. Johnstone, and R. Rendle-Buhring (2010), East Asian summer monsoon weakening after 7.5 Ma: Evidence from combined planktonic foraminifera Mg/Ca and $\delta^{18}O$ (ODP Site 1146; northern South China Sea), *Palaeogeography Palaeoclimatology Palaeoecology*, *289*(1-4), 33-43.

Wara, M. W., A. C. Ravelo, and M. L. Delaney (2005), Permanent El Nino-like conditions during the Pliocene warm period, *Science*, *309*(5735), 758-761.

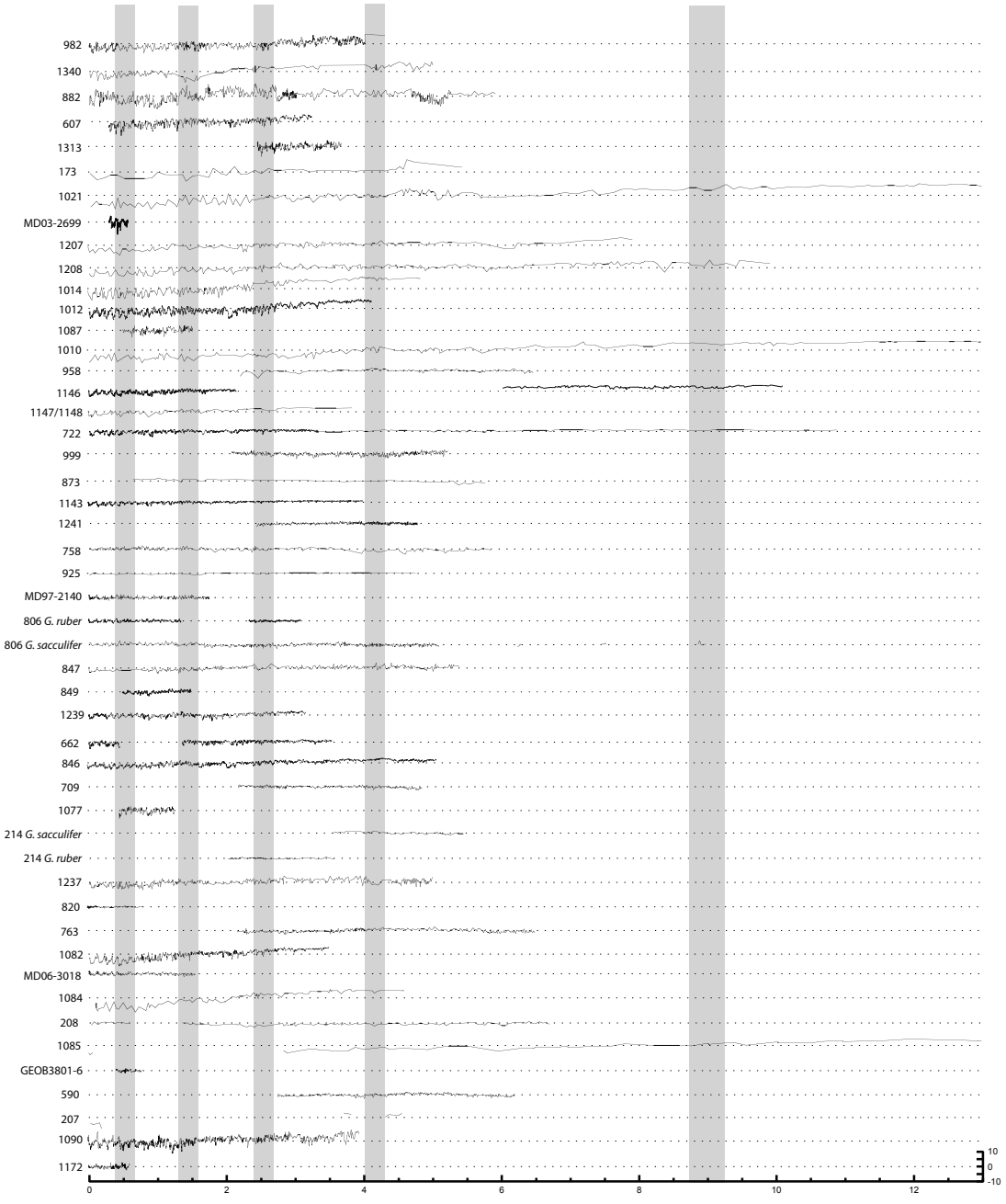

Figure 1. Compilation of all geochemical temperature records used in this study. Data is the difference from the mean SST of each record. Grey shading denotes time slices that correspond to the maps in figure 2-4. Details of original data references can be found in Table 1. Time series are ordered according to site latitude.

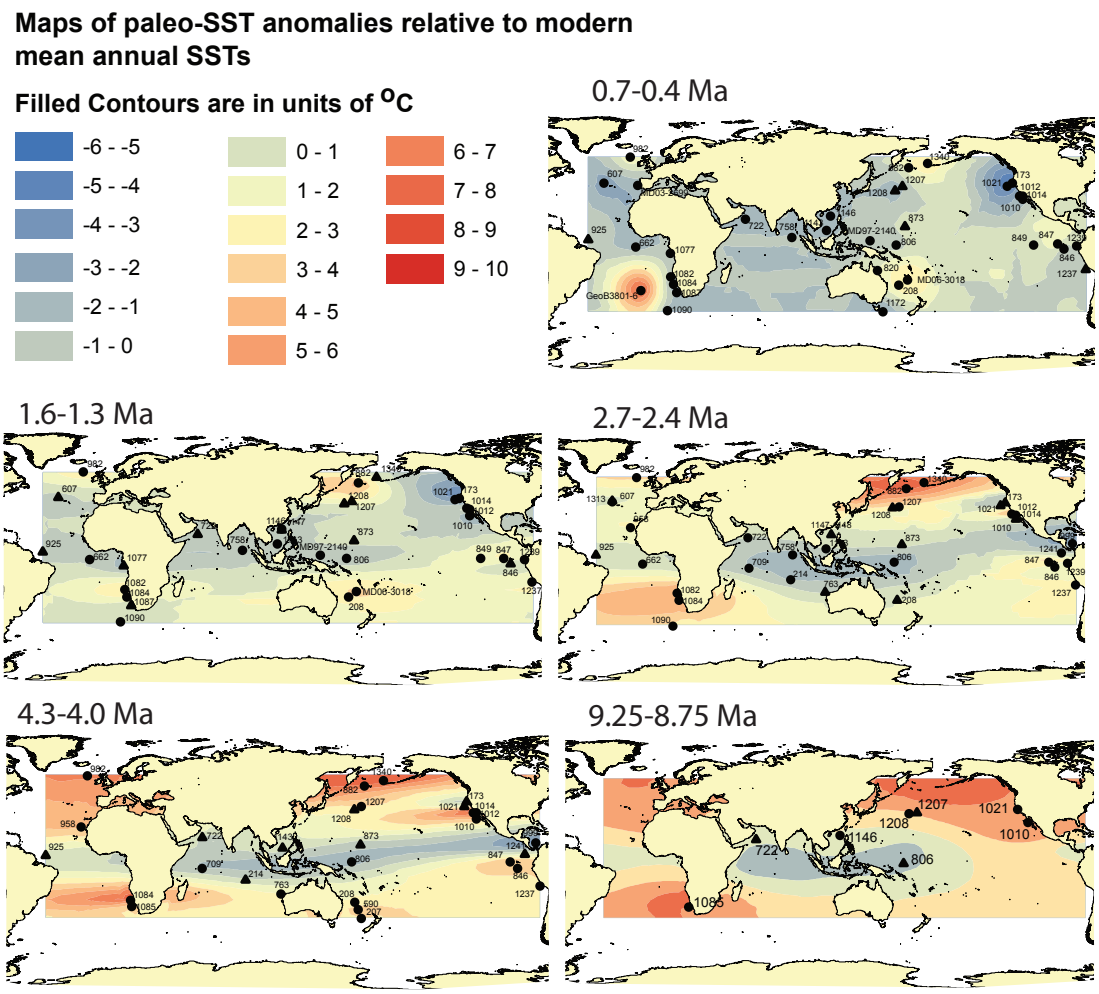

Figure 2. Maps of paleo sea surface temperature anomalies relative to modern mean annual SSTs. Site locations are denoted with circles and triangles. Circles denote sites where the median SST of the time slice is significantly different from the median SST of the monthly SSTs 1950-2007 [Carton and Geise, 2008]. Triangles denote sites where the median SST of the time slice is not significantly different from the median of the monthly SSTs 1950-2007.

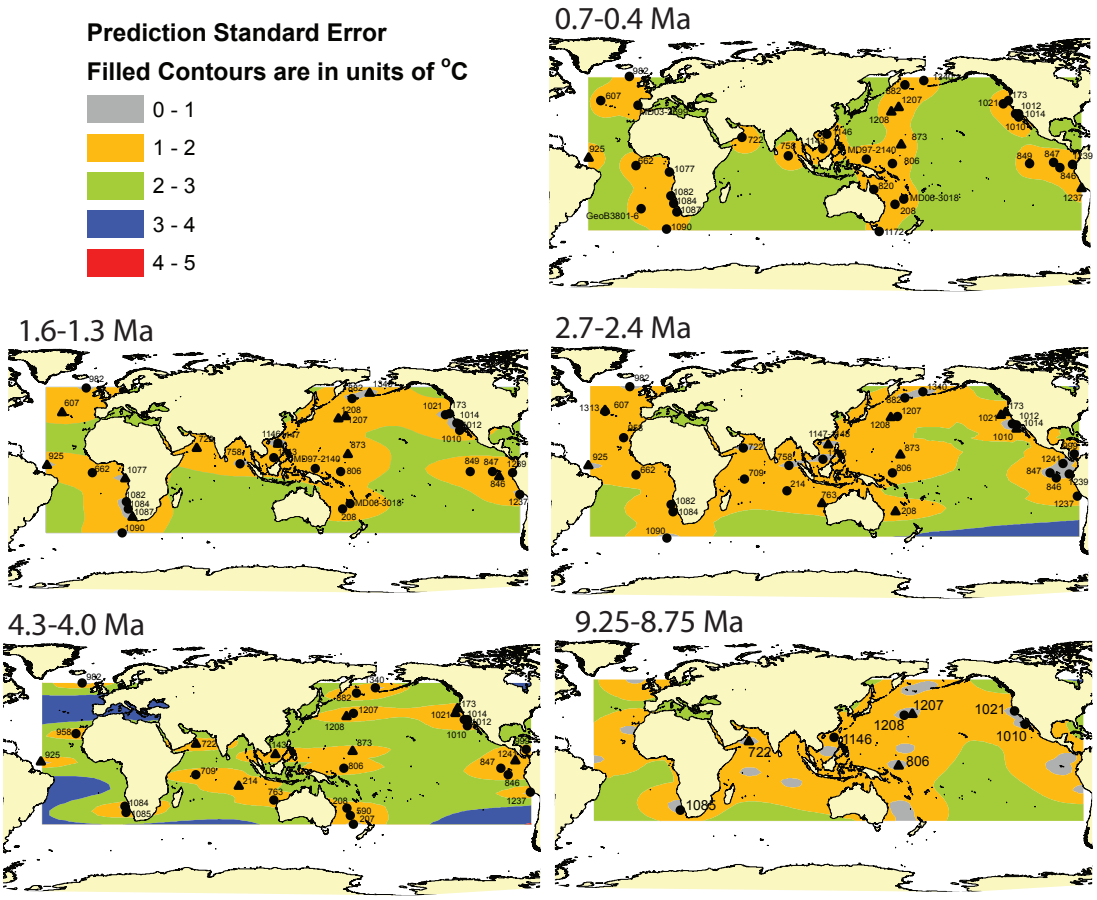

Figure 3. Prediction standard error maps for each interpolated SST anomaly map in figure 2. Site locations are denoted with circles and triangles. Circles denote sites where the median SST of the time slice is significantly different from the median SST of the monthly SSTs 1950-2007 [Carton and Geise, 2008]. Triangles denote sites where the median SST of the time slice is not significantly different from the median of the monthly SSTs 1950-2007. Gray shading that is not proximal to a site marker in the 9.25-8.75 Ma map denotes locations of early Pliocene sites used to aid in mapping (Table 2).

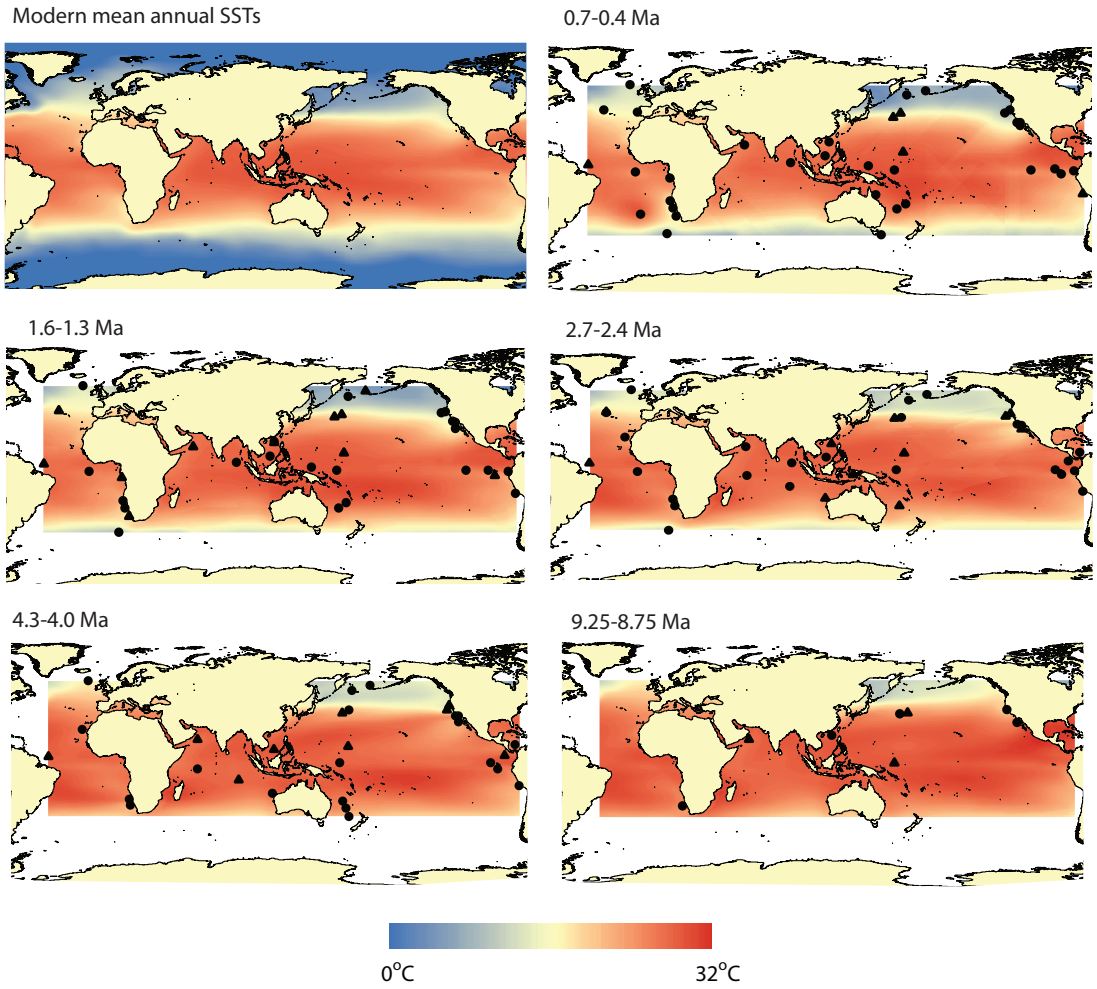

Figure 4. Time slice snapshots of basin-wide sea surface temperatures. Site locations are denoted with circles and triangles. Circles denote sites where the median SST of the time slice is significantly different from the median SST of the monthly SSTs 1950-2007 [Carton and Geise, 2008]. Triangles denote sites where the median SST of the time slice is not significantly different from the median of the monthly SSTs 1950-2007.

Figure 5. Development of large-scale SST gradients in the North Pacific. a. West Pacific meridional gradient. Alkenone based SST estimates from Shatsky Rise sites 1208 (purple)[*LaRiviere et al.*, 2012] and 1207 (gray) compared to Mg/Ca based SSTs from western tropical Pacific site 806 (brown)[*Wara et al.*, 2005; *Nathan and Leckie*, 2009]. b. Mid-latitude zonal gradient. Alkenone based SST estimates from Shatsky Rise sites 1208 (purple) and 1207 (gray) compared to northern California Current sites 1021 (light blue)[*LaRiviere et al.*, 2012] and 173 (dark blue). c. Zonal gradients of the tropical Pacific and comparison to eastern subtropical Pacific SSTs. Mg/Ca based SST estimates from site 806 (brown) compared to alkenone based SST estimates from EEP sites 846 (black)[*Lawrence et al.*, 2006] and 1338 (mustard)[*Rousselle et al.*, 2013], and southern California Current site 1010 (green)[*LaRiviere et al.*, 2012]. Heavy lines denote Stineman smoothing curves applied in KaleidaGraph software. Map shows mean annual SSTs [*Locarnini et al.*, 2010], site locations (white dots), and regional focus of each time series panel (letters).

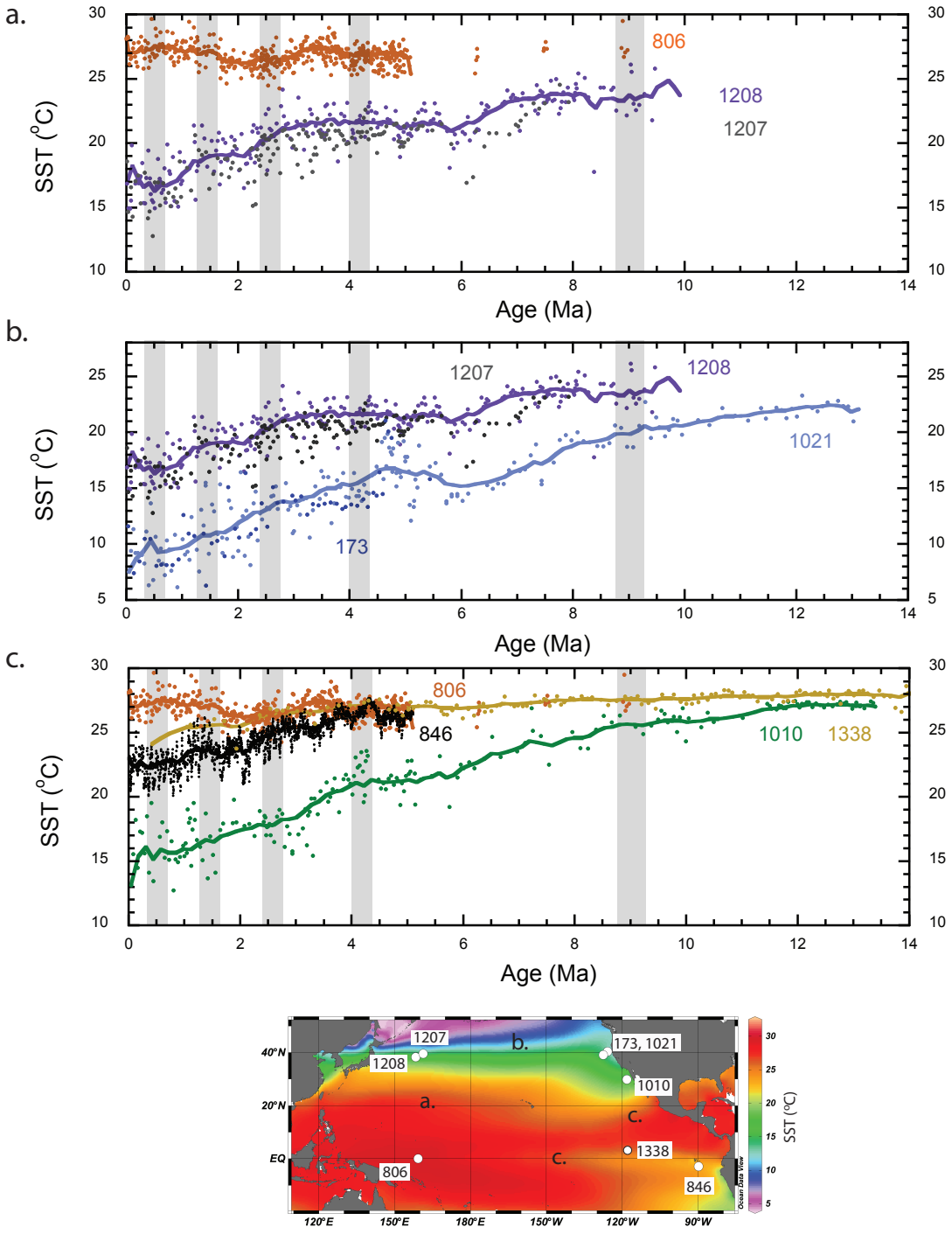
a.
SST (°C)
Age (Ma)
806
1208
1207
b.
SST (°C)
Age (Ma)
1207
1208
1021
173
c.
SST (°C)
Age (Ma)
806
846
1010
1338
1207
1208
b.
173, 1021
1010
a.
c.
1338
c.
806
846
40°N
20°N
EQ
120°E
150°E
180°E
150°W
120°W
90°W
SST (°C)

Figure 5.

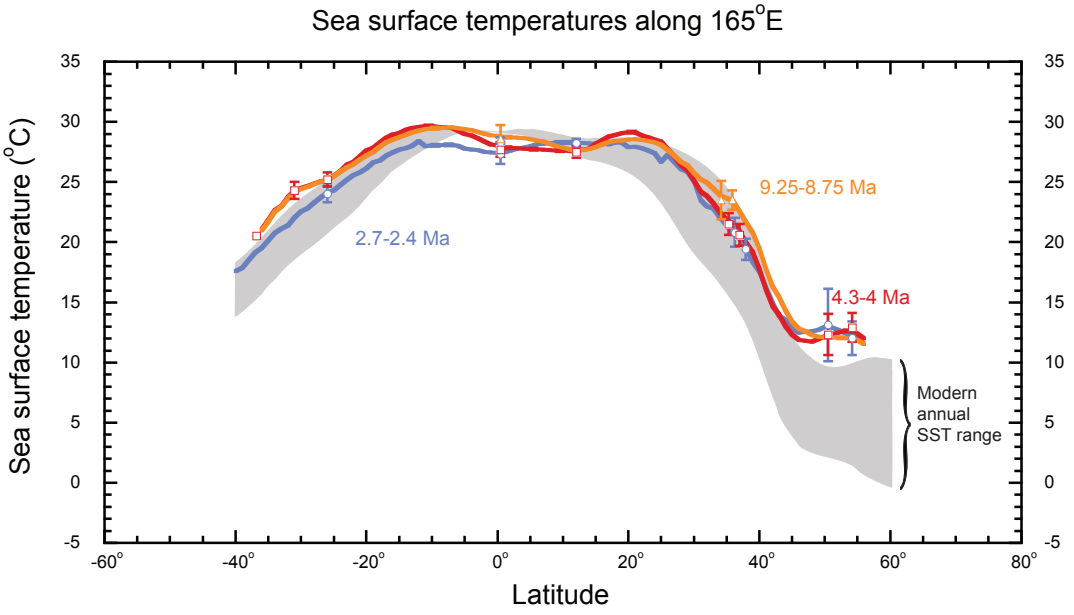

Figure 6. West Pacific meridional SST gradient of late Miocene, early Pliocene, and Plio-Pleistocene time slices. Curves denote the interpolated SST surface along 165°E in time slice maps of Figure 4. Symbols show mean SSTs from nearby sites in a N-S transect of the west Pacific. Error bars denote the standard deviation of SSTs in each time slice. Late Miocene (orange curve, triangles), early Pliocene (red curve, squares), and Plio-Pleistocene (blue curve, circles) values are overlaid on the modern annual SST range (gray shading) along 165°E. Annual SST range from the World Ocean Atlas [*Locarnini et al.,* 2010].

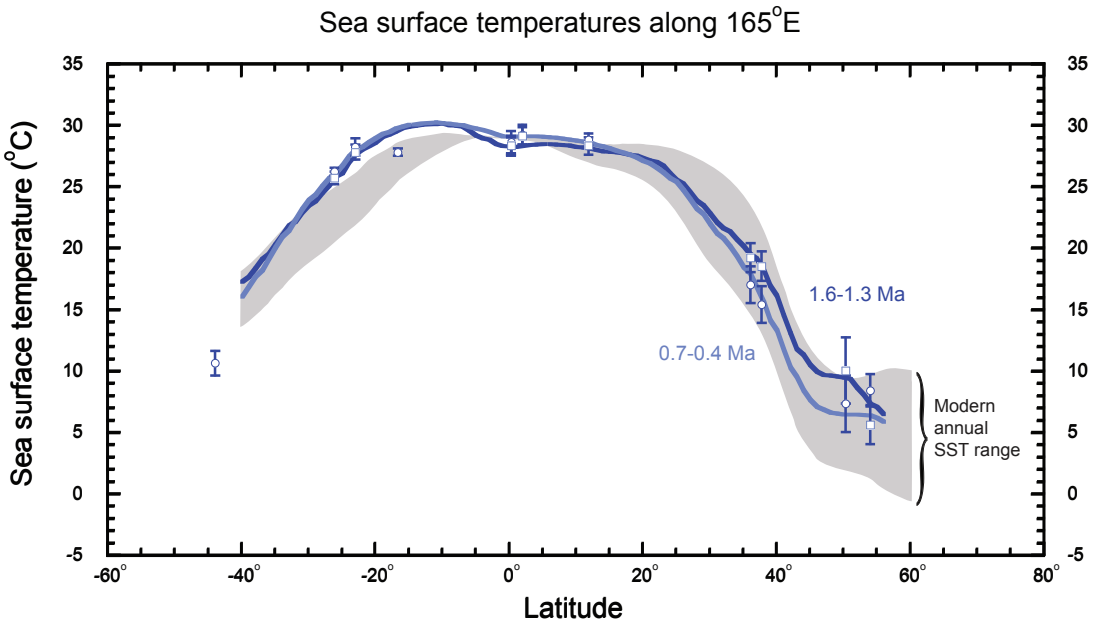

Figure 7. West Pacific meridional SST gradient of Pleistocene time slices. Curves denote the interpolated SST surface along 165°E in time slice maps of Figure 4. Symbols show mean SSTs from nearby sites in a N-S transect of the west Pacific. Error bars denote the standard deviation of SSTs in each time slice. 1.6-1.3Ma values (dark blue curve, squares) and 0.7-0.4Ma values (light blue curve, circles) are over-laid on the modern annual SST range (gray shading) along 165°E. Annual SST range from the World Ocean Atlas [*Locarnini et al.,* 2010].

Table 1. Site information

Site	Available data (Ma)	Geographic Region	Latitude	Longitude	Water Depth (m)	Proxy	Species	ΔCO_3^{2-} (µmol/kg)	Reference
173	0.72-0.42 1.62-1.38 2.71-2.42 4.32-4.03	Northern California Margin	40.0	-125.5	2927	alkenones			*this study*
207	4.33	Tasman Sea	-37.0	165.4	1389	alkenones			*this study*
208	0.57-0.36 1.63-1.35 2.53-2.39 4.34-3.96	Coral Sea	-26.1	161.2	1545	Mg/Ca	*G. sacculifer*	24.032	*this study*
214	2.74-2.36 4.34-3.96	Tropical east Indian Ocean	-11.3	88.7	1665	Mg/Ca	*G. sacculifer* *G. ruber*[a]	18.9	[*Karas et al., 2009*]
590	4.34-3.95	Tasman Sea	-31.2	163.4	1308	Mg/Ca	*G. sacculifer*	30.865	[*Karas et al.,* 2011b]
607	0.74-0.35 1.64-1.25 2.74-2.35	North Atlantic	41.0	-33.0	3427	alkenones			[*Lawrence et al.,* 2010]
662	0.46-0.35 1.64-1.37 2.74-2.35	Tropical Atlantic	-1.4	-11.7	3814	alkenones			[*Herbert et al.,* 2010]
709	2.74-2.37 4.34-3.95	Indian Ocean	-3.9	60.6	3041	Mg/Ca	*G. sacculifer*	7.055	[*Karas et al.,* 2011a]
722	0.74-0.35 1.64-1.25 2.74-2.35 4.3-3.96 9.21-8.92	Arabian Sea	16.6	59.8	2022	alkenones			[*Herbert et al.,* 2010][*Huang et al.,* 2007]
758	0.74-0.35 1.63-1.26 2.74-2.36 4.2-3.96	Indian Ocean	5.4	90.4	2926	Mg/Ca	*G. sacculifer*	7.406	[*Dekens et al.,* in prep]
763	2.74-2.36 4.33-3.95	Indian Ocean	-20.6	112.2	1367	Mg/Ca	*G. sacculifer*	20.375	[*Karas et al.*, 2011a]
806	0.73-0.36 1.63-1.25 2.73-2.35 4.34-3.95 8.98-8.86	Western equatorial Pacific	0.3	159.4	2520	Mg/Ca	*G. sacculifer, G. ruber*	5.692	[*Wara et al.*, 2005] [*Nathan and Leckie,* 2009]
820	0.73-0.36	Coral Sea	-16.6	146.3	278	alkenones			[*Lawrence and Herbert,* 2005]
846	0.74-0.35 1.64-1.25 2.74-2.35 4.34-3.95	East equatorial Pacific	-3.1	-90.8	3296	alkenones			[*Lawrence et al.,* 2006]
847	0.62-0.35 1.63-1.25 2.73-2.38 4.33-3.98	East equatorial Pacific	0.2	-95.3	3334	Mg/Ca	*G. sacculifer*	-6.345	[*Wara et al.,* 2005]
849	1.5-0.5	Tropical Pacific	0.2	-110.5	3837	alkenones			[*McClymont and Roselle-Melé*, 2005]
873	1.64-1.26 2.87, 2.18 4.42, 3.74	Tropical Pacific	11.9	164.9	1335	Mg/Ca	*G. sacculifer*	8.272	*this study*
882	0.74-0.35 1.64-1.26 2.74-2.37 4.34-3.96	Subarctic North Pacific	50.4	167.6	3255	alkenones			[*Haug*, 1995]
925	0.58-0.43 1.64-1.25 2.72-2.4 4.11- 3.99	Tropical Atlantic	4.2	-43.5	3042	alkenones			[*Pagani et al.*, 2010]
958	2.71-2.37 4.32-3.96	North west Africa	24.0	-20.0	3728	alkenones			[*Herbert and Schuffert*, 1998]
982	0.74-0.35 1.64-1.25 2.74-2.36 4.3-3.95	North Atlantic	57.5	-15.9	1334	alkenones			[*Lawrence et al.*, 2009] [*Pagani et al.*, 2010]
999	2.74-2.35 4.34-3.95	Caribbean	12.7	-78.7	2828	Mg/Ca	*G. sacculifer*	22.42	[*Groeneveld*, 2005]
1010	0.72-0.36 1.64-1.28 2.7-2.35 4.28-3.97	Southern California Margin	30.0	-118.1	3466	alkenones			[*LaRiviere et al.*, 2012]

1012	0.74-0.35 1.64-1.25 2.74-2.35 4.11-3.95 9.23-8.8	Southern California Margin	32.3	-118.4	1773	alkenones			[*Brierley et al.*, 2009]
1014	0.74-0.35 1.64-1.25 2.73-2.35 4.29-3.95	Southern California Margin	32.8	-120.0	1165	alkenones			[*Dekens et al.*, 2007]
1021	0.72-0.36 1.63-1.26 2.71-2.35 4.34-3.98 9.18-8.75	Northern California Margin	39.1	-127.8	4215	alkenones			[*LaRiviere et al.*, 2012]
1077	0.74-0.46 1.25-1.25	Angola Basin	-5.2	10.4	2381	alkenones			[*Schefuss et al.*, 2004]
1082	0.74-0.35 1.64-1.25 2.74-2.35	Eastern tropical South Atlantic	-21.1	11.8	1281	alkenones			[*Etourneau et al.*, 2009]
1084	0.73-0.37 1.63-1.31 2.71-2.35 4.25-4.13	Eastern subtropical South Atlantic	-25.5	13.0	1992	alkenones			[*Marlow et al.*, 2000]
1085	4.32-4.02 9.04-8.79	Eastern South Atlantic	-29.0	14.0	1713	alkenones			[*Rommerskirchen et al.*, 2011]
1087	0.74-0.5 1.52-1.25	Eastern South Atlantic	31.5	15.3	1374	alkenones			[*McClymont et al.*, 2005]
1090	0.74-0.35 1.64-1.25 2.71-2.35	South Atlantic	-42.9	8.9	3702	alkenones			[*Martinez-Garcia et al.,* 2010]
1143	0.74-0.35 1.64-1.25 2.74-2.35 4-3.95	South China Sea	9.4	113.3	2772	alkenones			[*Li et al.*, 2011]
1146	9.24-8.77	South China Sea	19.5	116.3	2091	alkenones, Mg/Ca	*G. sacculifer* *G. quadrilobatus*	-2.84	[*Herbert et al.*, 2010] [*Steinke et al.*, 2010]
1147-1148	0.74-0.4 1.64-1.28 2.74-2.42	South China Sea	18.8	116.6	3270	alkenones			[*Jia et al.*, 2008]
1172	0.61-0.35	East Tasman Plateau	-44.0	149.9	2622	Mg/Ca	*G. bulloides*	8.5	[*Nürnberg et al.*, 2006]
1207	0.7-0.38 1.63-1.29 2.71-2.37 4.34-3.97 7.92-7.49	North Pacific	37.8	162.8	3101	alkenones			*this study*
1208	0.73-0.36 1.63-1.26 2.73-2.36 4.34-3.95 9.19-8.77	North Pacific	36.1	158.2	3346	alkenones			[*LaRiviere et al.*, 2012]
1237	0.74-0.35 1.64-1.25 2.74-2.36 4.33-3.98	Eastern tropical South Pacific	-16.0	-76.4	3212	alkenones			[*Dekens et al.*, 2007]
1239	0.75-0.35 1.64-1.25 2.74-2.35	Eastern equatorial Pacific	-0.7	-82.1	1414	alkenones			[*Etourneau et al.*, 2010] [*Rincón-martinez et al.*, 2010]
1241	2.74-2.43 4.34-3.95	Eastern equatorial Pacific	5.8	-86.4	2027	Mg/Ca	*G. sacculifer*	2.381	[*Groeneveld et al.*, 2006] [*Dekens et al.*, 2008]
1313	2.74-2.46	North Atlantic	41.0	-33.0	3414	alkenones			[*Naafs et al.*, 2010]
1338[b]		Eastern equatorial Pacific	2.5	-118.0	4210	alkenones			[*Rousselle et al.,* 2013]
1340	0.74-0.35 1.61-1.34 2.74-2.37 4.33-4.02	Bering Sea	54.0	180.0	1295	alkenones			*this study*
MD03-2699	0.58-0.35	Iberian Slope	39.0	-10.7	1865	alkenones			[*Rodrigues et al.*, 2011]
MD06-3018	0.74-0.35 1.54-1.25	Western tropical Pacific	-23.0	166.1	2470	Mg/Ca	*G. ruber*	11.247	[*Russon et al.*, 2010]
MD97-2140	0.74-0.35 1.64-1.25	Western tropical Pacific	2.0	141.8	2547	Mg/Ca	*G. ruber*	7.9	[*de Garidel-Thoron et al.,* 2005]
GEOB3801-6	0.74-0.41	Central South Atlantic	-29.5	-8.3	4546	Mg/Ca	*G. ruber*	-8.81	[*Rackebrandt et al.*, 2011]

[a] *G. ruber* used over the 3.552-2.013Ma interval, *G. sacculife*r used over the 3.566-5.461Ma interval
[b] Data from *Rousselle et al.* [2013] is not included in the time slice maps.

Table 2. SST estimates for each time slice

Site	Modern mean annual SST (WOA09)[a] (°C)	Standard deviation of SODA SST 1958-2007 (°C)	proxy-based mean SST esimates				
			0.7-0.4Ma	1.6-1.3 Ma	2.7-2.4 Ma	4.3-4.0 Ma	9.25-8.75 Ma
173	13.8	1.8	8.7 ± 1.2, n=4	9.4 ± 2.1, n=4	13.5 ± 1.5, n=4	13.6 ± 0.3, n=4	
207	17.6	2				20.6, n=1	early plio. mean
208	23.1	1.8	26.2 ± 0.3, n=5	25.7 ± 0.5, n=8	24.1 ± 0.7, n=6	25.3 ± 0.6, n=11	early plio. mean
214	27.5	0.8			26.3 ± 0.3, n=19	27.4 ± 0.5, n=16	early plio. mean
590	21	1.9				24.4 ± 0.7, n=31	early plio. mean
607	17.9	2.8	15.1 ± 2.2, n=109	17.4 ± 1.8, n=105	18.3 ± 1.3, n=116		
662	26	1.7	24.3 ± 1.2, n=49	26 ± 0.8, n=111	26.3 ± 0.6, n=190		
709	28.4	0.8			27.4 ± 0.5, n=45	27.3 ± 0.7, n=45	early plio. mean
722	27	1.5	25.8 ± 0.9, n=203	26.6 ± 0.6, n=183	27 ± 0.6, n=204	26.9 ± 0.5, n=4	27.3 ± 0.3, n=4
758[b]	28.6	0.6	27.6 ± 0.7, n=43	27.7 ± 0.8, n=19	27.2 ± 0.9, n=22	25.8 ± 0.9, n=6	
763	25.3	1.7			25 ± 0.7, n=34	27.1 ± 0.5, n=32	early plio. mean
806 *G. sacculifer*	29.3	0.6	28.6 ± 0.9, n=23	28.3 ± 0.8, n=20	27.4 ± 0.8, n=48	27.8±0.6, n=50	28.7±1.1, n=5
806 *G. ruber*	29.3	0.6	28.3 ± 0.7, n=172		28.4 ± 0.4, n=219		
820	26.8	1.9	27.8 ± 0.3, n=30				
846	23.4	2.4	22.2 ± 0.9, n=159	23.6 ± 0.8, n=171	24.5 ± 0.8, n=199	26.7 ± 0.6, n=142	early plio. mean
847	24.4	2	26.3 ± 0.6, n=7	26.8 ± 0.9, n=23	28.1 ± 1.4, n=15	28.7 ± 1.2, n=15	early plio. mean
849	24.5	2.1	24.9±0.8, n=45	26±0.7, n=51			
873[c]	28	0.8	28.8±0.5, n=2	28.3 ± 0.7, n=7	28.3 ± 0.4, n=2	27.6 ± 0.5, n=2	early plio. mean
882	5.5	2.9	7.3 ± 2.3, n=61	10 ± 2.7, n=56	13.2 ± 3, n=52	12.4 ± 1.7, n=11	early plio. mean
925	27.5	0.4	27.3 ± 0.6, n=2	27.2 ± 0.5, n=5	27.7 ± 0.2, n=6	28 ± 0, n=2	early plio. mean
958	21.7	1.5			23.9 ± 1.8, n=7	26.3 ± 0.6, n=10	early plio. mean
982	10.7	1.5	12.8 ± 1.6, n=75	13.6 ± 1.5, n=142	14 ± 1.4, n=105	16.9 ± 1.9, n=34	early plio. mean
999	27.6	0.8			24.9 ± 1, n=66	24.1 ± 0.9, n=62	
1010[d]	17.7	1.7	16.2 ± 2.1, n=8	16 ± 1.7, n=8	17.9 ± 0.8, n=13	22 ± 1.3, n=13	26.4 ± 1.8, n=4
1012	16.7	1.9	15.9 ± 2, n=200	17.4 ± 1.5, n=200	18.9 ± 1.8, n=200	24 ± 0.5, n=85	
1014	16.3	1.9	15.2 ± 2, n=38	17.1 ± 1.6, n=28	21.9 ± 1.8, n=19	25.8 ± 0.6, n=25	
1021	14.5	2.1	9.3 ± 2.3, n=10	11.9 ± 2.6, n=10	13.2 ± 1.4, n=9	14.7 ± 0.7, n=10	19.8±1, n=5
1077	25.8	2.3	24.9 ± 1.7, n=73	24.3 ± 1.4, n=4			
1082	18.8	2	18 ± 1.8, n=70	22.2 ± 1.4, n=85	24.4 ± 1, n=114		
1084	17.9	1.7	15.2 ± 2.4, n=8	20 ± 1, n=7	23.3 ± 1, n=18	25.8 ± 0.9, n=4	early plio. mean
1085	17.9	1.9				21.3 ± 1.1, n=2	23.8 ± 0.7, n=4
1087	17.8	1.8	16.5 ± 1.4, n=35	17.9 ± 1.3, n=54			
1090	10.2	1.4	8.9 ± 1.7, n=182	10.4 ± 1.8, n=125	13.1 ± 1.4, n=105		
1143	28.3	1	27.1 ± 0.8, n=187	28 ± 0.5, n=171	28.4 ± 0.3, n=162	28.9 ± 0.1, n=12	early plio. mean
1146	26.7	2.2	24.7±1.1, n=286	26.2±0.7, n=231			28.5 ± 0.7, n=17
1147-1148	26.9	2.1	25.4 ± 1.1, n=16	26.5 ± 0.8, n=15	27.6 ± 0.6, n=4		
1172	13.1	1.7	10.6 ± 1, n=122				
1207[d,e]	16.5	3.9	15.4 ± 1.5, n=8	18.5 ± 1.2, n=6	19.5 ± 0.9, n=15	20.7 ± 0.9, n=12	23.6 ± 0.8, n=3
1208[d]	18.5	4.1	17 ± 1.5, n=16	19.2 ± 1.2, n=11	20.9 ± 1.2, n=12	21.6 ± 0.9, n=14	23.6 ± 1.6, n=7
1237	20	2.6	19.4 ± 1.4, n=54	21.9 ± 1, n=39	22.4 ± 1.1, n=33	22.1 ± 1.9, n=14	early plio. mean
1239	24.5	1.5	25.2 ± 0.9, n=105	25.6 ± 0.8, n=125	26.4 ± 0.7, n=89		
1241	27.4	1			27.1 ± 0.6, n=44	27.8 ± 0.5, n=141	early plio. mean
1313	17.9	2.7			18.9 ± 1.7, n=106		
1340	5.2	2.3	8.4 ± 1.3, n=29	5.6 ± 1.6, n=9	12.1 ± 1.4, n=18	13 ± 1.2, n=15	early plio. mean
MD03-2699	17.4	2.4	15.7 ± 1.7, n=722				
MD06-3018	24.3	1.6	28.2 ± 0.7, n=59	27.8 ± 0.6, n=42			
MD97-2140	29.2	0.5	29.2 ± 0.8, n=65	29.1 ± 0.7, n=66			
GEOB3801-6	20.6	2.3	28.7 ± 0.6, n=112				

[a] Modern mean annual SST of WOA09 was within 1°C of the mean of SODA 1958-2007 monthly SSTs at all sites

[b] Due to poor preservation and a likely dissolution bias we have omitted Site 758 4.3-4.0Ma SSTs from maps in figure 1

[c] 873 mean SST estimates for 2.7-2.4Ma from data at ~2.2 and ~2.9Ma. Mean SST estimates for 4.3-4Ma from data at ~3.7 and 4.4Ma.

[d] We used the modern SST at the 4 and 9Ma paleolocations to estimate anomalies for these sites

[e] 1207 mean SST estimates for 9.25-8.75Ma time slice from data 7.9-7.5Ma

Table3. Cross-validation errors

Anomaly map	Kriging Type	Kgriging Model	Cross-validation prediction errors					Number of samples
			Mean (°C)	Root-Mean-Square (°C)	Average Standard Error	Mean Standardized	Root-Mean-Square Standardized	
9.25-8.75 Ma time slice	Ordinary cokriging	Spherical	0.1675	2.069	1.819	0.06715	1.189	26
4.3-4.0 Ma time slice	Ordinary cokriging	Spherical	0.3938	1.943	2.467	0.1327	1.073	29
2.7-2.4 Ma time slice	Ordinary cokriging	Spherical	0.03073	1.404	1.817	0.02124	17.04	34
1.6-1.3 Ma time slice	Ordinary cokriging	Spherical	0.061	1.523	1.564	0.04398	1.114	33
0.7-0.4 Ma time slice	Ordinary cokriging	Spherical	-0.1314	2.168	1.935	-0.03946	1.046	37

Chapter 4. The utility of leaf-wax δD as proxy for precipitation in coastal western North America: a core-top transect and down-core pilot study

Abstract

A lack of well-dated, continuous records of precipitation has made it difficult to identify the mechanisms responsible for the development of the mediterranean climate in coastal western North America; however, there is an abundance of sedimentary core material from the California Margin that could be used to reconstruct the history of terrestrial climate in this region since the late Miocene. In this light, we used a transect of core-tops along the California Margin to test the utility of leaf-wax δD as a proxy for precipitation in coastal western North America. $\delta D_{n\text{-alkane}}$ values are offset from $\delta D_{precipitation}$ by ~90‰ from ~29-39°N. The *n*-alkanes ~29-36°N are reliable indicators of the $\delta D_{precipitation}$ in the southern coast region. However, *n*-alkanes ~37-39°N originate from an interior sediment source area and do not record the precipitation signal along the coast. The $\delta D_{n\text{-alkanes}}$ from core-tops ~39-42.5°N are offset from $\delta D_{precipitation}$ by ~70‰. This smaller isotopic offset may be the result of fog-harvesting by north coast vegetation; however, uncertainties in the north coast $\delta D_{precipitation}$, sediment sources, and vegetation source waters make interpretations of $\delta D_{n\text{-alkanes}}$ in this region difficult. A transect of early Pleistocene samples exhibits $\delta D_{n\text{-alkane}}$ values that are similar to the late Holocene *n*-alkanes and

indicates that sites from the southern California Margin are suitable for down-core studies.

Low-resolution $\delta D_{n\text{-alkane}}$ data from ODP Site 1010, offshore of Baja, shows an overall decrease of ~7‰ between the late Miocene and the late Pleistocene, with most of the decrease taking place after the early Pliocene. Because the modern winter precipitation in southern California generally originates from central and North Pacific air masses and is isotopically light compared to the summer precipitation that originates from the Gulf of Mexico, Gulf of California, and eastern tropical Pacific air masses, we believe that the isotopic values at Site 1010 reflect a transition from year-round precipitation during the late Miocene to an increasingly mediterranean climate in the late Pleistocene. This climate transition may have been related to strengthening of the North Pacific meridional sea surface temperature (SST) gradient and cooling of local SSTs after the early Pliocene, though a higher-resolution reconstruction of terrestrial climate in southern California is needed in order to test this idea.

4.1 Introduction

For at least the past 50 years, the accepted narrative of late Miocene and Pliocene climate in western North America described a gradual transition out of the wet/warm state of the middle Miocene to generally drier conditions by the Pleistocene [*Minnich*, 2007; *Raven and Axelrod*, 1978; *Retallack et al.*, 2002]. The ages of Tertiary floras scattered through the Sonoran, Mojave, and Great Basin deserts indicated that early Miocene rainfall was ample throughout the year and supported

rich woodlands, which included taxa that are now exotic to the West [*Axelrod*, 1977]. This floristic evidence implies that precipitation gradually decreased during the late Miocene and early Pliocene, eventually developing into the highly seasonal rainfall distribution and dry conditions of today [*Axelrod*, 1939; *Lyle et al.*, 2008; *Minnich*, 2007; *Raven and Axelrod*, 1978].

Although this history of late Miocene and Pliocene climate evolution in western North America is persuasive, the observations that support this narrative are often spatially limited and poorly dated. Many of the older plant macrofossil studies described indirect evidence of aridification, the dating of terrestrial data is poor (often the dates are described as "late Miocene" or "Pliocene"), and the records are discontinuous [*Wilson and Pitts*, 2010]. The absolute timing of aridification, the rate of climatic change, the spatial extent, and the amount of precipitation change are not well constrained. As such, it has not been possible to identify mechanisms that led to precipitation changes and to use climate records as a benchmark for climate modeling [*Brierley et al.*, 2009]. One paleo-proxy approach that has not yet been applied to this topic involves using the hydrogen isotopic composition of terrestrial organic-biomarkers, which are transported from land and then deposited and preserved in marine sediments, to reconstruct the hydrologic history on land. Using deep sea sediment cores has several possible advantages over terrestrial records; it can provide continuous well-dated records of continental climate change, it integrates over large spatial scales that encompass the sediment source region thereby providing a record that minimizes the effects of local heterogeneous responses to climate change, and it

can potentially be compared to isotope-enabled climate model simulations to advance mechanistic interpretations of continental climate change.

The isotopic composition of plant leaf-waxes preserved in marine sediments has the potential to monitor past changes in the isotopic composition of precipitation. The waxy coating on plant leaves contains a variety of lipids including linear alkanes (*n*-alkanes). These *n*-alkanes are ubiquitous components of ancient sedimentary organic matter because they are generally unreactive during transport and burial. Further, the carbon-bound hydrogen of *n*-alkanes does not readily exchange at low temperatures [*Schimmelmann et al.*, 2006], preserving the original isotopic composition after burial. Recently published analyses of *n*-alkane hydrogen isotopic composition (δD) demonstrate the utility of this measurement for paleoprecipitation studies. These studies show that plant-wax *n*-alkane δD reflects the isotopic composition of precipitation [e.g. *Feakins*, in press*; Hou et al.*, 2008; *Jia et al.*, 2008; *Liu and Yang*, 2008; *Polissar and Freeman*, 2010; *Sachse et al.*, 2004; *Sachse et al.*, 2006; *Sauer et al.*, 2001; *Smith and Freeman*, 2006; *Tipple et al.*, 2007] and can be used to reconstruct past precipitation δD values.

The *n*-alkane δD proxy ($\delta D_{n\text{-alkane}}$) could provide an opportunity to better understand the evolution of the mediterranean climate in western North America; however, because the degree to which leaf-wax δD found in sediments reflects precipitation in western North America is still uncertain, initial validation of the proxy is needed prior to conducting paleo-studies. Here we present $\delta D_{n\text{-alkane}}$ data from a N-S transect of core-top sediments in the California Margin. With this

transect we investigate the relationship between modern precipitation and $\delta D_{n\text{-alkane}}$ in marine sediments, with a focus on the influences of sediment source, plant physiology, and climate on the $\delta D_{n\text{-alkane}}$ signal. We also test the applicability of the δD proxy to studies of climate change on long time scales with a low-resolution reconstruction of $\delta D_{n\text{-alkanes}}$ in southern California at ODP Site 1010.

4.2 Background

4.2.1 Terrestrial sediment delivery to the California Margin

Coastal rivers are the largest terrestrial sediment source to the California Margin. The watersheds of these rivers delineate the major sediment source areas that deliver terrestrial material to the marine sediments [*Griggs and Hein*, 1980; *Hein et al.*, 2003]. Sediment delivery to the margin is highest in the mountainous northern coast region of California and decreases towards the relatively small and more arid watersheds of the southern coast regions [*Griggs and Hein*, 1980; *Hein et al.*, 2003]. The largest sediment source area drains to the margin through San Francisco Bay and consists of the Sacramento and San Joaquin river basins. These basins drain the Central Valley, the western slope of the Sierras, the eastern slope of the Coast Range, and interior parts of the northern mountains [*Griggs and Hein*, 1980]. Compared to this interior region, the other California Margin sediment source areas are coastal, though the north coast does receive some sediment from interior mountains of northern California [*Griggs and Hein*, 1980; *Hein et al.*, 2003] (Figure 1a, Table 1).

In our study, the sediment source areas identified by *Griggs and Hein* [1980] and *Hein et al.* [2003] provide a starting point for many of our interpretations. However, similar information was not available for the coastline of Baja, Mexico. As a result, we estimated the sediment source regions for Baja based primarily on topography. The division between the northern and southern Baja sediment source regions in Figure 1a was meant to outline areas that were roughly similar in size to the sediment source areas of southern California. The uncertainty in boundaries of sediment source areas of Baja does not affect our interpretations of the overall dataset.

4.2.2 Precipitation controls in modern California

Rainfall on the western coast of North America is highly seasonal, and tied to seasonal changes in the large-scale atmospheric pressure field of the North Pacific. In winter, the North Pacific High (NPH) pressure system is relatively weak and frequent storm systems are directed to the northwest US where they deliver substantial rainfall to central California. In the summer, the NPH is well-developed, directing storms further north and resulting in dry summers throughout California and to the south [*Lyle et al.*, 2008]. However, there is a weak low pressure feature that develops over the southwest US and northwest Mexican deserts: this produces a North American summer monsoon effect, which draws in moisture from the Gulf of Mexico and eastern subtropical Pacific [*Friedman et al.*, 1992], but the total summer rainfall is low. Though strong seasonality in precipitation is a primary feature throughout much of California, there is also a strong gradient in overall rainfall within the region.

Relatively high total annual rainfall characterizes northern California (North of ~38°N) while southern California and Baja are relatively arid [*Lyle et al.*, 2008] (Figure 1a, Table 1).

4.2.3 δD values in modern precipitation

The isotopic composition of precipitation reflects the source, transport and rainout processes that deliver moisture to a given location. In particular, condensation and rainout of water vapor during transport preferentially removes moisture that is enriched in the heavier isotopologues (HDO and $H_2{}^{18}O$), leaving the residual vapor depleted in ^{18}O and D. Both northern and southern California are dominated by winter precipitation. However, because the coastal climate is relatively dry in the south and becomes progressively wetter towards the north, the models of coastal California precipitation show a decrease (going from south to north) of ~20-30‰ from northern Baja to northern California (Figures 1b and 1c, Table 1) [*Bowen*, 2012; *Bowen and Revenaugh*, 2003; *Bowen et al.*, 2005; *Williams and Rodoni*, 1997].

In addition to the isotopic effect produced by the precipitation gradient in coastal California, the storms that provide moisture to the western coast of North America originate in several different regions and the addition/removal of water vapor along storm trajectories can impart different isotopic values on local precipitation. The majority of the winter storms in the region travel eastward from the North Pacific and result in precipitation that is isotopically depleted relative to that of any summer storms. Summer storms originate in the eastern subtropical Pacific and the Gulf of Mexico and produce precipitation that is isotopically enriched

relative to the winter precipitation [*Benson and Klieforth*, 1989; *Dawson*, 1998; *Friedman et al.*, 1992].

4.3 Methods and Materials

4.3.1 Sites used in this study

We used 28 core-top samples to ground-truth the relationship between modern $\delta D_{precipitation}$ and $\delta D_{n\text{-alkanes}}$ in the sediments. The core-top transect spans ~10° of latitude along the coast (Figure 1a,b, Table 2). Fourteen of the core-top samples came from sites with previously published sedimentation rates that were calculated using radiocarbon dating. With these sites it was possible to ensure that our sampling was limited to late Holocene sediments. However, radiocarbon-based sedimentation rates were not available for the remaining fourteen core-tops. Based on the depth of the un-dated core-tops and an average sedimentation rate of the well-dated cores, of ~ 20 cm/kyr, it is likely that the un-dated cores are late Holocene aged as well (Table 2).

To generate the paleo δD records we sampled four ODP sites that also comprise a north-south transect along the coast (Table 2). Dating for these samples was based on shipboard age models [*Lyle et al.*, 1997]. At each core a sample from ~1.5 Ma was used to construct a 'snapshot' of early Pleistocene $\delta D_{n\text{-alkanes}}$. At ODP Site 1010 a low-resolution down-core record was constructed from five samples dated at ~10.5, 7, 4, 1.5, and 0.5 Ma.

4.3.2 Methods

Lipids were extracted from ~5-60g of crushed dry sediment with a 9:1 dichloromethane:methanol mix using a Dionex Accelerated Solvent Extractor (ASE200). The total lipid extract was evaporated under a stream of N_2 (Zymark Turbovap, water bath at 20°C) and subsequently split into three compound class fractions using silica gel chromatography.

The total lipid extract was transferred to ashed 8" Pasteur pipettes plugged at the tip with ashed glass wool and filled with 0.5g of silica gel (solvent rinsed, 70-230 mesh, activated at 200°C for 2 hours). Aliphatic, ketone, and alcohol/acid fractions were collected from the silica column using 4ml each of hexane, dichloromethane, and methanol, respectively. The ketone and alcohol fractions were dried and archived. Elemental sulfur (S_8) was removed from the aliphatic fraction by passing the fraction in hexane through an ashed 8"pasteurre pipette plugged at the tip with ashed glass wool and filled with activated copper (-40-100 mesh, rinsed in 4 volumes of dilute HCl, water, acetone, and dichloromethane) and collecting a total of 4ml of hexane [*Wakeham and Pease*, 1992]. The sulfur-free aliphatic fraction of each sample was run on a GC-MS to confirm the presence of long-chained *n*-alkanes.

GC-IRMS analysis of δD is quite sensitive to co-elution of chromatographic peaks and as a result it is often necessary to purify samples as much as possible prior to running on the GC-IRMS. For example, the *n*-alkyl lipids from Santa Barbara Basin sediments span an isotopic range of 120‰ [*Li et al.*, 2009]; co-elution over such a substantial isotopic range has the potential to severely limit the accuracy of the compound specific δD measurements. To reduce the potential of contamination from

co-elution, saturated strait chain *n*-alkanes were isolated from the desulfurized aliphatic fraction prior to isotopic analysis by GC-IRMS. Saturated compounds were separated from unsaturated aliphatic compounds using silver ion chromatography. Samples were transferred in hexane to an 8"pasteurre pipette filled with 0.5g of silver impregnated silica gel (10% w/w $AgNO_3$ on 60-200 mesh gel, activated at 120°C overnight). The saturated fraction was collected with 4ml of hexane and the unsaturated fraction was collected with 4mL of ethyl acetate. Normal and iso-alkanes were separated from cyclic and branched alkanes using urea adduction. Samples were dried under N_2 and 200μl each of urea-saturated methanol, acetone and pentane were each added to the sample vial. Vials were capped and placed in a freezer for 30 minutes. Immediately after removal from the freezer, excess solvent was evaporated under a stream of N_2 leaving visible urea crystals on the bottom of each vial. Non-adducts were washed from the crystals using hexane. The urea crystals were then dissolved in 500μl of DI water and 500μl of methanol. *N*-Alkanes were extracted from the water and methanol solution using hexane. The entire process was repeated on the adduct fraction to minimize any residual cyclic and branched compounds [*Wakeham and Pease*, 1992]. Purification of each sample was checked by GC-MS analysis and sample concentrations were determined using a GC-FID.

Biomarker δD values from the purified *n*-alkane samples were measured with a Thermo Trace capillary gas chromatograph coupled to a Thermo Delta Plus XP continuous-flow isotope ratio mass spectrometer through a high-temperature pyrolysis interface. Samples were injected using a PTV inlet in splitless mode.

Compounds were separated using a fused silica DB5-MS column (30m, 0.25mm I.D., 0.25µm film thickness). The initial GC oven temperature was 60°C. The oven temperature was increased at a rate of 30°C/min until reaching 225°C, followed by 10°C/min until reaching 325°C, where it was held constant for 13 minutes. Separated compounds were converted to C and H_2 in an alumina reactor held at 1425°C. *n*-alkane peaks were identified based on elution times and isotopic composition of each peak was determined using Isodat software. The H_3^+ factor was determined from reference gas pulses of increasing size using Isodat software at the start of each day. Isotopic ratios of the samples were calibrated using an *n*-alkane standard of known isotopic composition expressed relative to Vienna Standard Mean Ocean Water (VSMOW). The standard, *MixA2*, was prepared by Arndt Schimmelmann at Indiana University and includes fifteen *n*-alkanes (C_{16}-C_{30}). *MixA2* was run every 4-6 samples. In addition, a lab standard was run at a range of concentrations each day to quantify any size effects. The long-term reproducibility of δD_{C29} from *MixA2* was ±3.7‰ (s.d., *n*=45).

4.4 Results

4.4.1 Modern core-tops

The average chain length (ACL) and carbon preference index (CPI) of each core-top sample can be used to help evaluate the source of *n*-alkane compounds in the sediments. ACL values of terrestrial higher plants typically range from C_{27}-C_{33} [*Eglinton and Eglinton*, 2008; *Pancost and Boot*, 2004]. Small variations in terrestrial

higher plant ACLs may be due to vegetation type, aridity, and/or growth temperature [*Schefuß et al.,* 2003; *Tipple and Pagani*, in press]. ACLs were determined from chromatographic peak areas using the following equation:

$$ACL = 25(nC_{25\ peak\ area}) + 27(nC_{27\ peak\ area}) + 29(nC_{29\ peak\ area}) + 31(nC_{31\ peak\ area}) + 33(nC_{33\ peak\ area}) / nC_{25\ peak\ area} + nC_{27\ peak\ area} + nC_{29\ peak\ area} + nC_{31\ peak\ area} + nC_{33\ peak\ area}$$

ACL values range from 28.6-30 with a mean of 29.5 (Table 3). There is a small negative relationship between ACL and latitude (slope= -0.1, R^2=0.64, P<.0001), with the shortest ACLs in the north and longest ACLs in the south.

CPI values represent the odd-over-even tendency of the *n*-alkanes in a sample and can be used as a first-order assessment of non-terrestrial plant *n*-alkane inputs, sample maturity, and contamination from oil. Terrestrial plant leaf-waxes generally have a CPI >4, though there is large CPI variability between plant species [*Diefendorf et al.*, 2011]. CPI values less than ~4 are typically interpreted as an indication of petroleum contamination (the CPI of petroleum is ~1), algal or microbial *n*-alkane inputs, and/or thermal maturity and degradation of a sample [*Pancost and Boot*, 2004; *Pearson and Eglinton*, 2000]. CPI values were calculated according the CPI2 equation of *Marzi et al.* [1993]:

$$CPI2=1/2((nC_{25\ peak\ area} + nC_{27\ peak\ area} + nC_{29\ peak\ area} + nC_{31\ peak\ area} + nC_{33\ peak\ area} / nC_{24\ peak\ area} + nC_{26\ peak\ area} + nC_{28\ peak\ area} + nC_{30\ peak\ area} + nC_{32\ peak\ area}) + (nC_{25\ peak\ area} + nC_{27\ peak\ area} + nC_{29\ peak\ area} + nC_{31\ peak\ area} + nC_{33\ peak\ area} / nC_{26\ peak\ area} + nC_{28\ peak\ area} + nC_{30\ peak\ area} + nC_{32\ peak\ area} + nC_{34\ peak\ area}))$$

CPI values range from 2.50-10.71 (Table 3) with a mean of 6.87. There is a negative relationship between CPI and latitude (slope=-0.55, R^2=0.51, P<.0001). In three of the samples the even *n*-alkane peak areas were too small to integrate at the concentration run; however, in each of these samples there were abundant odd *n*-alkanes, indicating that the CPI was relatively high (denoted as >10 in Table 3).

The δD_{C29} and δD_{C31} values have a range of 18‰ over the entire late Holocene transect (Figure 2, Table 3). δD_{C29} values range from -151 to -169‰ and δD_{C31} values range from -149 to -167‰. Despite this large overall range, the northern and southern regions have similar $\delta D_{n\text{-alkane}}$ signatures; the mean δD_{C29} and mean δD_{C31} from sites ~29-35°N are 156‰ in both cases, similar to values from sites from ~39-42°N that exhibit mean δD_{C29} and δD_{C31} values of -159‰ and -158‰, respectively. Sites between ~37° and 39°N exhibit the lowest $\delta D_{n\text{-alkane}}$ values in the transect. In this region the mean δD_{C29} is -166‰ and the mean δD_{C31} is -167‰.

4.4.2 δD of paleo-records

The transect of early Pleistocene samples has a smaller range of $\delta D_{n\text{-alkane}}$ values than the transect of late Holocene samples (Figure 2, Table 3). The early Pleistocene δD_{C29} values have a range of ~12‰ and the δD_{C31} values have a range of ~15‰. The absolute δD_{C29} and δD_{C31} values of the early Pleistocene samples are similar to those of the late Holocene samples, approximately -154 to 168‰. Except for the δD_{C29} at ODP Site 1021, the site-to-site variation in the early Pleistocene samples generally follows a trend of decreasing δD values associated with increasing latitude.

ODP Site 1010 exhibits a trend of decreasing *n*-alkane δD since the early Pliocene (Figure 3, Table 3). The late Pleistocene δD_{C29} is ~7‰ lower than the δD_{C29} at ~10.5Ma. Most of the depletion in δD_{C29} occurs within the last ~4 myrs; isotopic values appear to be stable through the late Miocene and early Pliocene with a mean δD_{C29} of ~-152‰. By ~1.5Ma the δD_{C29} was ~-155‰ and by ~0.5myrs ago the δD_{C29} had reached -158‰. A one-way analysis of variance using the replicate analyses of each sample confirmed statistical significance of this down-core trend ($F(4,20)=12.23$, $p<0.0001$). Post-hoc Student-t tests show that the Pleistocene δD values are significantly different from Pliocene and late Miocene values ($p<0.05$ in all cases).

4.5 Discussion

4.5.1 Delivery of terrestrial *n*-alkanes to the California Margin

The ACL, CPI, and *n*-alkane concentration data indicate that the long-chain odd *n*-alkanes in the California Margin core-top samples originated from terrestrial plants and were delivered to the margin by rivers.

ACL variation in the core-top samples is small (28.6-30) and corresponds with the range expected for higher plant leaf waxes (C_{27}-C_{33})[*Pancost and Boot,* 2004]. The slight anti-correlation between ACL and latitude (slope= -0.1, R^2=0.64, P<.0001) may reflect the latitudinal changes in vegetation type, temperature, and/or aridity along coastal California, with both warmer and drier conditions characterized by longer ACLs [*Schefuß et al.*, 2003; *Tipple and Pagani*, in press]. Thus, the latitudinal trend in ACLs from core-tops can be explained by any of these mechanisms, all of which are consitent with local sources of *n*-alkanes.

The CPI range that we observe (2.5-10.71) reflects higher-plant leaf-wax inputs to the core-top sediments [*Tipple and Pagani*, 2010]. Several of the northern sites in our transect have CPIs <4, which is often considered to be the minimum for modern-plant CPIs and indicative of some mixing from fossil or petroleum sourced *n*-alkanes [*Jeng*, 2006]. However, radiocarbon analysis of Eel River sediments showed that petrogenic inputs in this region were minor [*Drenzek et al.*, 2009]. Therefore, the fact that the core-top CPIs are anti-correlated with latitude (slope=-0.55, R2=0.51, P<.0001) indicates that the trend in CPI is likely the result of latitudinal variation in vegetation. *Diefendorf et al.* [2011] showed that CPI values can vary greatly between plant species. *Pseudotsuga menziesii* (Douglas fir, CPI=1.6), *Abies concolor* (white fir, CPI=2.4) [*Diefendorf et al.*, 2011], and *Sequoia sempervirens* (California

Redwood, CPI=2.6) [*Oros*, 1999] all have exceptionally low CPIs and are main components of the Klamath and Sierra montane forests, northern California mixed evergreen forests, and redwood forests [*Fites-Kaufman et al.,* 2007; *Kulcher*, 1990; *Sawyer,* 2007]. Thus the vegetation shift from shrub-dominated in southern sediment source areas to conifer forest-dominated in the northern sediment source areas is the likely cause for the latitudinal trend in core-top CPIs (Table 1).

The concentrations of *n*-alkanes in these sediments suggest that the primary source of long-chain odd *n*-alkanes was rivers rather than aeolian input. The concentrations of C_{25}-C_{31} *n*-alkanes in the core-tops varied from ~1-5µg/g sediment. An approximation of C_{25}-C_{31} mass accumulation rates (MARs) indicates that the core-top MARs are over ten times higher than MARs in sites associated with wind delivery of leaf waxes [*Jia et al.*, 2012] (MAR estimate based on average dry bulk density of ODP 1019, 0.9 g cm^{-3} [*Ravelo et al.,* 1997], and a minimum core-top sedimentation rate of 10cm kyr^{-1}).

Thus, it is probable that the sedimentary leaf waxes in California Margin sediments originated from proximal sediment source regions that are similar to those outlined by the clay-mineral provenance investigations of *Griggs and Hein* [1980] and *Hein et al.* [2003] (Figure 1a).

4.5.2 δD of the core-top transect

The first order interpretation presented here is made by comparing the $\delta D_{n\text{-}alkanes}$ data in core-tops to the Online Isotopes in Precipitation Calculator (OIPC)

estimates of $\delta D_{precipitation}$ [*Bowen*, 2012; *Bowen and Revenaugh*, 2003; *Bowen et al.*, 2005], and therefore the initial assumption is that the OIPC estimates are accurate in the region of our study. However, implications of uncertainties in the OIPC estimates are also considered. As a starting point, $\delta D_{n\text{-alkanes}}$ measured in core-tops are compared to the $\delta D_{precipitation}$ in the watersheds of nearby source areas to assess whether $\delta D_{n\text{-alkanes}}$ in deep sea sediments are a promising proxy capable of monitoring past climate-induced changes in the broad spatial patterns of $\delta D_{precipitation}$. Since climate not only impacts the $\delta D_{precipitation}$ patterns on land, but also impacts the isotopic fractionation between leaf-waxes and the source water ($\varepsilon_{C29/source\ water}$), then it is also important to assess whether the mathematical difference between the $\delta D_{n\text{-alkanes}}$ and $\delta D_{precipitation}$, which is the implied $\varepsilon_{C29/source\ water}$, is consistent with what is expected for the vegetation type and climate conditions in the source regions. The discussion below begins by assessing the large-scale trends in $\delta D_{n\text{-alkanes}}$, but later incorporates an evaluation of the implied $\varepsilon_{C29/source\ water}$.

Most of the sediment sources to the California Margin are located along the coast, but because one large source area, the Central Valley (region 10 in Figure 1a and 1b), is located inland, the expected $\delta D_{n\text{-alkanes}}$ differs from the monotonic low-to-high $\delta D_{precipitation}$ trend that characterizes the sediment source areas along the coast (regions 1-9 in Figure 1b). The delivery of Central Valley sediments to the California Margin via outflow from the San Francisco Bay causes a local low in the expected $\delta D_{n\text{-alkane}}$ values. This is because the Central valley sediment source region includes relatively D-depleted inland source waters and further D-depleted waters of the

western Sierra Nevada Mountains. Taking all of these features into account, we can construct a latitudinal profile of expected $\delta D_{source\ waters}$ along the Margin (Figure 1c) and use this framework to interpret the relationship between precipitation in the sediment source regions and observed $\delta D_{n\text{-alkane}}$ values from the marine sediments.

Based on the OIPC $\delta D_{precipitation}$ estimate, the $\delta D_{n\text{-alkanes}}$ should exhibit an isotopic gradient, and possibly, because of variability in fractionation along the transect, an even steeper gradient than observed in the $\delta D_{precipitation}$. However, the $\delta D_{n\text{-alkane}}$ data does not exhibit a strong, monotonic continuous trend. Rather, core-tops from the California Margin have the highest $\delta D_{n\text{-alkane}}$ values in the south and north, and lowest values in the north-central region (Figure 4). This pattern is explained below by considering both the $\delta D_{precipitation}$ of the *n*-alkane source areas and differences in plant-water utilization in each region (e.g. plants utilize precipitation in the south and north-central regions, but a combination of precipitation and fog in the north).

Relatively positive core-top $\delta D_{n\text{-alkane}}$ values from ~29° to 36° N reflect a local source of southern California leaf-waxes to the marine sediments. For all but one of the samples in this region, the δD_{C29} and δD_{C31} leaf-waxes range from -151 to -159‰ and -152 to -162‰, respectively. This isotopic range is offset from the $\delta D_{precipitation}$ of the southern California sediment source areas by a magnitude that is consistent with observed apparent fractionation processes in the region (Figure 4). *Feakins and Sessions* [2010] found that the $\varepsilon_{C29/source\ water}$ of southern California vegetation was ~-90‰, which is similar in magnitude to the $\varepsilon_{C29/source\ water}$ observed in shrubs [*Sachse et*

al., 2012]. While the observed isotopic offset between the core-top $\delta D_{n\text{-alkanes}}$ and $\delta D_{precipitation}$ is variable, and difficult to associate with a particular month or the estimate of mean annual precipitation (MAP) values, it agrees more closely with previously published arid region/shrub $\varepsilon_{C29/source\ water}$ values than with the $\varepsilon_{C29/source\ water}$ of humid-region and non-shrub growth forms. In all, the core-top $\delta D_{n\text{-alkane}}$ values in the southern part of the transect are reliable indicators of the $\delta D_{precipitation}$ and the $\varepsilon_{C29/source\ water}$ expected from arid region/shrub vegetation in that region.

In the central portion of the north-south transect, at ~38°N, relatively negative core-top $\delta D_{n\text{-alkane}}$ values reflect Sacramento/San Joaquin river delivery of Central Valley and Western Sierra *n*-alkanes to the California Margin. The δD_{C29} and δD_{C31} values between ~37° and 39°N are the lowest in the *n*-alkane transect and range from -165 to -168‰ (Figure 4). The isotopic offset between Central Valley precipitation and these leaf waxes is consistent with a ~-90‰ $\varepsilon_{C29/source\ water}$, which is similar to that observed in the southern part of the transect. In addition, because these relatively negative $\delta D_{n\text{-alkane}}$ values are in close proximity to San Francisco Bay, they also agree spatially with the expected $\delta D_{n\text{-alkane}}$ low that corresponds to the $\delta D_{precipitation}$ of the Central Valley sediment source area (Figure 1b). Though the $\delta D_{n\text{-alkane}}$ values in this region are low relative to the southern part of the transect, a simple latitudinal control on $\delta D_{n\text{-alkane}}$ is unlikely. A latitudinal gradient does not exist within the southern region 29°-36°N, nor does it exist in the overall transect (29°-42°N).

North of ~39°N the $\delta D_{n\text{-alkane}}$ isotopic range is similar to that of southern California (Figure 4). This lack of a strong $\delta D_{n\text{-alkane}}$ gradient between north and

south indicates that some factor(s) other than $\delta D_{precipitation}$ must play a role in determining the isotopic composition of northern California leaf waxes. The δD_{MAP} in the most northern sediment source area of the study (Region 9 in figure 1b) is approximately 30‰ lower than that of the most southern region (Table 1). However, the -150 to -162 ‰ $\delta D_{n\text{-alkane}}$ range in the North overlaps with the $\delta D_{n\text{-alkane}}$ range in the south and results in a much smaller offset from $\delta D_{precipitation}$ than is observed throughout the rest of the transect. In the north, the offset of the mean $\delta D_{n\text{-alkane}}$ from MAP is ~70‰. One likely explanation for the relatively high $\delta D_{n\text{-alkane}}$ values is that the vegetation in the north coast sediment source area derives a substantial portion of its source water from fog.

Vegetation in northern California's coastal forests has been shown to utilize fog or fog-drip as a major water source [*Dawson*, 1998] and such fog utilization could dampen the expected offset between $\delta D_{precipitation}$ and $\delta D_{n\text{-alkanes}}$. In the summer months, when fog utilization is highest, the fog has δD values (δD_{fog}) that are ~40‰ more positive than the $\delta D_{precipitation}$ in northern California. In the winter months this difference increases to ~55‰ [*Dawson*, 1996; *Dawson*, 1998]. The mean value of measured core-top δD_{C29} is -159‰ which, when combined with expected fractionation $\varepsilon_{C29/source\ water}$ of ~90‰, implies that the source water has a seasonally integrated δD value of -70‰. This $\delta D_{source\ water}$ is possible if ~50% of the north coast source waters are from fog or fog-drip and ~50% of the north coast source waters are precipitation (estimate is based on an average offset between δD_{fog} and $\delta D_{precipitation}$ of 49‰ [*Dawson*, 1996; *Dawson*, 1998] and OIPC δD_{MAP}=-94‰). This estimate of fog

input is larger than the average annual hydrologic input of fog and fog-drip in North coast forests, which is estimated to be 34% where redwoods are present, and 17% in open areas [*Dawson*, 1998]. Overall, our estimate of the magnitude of fog-derived source waters hinges on the accuracy of the OIPC $\delta D_{precipitation}$ and the accuracy of the areal extent of the sediment source area.

Another possibility is that the OIPC estimates of $\delta D_{precipitation}$ underestimate the actual isotopic values. Three years of observations of $\delta D_{precipitation}$ from 41.5°N, 124.1°W show mean winter (December-May) δD of -61‰ [*Dawson*, 1996; *Dawson,* 1998], which is ~19‰ higher than the OIPC estimates for the same location. These observations imply that that fog waters are not needed to explain the enriched $\delta D_{n\text{-}alkanes}$ at this site. Rather, these relatively positive precipitation values indicate that, at this site, either the $\varepsilon_{C29/source\ water}$ of ~90‰ is too small or that *n*-alkane production is limited to the months when $\delta D_{precipitation}$ is more negative than the mean winter values [*Dawson*; 1998]. With $\delta D_{precipitation}$ observations from only one site near the western edge of the OIPC interpolation, it seems premature to conclude that the integrated OIPC north coast $\delta D_{precipitation}$ estimate is inaccurate. Similarly, though there is evidence that in southern California the $\delta D_{precipitation}$ of the 2006/2007 winter was underestimated by the OIPC (by ~16‰) [*Feakins and Sessions*, 2010], the southern California core-top data are consistent with the OIPC model and measured $\varepsilon_{C29/source\ water}$ for this region. Nonetheless, the disagreements between observed and modeled $\delta D_{precipitation}$ values indicate that more observations of $\delta D_{precipitation}$ are needed to

adequately test the accuracy of the OIPC interpolation, especially in the north coast region.

The 50% fog-water estimate represents an end-member value needed to reconcile the $\delta D_{n\text{-alkanes}}$ with the δD_{MAP} for the north coast sediment source area (Figure 1b, region 9). It is possible that the sediment source area boundaries overestimate the areal extent of sedimentary *n*-alkane delivery to the margin. If the eastern boundary of the source area is revised to a more western location, the integrated δD_{MAP} value would be higher and less fog input is needed to explain the $\delta D_{n\text{-alkanes}}$. Thus, accurate bounding of *n*-alkane source regions is an important part of interpretation of $\delta D_{n\text{-alkanes}}$, especially in areas with large $\delta D_{precipitation}$ gradients.

The summer drought conditions in California typically limit peak vegetation growth to the spring months when light availability is increasing, temperatures are warming, and winter season moisture is still available [*Minnich*, 2007; *Royce and Barbour*, 2001; *Xu et al.*, 2004]. However, fog-harvesting in northern California can effectively extend the growing season into the summer-drought conditions [*Dawson*, 1998], making it difficult to determine the boundary conditions of the isotopic system recorded by the $\delta D_{n\text{-alkanes}}$. Because of the major isotopic offset between fog and precipitation δD, constraints on source-water utilization may be critical to accurately interpreting down-core $\delta D_{n\text{-alkanes}}$ records in this region. Furthermore, the tight coupling between fog and oceanic conditions (e.g. wind-driven upwelling, the Pacific Decadal Oscillation [*Johnstone and Dawson*, 2010]) implies that the $\delta D_{n\text{-alkane}}$ signal

in northern coastal California is susceptible to a larger range of controls than regions without the potential for fog source waters.

The interpretations discussed above are based on the assumption that leaf-wax compounds were delivered to the California Margin with little pre-aging in terrestrial soils prior to marine sedimentation. However, there is evidence from radiocarbon analyses of Eel River sediments that some pre-aging, on the order of several kyrs, occurs prior to marine sedimentation of leaf-wax compounds in northern California [*Drenzek et al.*, 2009]. Radiocarbon studies can provide some estimate of pre-aging time-scales for leaf-waxes. For example, *Drenzek* [2007] found that in Cariaco Basin and Saanich Inlet sediments, fatty acids derived from vascular plant detritus resided in soils for decades to ~5.2 kyrs before being incorporated into marine sediments. Roughly 70-90% of the plant-derived compounds in these marine sediments were pre-aged in soils for ~2.5-5.2 kyrs and 30-10% of the compounds were pre-aged in soils for decades [*Drenzek*, 2007]. To an extent, the pre-aging of *n*-alkanes in California Margin core-tops would help to time-average the $\delta D_{n\text{-alkane}}$ signal and facilitate our comparisons to climatological estimates of $\delta D_{precipitation}$, such as the OIPC dataset. However, pre-aging could also complicate the core-top $\delta D_{n\text{-alkane}}$ signal because it may result in a record of middle Holocene $\delta D_{precipitation}$ in the core-top samples.

In the case of the Northern California margin sediments, pre-aging of *n*-alkanes could partly explain the relatively small isotopic offset of $\delta D_{n\text{-alkanes}}$ from $\delta D_{precipitation}$. A high-resolution multi-proxy study of the Holocene climate in northern

California suggests that middle Holocene conditions ~8.2-3.2 ka were warmer and drier than the conditions of the late Holocene [*Barron et al.*, 2003]. Less precipitation in the middle Holocene, compared to modern, could have resulted in the relatively high $\delta D_{n\text{-alkane}}$ values that we observe in northern California Margin sediments. The transition from the relatively warm/dry conditions of the middle Holocene to the cooler/wetter conditions of the late Holocene and modern occurred ~5.2-3.5 ka [*Barron et al.*, 2003]. Because these more recent conditions are characterized by coastal fog, which also acts to enrich the $\delta D_{n\text{-alkane}}$ signal, it is not fully clear if the $\delta D_{n\text{-alkane}}$ values in core-tops are a result of a middle-Holocene climate signal or fog utilization, as we discussed earlier. Ultimately, compound specific radiocarbon dating of *n*-alkanes in the California Margin sediments will be needed to fully quantify the influence of pre-aged leaf-waxes on the *n*-alkane isotopic signal.

4.5.3 Paleohydrology

4.5.3.1 Pleistocene transect

Data from southern sites in the early Pleistocene transect show *n*-alkanes that are enriched in D, relative to the more northern sites, and indicate that the southern sites may be suitable for down-core studies. The $\delta D_{n\text{-alkane}}$ values at each site overlap with the core-top values in each region and capture the contrast between the relatively high $\delta D_{n\text{-alkane}}$ values of southern California and low values of the north-central region (Figure 2). If transport of terrestrial material via winds or ocean currents had

substantially homogenized inputs along the coast, then it would not be possible to resolve the isotopic contrast between central and southern California. In addition, there is excellent agreement between the early Pleistocene data from Site 1016 (34.5° N) and the $\delta D_{alkanes}$ from recent Santa Barbara basin (SBB) sediments in our study (Figure 2), as well as an independent study by *Li et al.* [2009] that shows mean δD values of C_{25}-C_{33} odd *n*-alkanes of -155‰ and -159‰ in two recent SBB cores. This agreement between the offshore ODP sites and the nearshore recent sediments confirms that the offshore ODP sites reflect the $\delta D_{n\text{-alkane}}$ signal from adjacent coastal locations, which are dominated by fluvial input. Overall, the early Pleistocene observations preclude (i) a significant inland source for the plant-waxes in southern California and (ii) latitudinal mixing of coastal sources in both our late Holocene and early Pleistocene data.

4.5.3.2 ODP Site 1010 down-core

The downcore record of $\delta D_{n\text{-alkanes}}$ from ODP Site 1010 suggests that there was a shift from year-round precipitation in the late Miocene and early Pliocene to a more summer-dry mediterranean climate in the Pleistocene (Figure 3). Relative to the $\delta D_{n\text{-alkanes}}$ in the Pleistocene, the high values of the late Miocene and early Pliocene are indicative of higher amounts of summer precipitation. This interpretation is based on the fact that the modern winter precipitation in southern California generally originates from central and North Pacific air masses and is isotopically light compared to the summer precipitation that originates from Gulf of Mexico and Gulf

of California air masses [*Benson and Klieforth*, 1989; *Dawson*, 1998; *Friedman et al.*, 1992]. This interpretation is consistent with low-resolution pollen data from the same site that shows >10% decline in summer-wet taxa between the latest Miocene and the Pleistocene [*Heusser;* unpublished](Figure 5).

The pollen and isotope data from Site 1010 record a change in the seasonality of precipitation, but do not show changes in precipitation amount. A simple shift to more arid conditions would have resulted in increasing $\delta D_{n\text{-alkane}}$ values since the late Miocene, as opposed to the decrease in values observed in the Site 1010 record. It is possible that an overall decrease in precipitation amount muted the seasonal signal; however, this cannot be determined from the available data. Vegetation shifts in the sediment source area to 1010 cannot explain the decrease in $\delta D_{n\text{-alkanes}}$ either; rather it may have muted the amplitude in the $\delta D_{n\text{-alkane}}$ shift from relatively high to low values. Based on the pollen analyses, there was a shift from the tree-dominated vegetation in the Miocene to shrub-dominant in the present (*chaparral*) [*Heusser, unpublished*]. This shift from forest to shrubland would tend to increase evapotranspiration, resulting in a smaller $\varepsilon_{C29/\text{source water}}$ [*Sachse et al.*, 2012], and higher $\delta D_{n\text{-alkanes}}$. In all, the decreasing $\delta D_{n\text{-alkanes}}$ values, and changes in pollen assemblage, are strong evidence for a shift from wet-summer climate in the late Miocene to the dry-summer climate of today.

Along with the pollen evidence for a vegetation shift, there is isotopic evidence indicating that the distribution of photosynthetic pathway types has changed since the late Miocene, also possibly affecting the $\varepsilon_{C29/\text{source water}}$ in southern

California. Vegetation possessing the C_3 photosynthetic pathway is often found in regions such as modern coastal California, which is characterized by cool growing seasons and substantial winter precipitation. In contrast, plants with the C_4 pathway tend to outcompete C_3 vegetation in regions with warm growing season and adequate summer precipitation. The summer-dry conditions that characterize the modern Mediterranean climate of California strongly favor the C_3 photosynthetic pathway [*Sage et al.*, 1999]. However, carbon isotopes in fossil horse teeth provide evidence of greater C_4 vegetation in California during the middle Miocene [*Crowley and Koch*, 2007], possibly reflecting higher summer precipitation. An abrupt decrease, at ~2 Ma, in the $\delta^{13}C$ values of southern California fossil horse teeth indicates a shift to less C_4 influence in the region [*Spero et al.*, 2003]. A shift to less C_4 vegetation would result in a smaller offset due to $\varepsilon_{C29/source\ water}$ [*Sachse et al.*, 2012] and would also mute the amplitude of the isotopic shift from relatively high to lower values in the 1010 $\delta D_{n\text{-}alkane}$ record.

The timing of changes in the $\delta D_{n\text{-}alkane}$ record agrees with that of the horse-teeth $\delta^{13}C$ values [*Spero et al.*, 2003] and indicates that most of the hydrologic change in southern California occurred after the early Pliocene. This timing differs from the paleobotanical evidence, which describes marked changes taking place earlier in the late Miocene, and then a relatively stable hydrologic cycle over the past 5 myrs. Pollen assemblages from offshore southern California (DSDP site 467, 33.8° N) indicate that the change from a relatively humid, summer-wet climate to drier summer-dry conditions started during the late Miocene. Genera now exotic to the

west (*Carya* (hickory), *Liquidambar* (sweet gum), *Fagus* (beech)), which are indicative of summer-wet conditions, decreased in southern coastal California by the early Pliocene [*Ballog and Malloy*, 1981]. Because DSDP Site 467 is located ~4°N of Site 1010, it is possible that the two sites may have experienced different regional hydrologic change, or that the low-resolution of the 1010 record is aliasing higher frequency variations in the hydrologic cycle of western North America. This discrepancy highlights the lack of understanding of the evolution of the mediterranean climate of western North America and a need for robust multi-proxy records from individual cores that can be compared to model simulations for the region.

The late Pliocene/early Pleistocene timing of changes in the $\delta D_{n\text{-alkane}}$ record is also roughly coincident with the strengthening of basin-wide meridional sea surface temperature (SST) gradients; a global-scale oceanic trend that could have played a role in establishing the mediterranean climate after the early Pliocene. Recent model results have shown that, relative to modern conditions, a reduction in the meridional SST gradients causes a weakening of the Hadley circulation, and a redistribution of precipitation patterns [*Brierley and Fedorov*, 2010; *Brierley et al.*, 2009] (Figure 6). The reduced meridional SST gradient increases summer season precipitation in southern California/western Mexico. This occurs because the ITCZ is less intense in the modeled early Pliocene climate, allowing for enhanced moisture flux from ocean to land as part of the southwest summer monsoon. Although these model predictions were for the early Pliocene, new SST records show warm subtropical North Pacific

SSTs during the late Miocene and indicate that reduced meridional SST gradients characterized the late Miocene as well [*LaRiviere et al.*, in prep; *LaRiviere et al.*, 2012]. These model results are consistent with the $\delta D_{n\text{-alkane}}$ and pollen evidence for year-round precipitation during the warm early Pliocene and late Miocene, as well as a transition to summer-dry conditions as the SST gradients strengthened.

It is also possible that local SST changes affected the seasonality of precipitation in southern California. Cyclones from the eastern tropical Pacific deliver more than 20% of the warm season precipitation to southern California and northern Baja [*Corbosiero et al.*, 2009]. Compared to the total number of cyclones that form in the eastern tropical Pacific, the number that travel north and eventually reach California is small. This is because cool SSTs off of southern California and high wind shear, associated large-scale atmospheric circulation, weaken the storms before they make contact with the land [*Corbosiero et al.*, 2009]. However, there is evidence that SSTs during the late Miocene and early Pliocene, off of southern California and throughout the California Current, were warmer than modern, perhaps enabling more tropical cyclones to affect the region.

The long-term, SST records from ODP Sites 1021 and 1010 show cooling throughout the California Current since the start of the late Miocene, and the nearshore sites ODP 1012 and ODP 1014 exhibit cooling since the early Pliocene (Figure 7) [*Brierley et al.*, 2009; *Dekens et al.*, 2007; *LaRiviere et al.*, 2012]. The nearshore southern California sites exhibit warmer early Pliocene SSTs than Site 1010, which is located further south, and further offshore than Sites 1012 and 1014.

However, the difference in Pliocene SSTs among the southern California sites may be a reflection of the small-scale variability of alkenone production within upwelling regions [*Bac et al.*, 2003] and/or a tendency for open ocean deep-water sites to record slightly cooler alkenone-based SSTs than shallower nearshore sites [*Herbert et al.*, 1998]. Overall, the local waters of southern California were warmer than modern during the late Miocene and Pliocene and would have been more conducive to eastern tropical Pacific cyclones progressing northward and delivering summer precipitation to southern California. In addition, the reduction in wind shear, relative to modern, that is associated with the reduced late Miocene and early Pliocene basin-wide SST gradients would also enable more tropical cyclones to reach southern California, a trend which has been predicted by models of early Pliocene climate [*Fedorov et al.*, 2010].

4.6 Summary and Conclusions

We measured the hydrogen isotopic composition of leaf-wax *n*-alkanes in California Margin sediments to evaluate whether the $\delta D_{n\text{-alkane}}$ proxy is capable of monitoring changes in coastal western North American precipitation since the late Miocene. $\delta D_{n\text{-alkane}}$ values from ~29-36°N are offset from $\delta D_{precipitation}$ by an amount that is consistent with the $\varepsilon_{C29/source\ water}$ expected for arid regions and are reliable indicators of the region's $\delta D_{precipitation}$. $\delta D_{n\text{-alkane}}$ values from ~37-39°N also exhibit an offset from $\delta D_{precipitation}$ that is similar to arid region $\varepsilon_{C29/source\ water}$; however, *n*-alkanes from this region originate from a large interior sediment source area that is influenced

by the D-depleted precipitation of the western Sierras and the rain shadow from the coast ranges. The $\delta D_{n\text{-alkanes}}$ ~39-42.5°N show the smallest offset from $\delta D_{precipitation}$ along the transect, possibly due to fog-water utilization in north coast vegetation. Uncertainties in vegetation source water, $\delta D_{precipitation}$, extent of the sediment source area, and *n*-alkane pre-aging in soils complicate the use of the $\delta D_{n\text{-alkane}}$ proxy in this region.

The $\delta D_{n\text{-alkanes}}$ of early Pleistocene sediments confirm the utility of southern California Margin *n*-alkanes for monitoring local precipitation. The down-core record from ODP Site 1010 shows relatively stable δD_{C29} values during the late Miocene and early Pliocene, followed by a shift to lower values after the early Pliocene. These data, combined with pollen data from Site 1010, and $\delta^{13}C$ isotopes from fossil horse teeth [*Spero et al.,* 2003] indicate that the establishment of the mediterranean climate in western North America may have occurred in the late Pliocene or early Pleistocene, later than previously thought. This shift in terrestrial climate may have resulted from a combination of strengthening basin-wide SST gradients and cooling of local SSTs. However, it will not be possible to accurately identify correlations between precipitation on land and SSTs unless more continuous and higher resolution records of precipitation in western North America are generated.

References

Axelrod, D. (1977), Outline history of California vegetation, in *Terrestrial vegetation of California*, edited by M. Barbour and J. Major, p. 1002, John Wiley & Sons, New York.

Axelrod, D. I. (1939), *A Miocene Flora from the Western Border of the Mohave Desert*, Carnegie Institution of Washington, Washington, D. C.

Bac, M. G., K. R. Buck, F. P. Chavez, and S. C. Brassell (2003), Seasonal variation in alkenones, bulk suspended POM, plankton and temperature in Monterey Bay, California: Implications for carbon cycling and climate assessment, *Organic Geochemistry*, *34*(6), 837-855.

Ballog, R. A., and R. E. Malloy (1981), Neogene palynology from the southern California continental borderland, Site 467, Deep Sea Drilling Project Leg 63, *Initial Reports of the Deep Sea Drilling Project*, *63*, 565-577.

Barron, J.A., L. Heusser, T. Herbert, and M. Lyle (2003), High-resolution climatic evolution of coastal northern California during the past 16,000 years, *Paleoceanography*, *18*(1), 20-1-20-14.

Benson, L., and H. Klieforth (1989), Stable isotopes in precipitation and ground water in the Yucca Mountain region, southern Nevada: Paleoclimatic Implications, in *Aspects of Climate Variability in the Pacific and the Western Americas*, edited by D. Peterson, p. 445, American Geophysical Union, Washington, D.C.

Bowen, G. J. (2012), Gridded maps of the isotopic composition of meteoric waters, http://www.waterisotopes.org.

Bowen, G. J., and J. Revenaugh (2003), Interpolating the isotopic composition of modern meteroic precipitation, *Water Resources Research*, *39*(10).

Bowen, G. J., L. I. Wassenaar, and K. A. Hobson (2005), Global application of stable hydrogen and oxygen isotopes to wildlife forensics, *Oecologia*, *143*(3), 337-348.

Brierley, C. M., and A. V. Fedorov (2010), Relative importance of meridional and zonal sea surface temperature gradients for the onset of the ice ages and Pliocene-Pleistocene climate evolution, *Paleoceanography*, *25*, 16.

Brierley, C. M., A. V. Fedorov, Z. H. Liu, T. D. Herbert, K. T. Lawrence, and J. P. LaRiviere (2009), Greatly expanded tropical warm pool and weakened Hadley circulation in the early Pliocene, *Science*, *323*(5922), 1714-1718.

California Department of Forestry and Fire Protection, CDF-FRAP (2010), Map of average annual rainfall 1900-1960, digitized from source map of S.E. Rantz, *US Geological survey, 1972*, Sacramento, CA.

Corbosiero, K. L., M. J. Dickinson, and L. F. Bosart (2009), The contribution of eastern North Pacific tropical cyclones to the rainfall climatology of the southwest United States, *Monthly Weather Review*, *137*(8), 2415-2435.

Crowley, B. E., and P. L. Koch (2007), The isotopic history of western North American grasslands, *EOS Transaction of the American Geophysical Union*, *88*(52), Fall Meeting Supplement.

Dawson, T. E. (1996), The use of fog precipitation by plants in coastal redwood forests, in *Proceedings of the conference on coastal redwood forest ecology and management*, edited by J. LeBlanc, p. 170, University of California Cooperative Extension Forestry Publication, Humboldt.

Dawson, T. E. (1998), Fog in the California redwood forest: ecosystem inputs and use by plants, *Oecologia*, *117*(4), 476-485.

Dekens, P. S., A. C. Ravelo, and M. McCarthy (2007), Warm upwelling regions in the Pliocene warm period, *Paleoceanography, 22,* 12.

Diefendorf, A. F., K. H. Freeman, S. L. Wing, and H. V. Graham (2011), Production of *n*-alkyl lipids in living plants and implications for the geologic past, *Geochimica Et Cosmochimica Acta*, *75*(23), 7472-7485.

Drenzek, N.J. (2007), The temporal dynamics of terrestrial organic matter transfer to the oceans: Initial assessment and application, PhD thesis, Massachusetts Institute of Technology and the Woods Hole Oceanographic Institution, Woods Hole, Massachusetts, United States.

Drenzek, N.J., K.H. Hughen, D.B. Montlucon, J.R. Southon, G.M. dos Santos, E.R.M. Druffel, L. Giosan, and T.I. Eglinton (2009), A new look at old carbon in active margin sediments, *Geology*, *37*(3), 239-242.

Eglinton, T. I., and G. Eglinton (2008), Molecular proxies for paleoclimatology, *Earth and Planetary Science Letters*, *275*(1-2), 1-16.

Feakins, S. J. (*in press*), Pollen-corrected leaf wax D/H reconstructions of northeast African hydrological changes during the late Miocene, *Palaeogeography, Palaeoclimatology, Palaeoecology*.

Feakins, S. J., and A. L. Sessions (2010), Controls on the D/H ratios of plant leaf waxes in an arid ecosystem, *Geochimica et Cosmochimica Acta*, *74*(7), 2128-2141.

Fedorov, A., C. Brierley, and K. Emanuel (2010), Tropical cyclones and permanent El Nino in the early Pliocene epoch, *Nature, 463*, 1066-1071.

Fites-Kaufman, J., P. Rundel, N. Stephenson, and D. A. Weixelman (2007), Montane and subalpine vegetation of the Sierra Nevada and Cascade ranges, in *Terrestrial Vegetation of California, 3rd ed.*, edited by M. Barbour, p. 734, University of California Press, Berkeley.

Friedman, I., G. I. Smith, J. D. Gleason, A. Warden, and J. M. Harris (1992), Stable Isotope Composition of waters in Southeastern California 1. Modern precipitation, *Journal of Geophysical Research-Atmospheres*, *97*(D5), 5795-5812.

Gardner, J. V., W. E. Dean, and P. Dartnell (1997), Biogenic sedimentation beneath the California Current system for the past 30 kyr and its paleoceanographic significance, *Paleoceanography*, *12*(2), 207-225.

Griggs, G. B., and J. R. Hein (1980), Sources, dispersal, and clay mineral composition of fine-grained sediment off central and northern California, *Journal of Geology*, *88*(5), 541-566.

Hein, J. R., J. S. Dowling, A. Schuetze, and H. J. Lee (2003), Clay-mineral suites, sources, and inferred dispersal routes: Southern California continental shelf, *Marine Environmental Research*, *56*(1-2), 79-102.

Herbert, T. D., J. D. Schuffert, D. Thomas, C. Lange, A. Weinheimer, A. Peleo-Alampay, and J. C. Herguera (1998), Depth and seasonality of alkenone production along the California margin inferred from a core top transect, *Paleoceanography*, *13*(3), 263-271.

Heusser, L.E. (*unpublished*), Pollen records from ODP Sites 1010, 1016, 1021, and 1022.

Hou, J. Z., W. J. D'Andrea, and Y. S. Huang (2008), Can sedimentary leaf waxes record D/H ratios of continental precipitation? Field, model, and experimental assessments, *Geochimica Et Cosmochimica Acta*, *72*(14), 3503-3517.

Jeng, W. L. (2006), Higher plant *n*-alkane average chain length as an indicator of petrogenic hydrocarbon contamination in marine sediments, *Marine Chemistry*, *102*(3-4), 242-251.

Jia, G., K. Wei, F. Chen, and P. A. Peng (2008), Soil n-alkane δD vs. altitude gradients along Mount Gongga, China, *Geochimica et Cosmochimica Acta*, *72*(21), 5165-5174.

Jia, G., Z. Li, P. Peng, and L. Zhou (2012), Aeolian *n*-alkane isotopic evidence from North Pacific for a late Miocene decline of C_4 plant in the arid Asian interior, *Earth and Planetary Science Letters*, *321-322*, 32-40.

Johnstone, J. A., and T. E. Dawson (2010), Climatic context and ecological implications of summer fog decline in the coast redwood region, *Proceedings of the National Academy of Sciences of the United States of America*, *107*(10), 4533-4538.

Kulcher, A. W. (1990), Natural vegetation of California (Map), in *Terrestrial vegetation of California*, edited by M. G. Barbour and J. Major, Native Plant Society, Special Publication Number 9, p. 1020, Davis, CA.

LaRiviere, J. P., A. C. Ravelo, H. Ford, and M. Aung (*in prep.*), Basin-wide sea surface temperature distributions of the Pleistocene, Pliocene, and late Miocene.

LaRiviere, J. P., A. C. Ravelo, A. Crimmins, P. S. Dekens, H. L. Ford, M. Lyle, and M. W. Wara (2012), Late Miocene decoupling of oceanic warmth and atmospheric carbon dioxide forcing, *Nature*, *486*(7401), 97-100.

Li, C., A. L. Sessions, F. S. Kinnaman, and D. L. Valentine (2009), Hydrogen-isotopic variability in lipids from Santa Barbara Basin sediments, *Geochimica et Cosmochimica Acta*, *73*(16), 4803-4823.

Liu, W., and H. Yang (2008), Multiple controls for the variability of hydrogen isotopic compositions in higher plant *n*-alkanes from modern ecosystems, *Global Change Biology*, *14*(9), 2166-2177.

Lyle, M., I. Koizumi, C. Richter, and S. S. Party (1997), Leg 167, *Proceedings of the Ocean Drilling Program, Initial Reports*, *167*.

Lyle, M., J. Barron, T. J. Bralower, M. Huber, A. Olivarez-Lyle, A. C. Ravelo, D. K. Rea, and P. A. Wilson (2008), Pacific Ocean and Cenozoic evolution of climate, *Reviews of Geophysics*, *46*(2002), 47.

Marzi, R., B. E. Torkelson, and R. K. Olson (1993), A revised carbon preference index, *Organic Geochemistry*, *20*(8), 1303-1306.

Minnich, R. A. (2007), California climate, paleoclimate and paleovegetation, in *Terrestrial Vegetation of California, 3rd ed.*, edited by M. Barbour, p. 734, University of California Press, Berkeley.

Normark, W. R., M. McGann, and R. W. Sliter (2009), Late Quaternary sediment-accumulation rates within the inner basins of the California Continental Borderland in support of geologic hazard evaluation, in *Earth science in the urban ocean: the Southern California continental borderland*, edited by H. J. Lee and W. R. Normark, p. 481, Geological Society of America, Boulder, Colorado.

Oros, D. R. (1999), Application of biomarker compounds as tracers for sources and fates of natural and anthropogenic organic matter in the environment, PhD thesis, Oregon State University, Corvallis, Oregon.

Pancost, R. D., and C.S. Boot (2004), The palaeoclimatic utility of terrestrial biomarkers in marine sediments, *Marine Chemistry*, *92*, 239-261.

Pearson, A., and T. I. Eglinton (2000), The origin of *n*-alkanes in Santa Monica Basin surface sediment: a model based on compound-specific $\Delta^{14}C$ and $\delta^{13}C$ data, *Organic Geochemistry*, *31*(11), 1103-1116.

Pisias, N. G., A. C. Mix, and L. Heusser (2001), Millennial scale climate variability of the northeast Pacific Ocean and northwest North America based on radiolaria and pollen, *Quaternary Science Reviews*, *20*(14), 1561-1576.

Polissar, P. J., and K. H. Freeman (2010), Effects of aridity and vegetation on plant-wax δD in modern lake sediments, *Geochimica et Cosmochimica Acta*, *74*(20), 5785-5797.

Ravelo, A. C., M. Lyle, I. Koizumi, J. P. Caulet, E. Fornaciari, A. Hayashida, F. Heider, J. Hood, S. Hovan, T. Janecek, A. Janik, R. Stax, M. Yamamoto, and the ODP Leg 167 Shipboard Scientific Party (1997), Pliocene carbonate accumulation along the California margin, *Paleoceanography*, *12*(6), 729-741.

Raven, P. H., and D. I. Axelrod (1978), *Origin and Relationships of the California Flora*, University of California Press, Berkeley.

Retallack, G. J., S. Tanaka, and T. Tate (2002), Late Miocene advent of tall grassland paleosols in Oregon, *Palaeogeography Palaeoclimatology Palaeoecology*, *183*(3-4), 329-354.

Royce, E. B., and M. G. Barbour (2001), Mediterranean climate effects. II. Conifer growth phenology across a Sierra Nevada ecotone, *American Journal of Botany*, *88*(5), 919-932.

Sachse, D., J. Radke, and G. Gleixner (2004), Hydrogen isotope ratios of recent lacustrine sedimentary *n*-alkanes record modern climate variability, *Geochimica et Cosmochimica Acta*, *68*(23), 4877-4889.

Sachse, D., J. Radke, and G. Gleixner (2006), δD values of individual *n*-alkanes from terrestrial plants along a climatic gradient - Implications for the sedimentary biomarker record, *Organic Geochemistry*, *37*(4), 469-483.

Sachse, D., et al. (2012), Molecular Paleohydrology: Interpreting the hydrogen-isotopic composition of lipid biomarkers from photosynthesizing organisms, *Annual Review of Earth and Planetary Sciences, 40*(40), 221-249.

Sage, R. F., D. A. Wedin, and L. Meirong (1999), The biogeography of C_4 photosynthesis: patterns and controlling factors, in *C_4 Plant Biology*, edited by R. F. Sage and R. K. Monson, p. 596, Academic Press, San Diego.

Sauer, P. E., T. I. Eglinton, J. M. Hayes, A. Schimmelmann, and A. L. Sessions (2001), Compound specific D/H ratios of lipid biomarkers from sediments as a proxy for environmental and climatic conditions, *Geochimica et Cosmochimica Acta*, *65*(2), 213-222.

Sawyer, J.O. (2007), Forests of northwestern California, in *Terrestrial Vegetation of California, 3rd ed.*, edited by M. Barbour, p. 734, University of California Press, Berkeley.

Schefuß, E., V. Ratmeyer, J. B. W. Stuut, and J. H. F. Jansen (2003), Isotope analyses of *n*-alkanes in dust from the lower atmosphere over the central eastern Atlantic, *Geochimica et Cosmochimica Acta, 67*(10), 1757-1767.

Schimmelmann, A., A. L. Sessions, and M. Mastalerz (2006), Hydrogen isotope (D/H) composition of organic matter during diagenesis and thermal maturation, *Annual Review of Earth and Planetary Science*, *34*, 501-533.

Smith, F. A., and K. H. Freeman (2006), Influence of physiology and climate on δD of leaf wax *n*-alkanes from C_3 and C_4 grasses, *Geochimica et Cosmochimica Acta*, *70*(5), 1172-1187.

Spero, H. J., C. B. Brogenski, G. T. Jefferson, J. M. Harris, and T. E. Cerling (2003), Initiation of modern Pacific atmospheric circulation at the Plio-Pleistocene boundary recorded in horse teeth enamel, *Geological Society of America Abstracts with Programs*, *35*(6), 586.

Stott, L. D., M. Neumann, and D. Hammond (2000), Intermediate water ventilation on the northeastern Pacific margin during the late Pleistocene inferred from benthic foraminiferal $\delta^{13}C$, *Paleoceanography*, *15*(2), 161-169.

Tipple, B., M. Pagani, R. Smith, and A. Anders (2007), Orographic and climatic influences on leaf wax carbon and hydrogen isotope ratios: A field survey from northern California, *EOS Transaction of the American Geophysical Union*, *88*(52), Fall Meeting Supplement.

Tipple, B. J., and M. Pagani (2010), A 35 Myr North American leaf-wax compound-specific carbon and hydrogen isotope record: Implications for C_4 grasslands and hydrologic cycle dynamics, *Earth and Planetary Science Letters*, *299*(1-2), 250-262.

Tipple, B. J., and M. Pagani (*in press*), Environmental control on eastern broadleaf forest species' leaf wax distributions and D/H ratios, *Geochimica et Cosmochimica Acta*.

Wakeham, S. G., and T. K. Pease (1992), Lipid analysis in marine particle and sediment samples, p. 36, Skidaway Institute of Oceanography, Savannah.

Williams, A. E., and D. P. Rodoni (1997), Regional isotope effects and application to hydrologic investigations in southwestern California, *Water Resources Research*, *33*(7), 1721-1729.

Wilson, J. S., and J. P. Pitts (2010), Illuminating the lack of consensus among descriptions of earth history data in the North American deserts: A resource for biologists, *Progress in Physical Geography*, *34*(4), 419-441.

Xu, L. K., D. D. Baldocchi, and J. W. Tang (2004), How soil moisture, rain pulses, and growth alter the response of ecosystem respiration to temperature, *Global Biogeochemical Cycles*, *18*(4), 10.

Figure 1. Rainfall, $\delta D_{precipitation}$, and sediment source areas relative to site locations. **a.** Mean annual rainfall in the study area. A pronounced rainfall gradient exists within the study area, with high rainfall north of ~38°N and relatively dry conditions south of ~38°N. GIS dataset from *CDF-FRAP* [2010]. Sediment source areas, outlined in red, are numbered and correspond to *Map IDs* in Table 1. Circles denote site locations. Site numbers correspond to *Map IDs* in table 2. **b.** Mean annual hydrogen isotopic composition of precipitation in the study area. $\delta D_{precipitation}$ from OIPC GIS gridded dataset [*Bowen*, 2012; *Bowen and Revenaugh*, 2003]. **c.** Latitudinal profiles of $\delta D_{precipitation}$ showing the monthly variation in $\delta D_{precipitation}$ for each sediment source area. Data points represent the mean of all OIPC cell values within each sediment source area. $\delta D_{precipitation}$ values plotted at the midpoint latitude of each sediment source area, except for area 10. The $\delta D_{precipitation}$ of area 10 is plotted at the latitude of the mouth of San Francisco Bay.

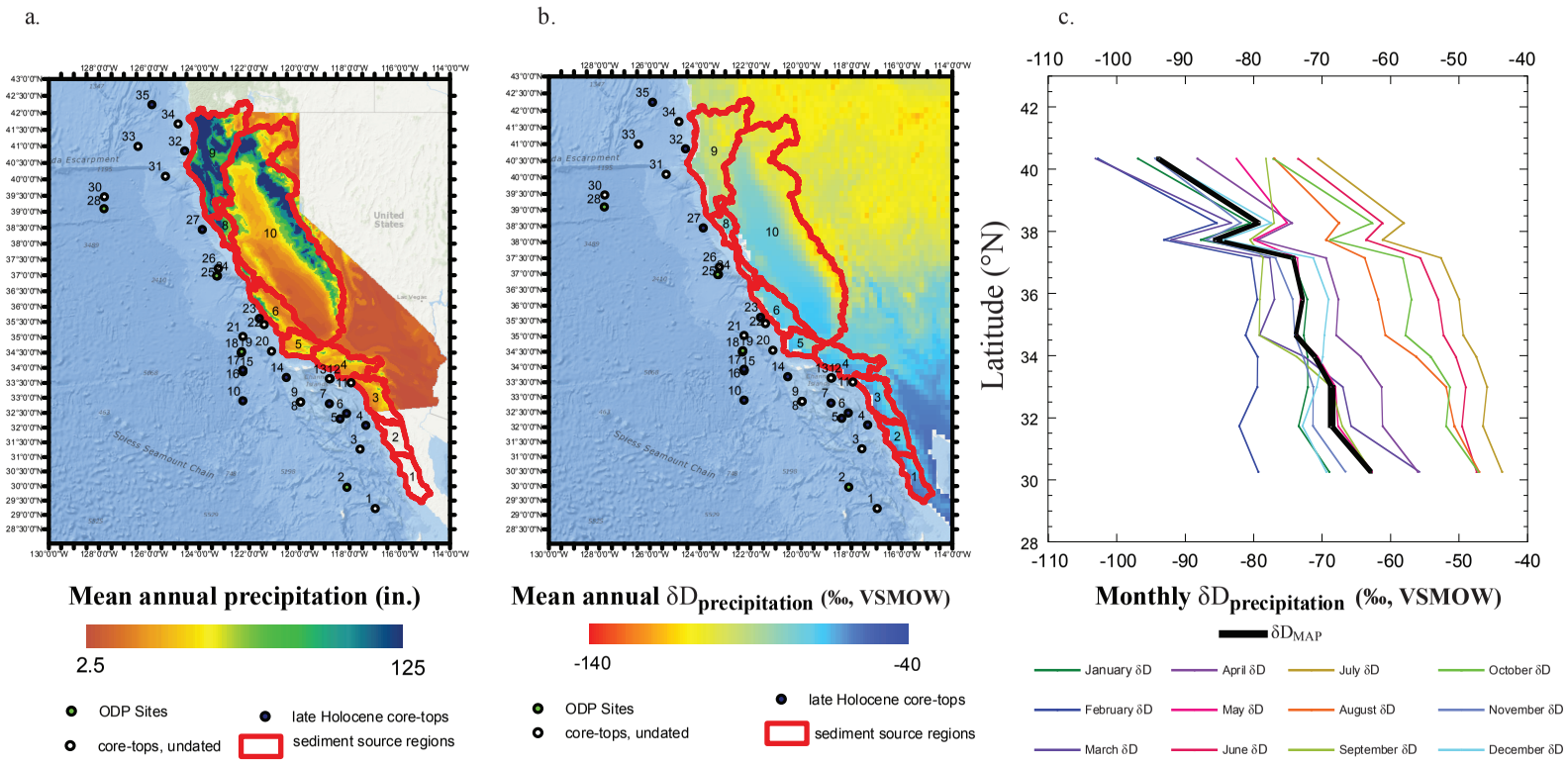
a.
b.
c.
Mean annual precipitation (in.)
2.5
125
ODP Sites
core-tops, undated
late Holocene core-tops
sediment source regions
Mean annual δD precipitation (‰, VSMOW)
-140
-40
ODP Sites
core-tops, undated
late Holocene core-tops
sediment source regions
Latitude (°N)
Monthly δD precipitation (‰, VSMOW)
δD MAP
January δD
February δD
March δD
April δD
May δD
June δD
July δD
August δD
September δD
October δD
November δD
December δD

Figure 1.

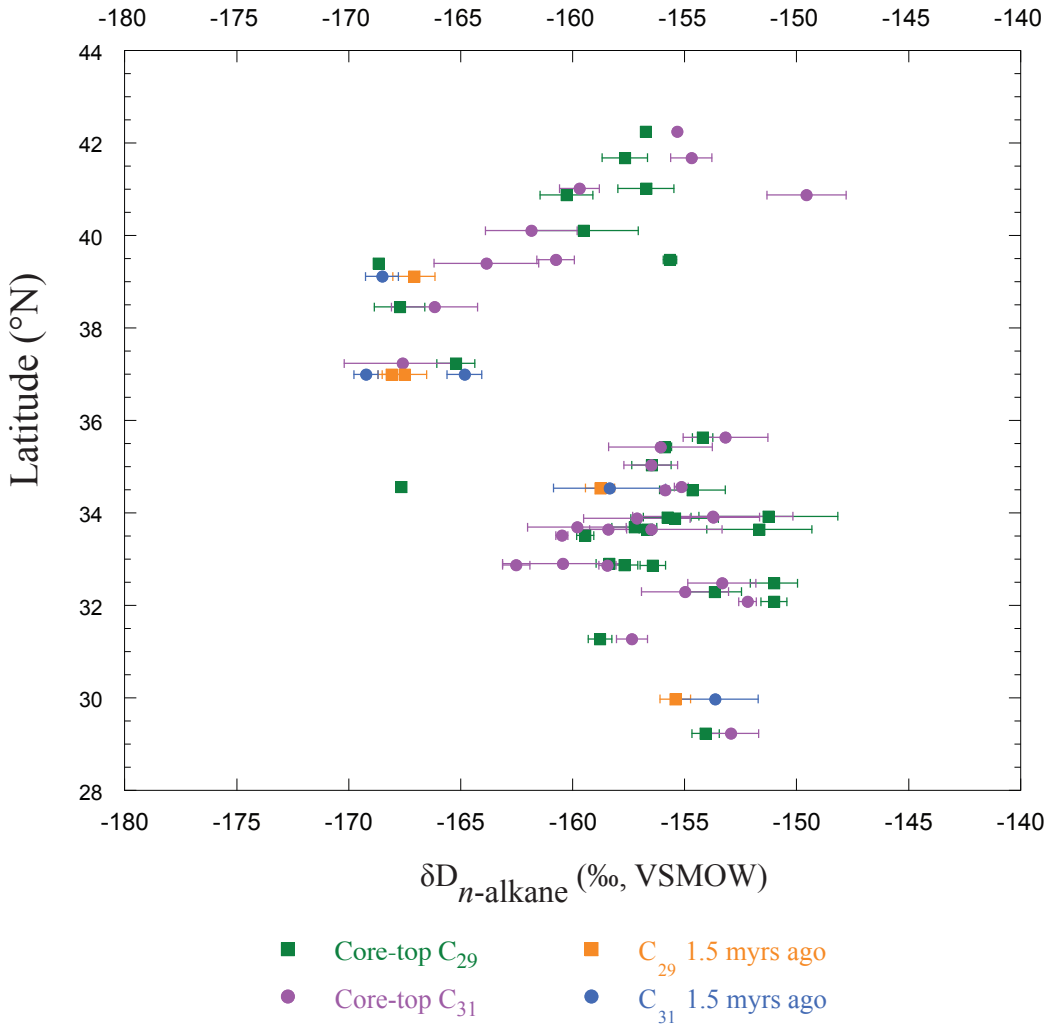

Figure 2. Core-top and early Pleistocene $\delta D_{n\text{-alkanes}}$. The mean of replicate analyses of C_{29} *n*-alkanes (squares) and C_{31} *n*-alkanes (circles) is plotted for late Holocene core-top (green, purple) and early Pleistocene (orange, blue) samples. Error bars show standard error of replicate analyses.

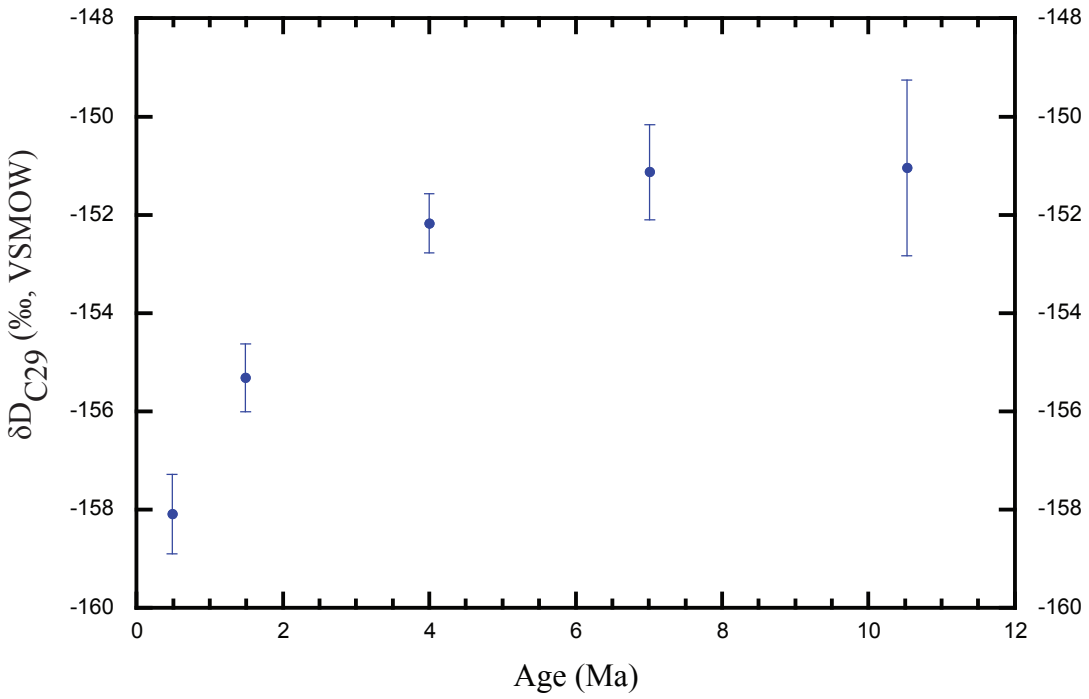

Figure 3. The downcore record of leaf wax δD at southern California Site 1010. Stable values persisted during the late Miocene and early Pliocene before trending towards lighter values. This long-term trend towards lighter δD values may reflect a shift to a more seasonal climate with dry summers and wet winters. Circles denote the mean of replicate analyses. Error bars show standard error of replicate analyses.

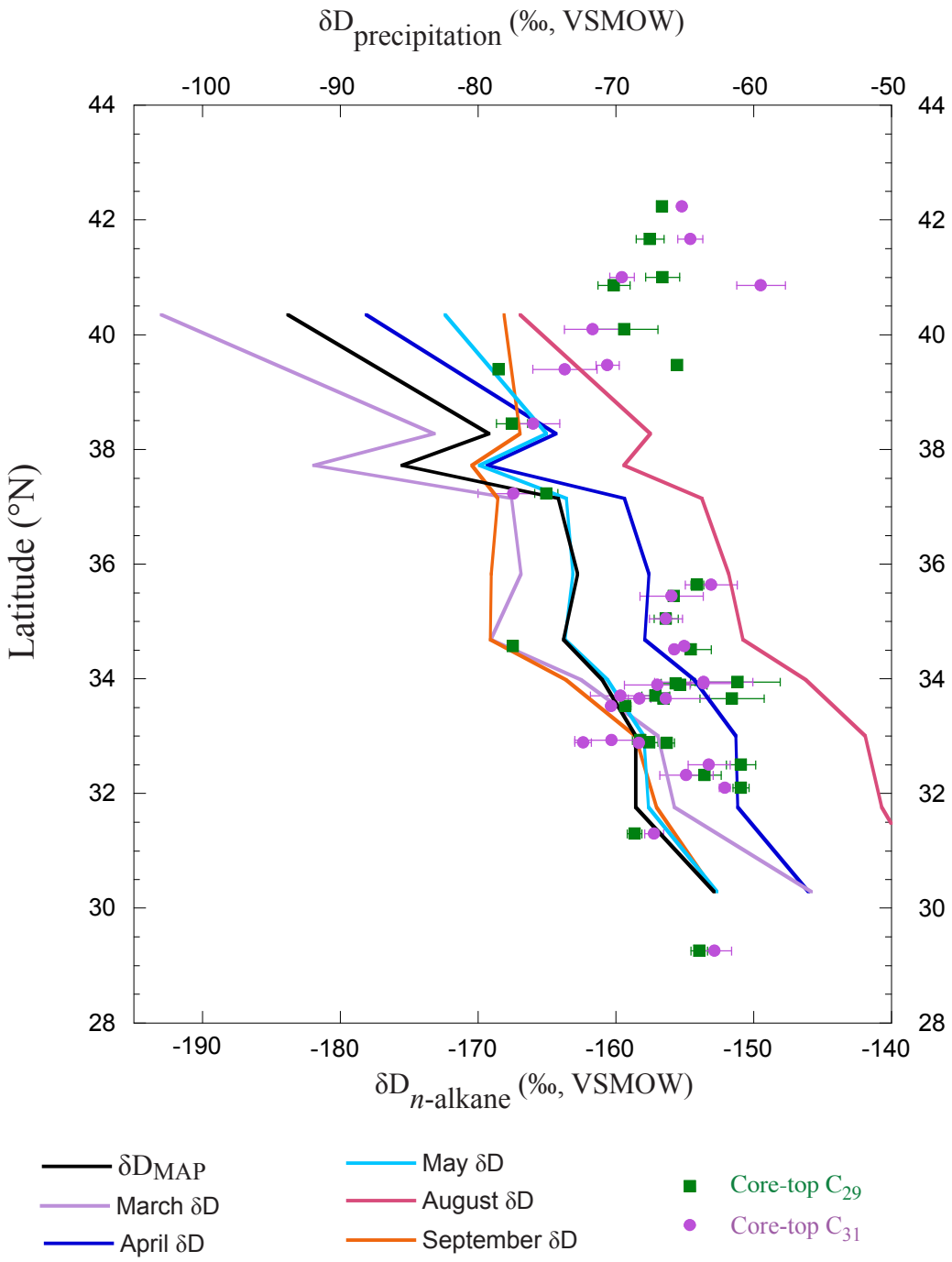

Figure 4. Core-top $\delta D_{n\text{-alkanes}}$ and $\delta D_{precipitation}$. The x axis of $\delta D_{precipitation}$ is shifted by 90‰ relative to the $\delta D_{n\text{-alkane}}$ axis. The mean of replicate analyses of C_{29} *n*-alkanes (squares) and C_{31} *n*-alkanes (circles) is plotted. Error bars show standard error of replicate analyses. $\delta D_{precipitation}$ of spring (March-May), late summer (August, September), and mean annual δD from figure 1c.

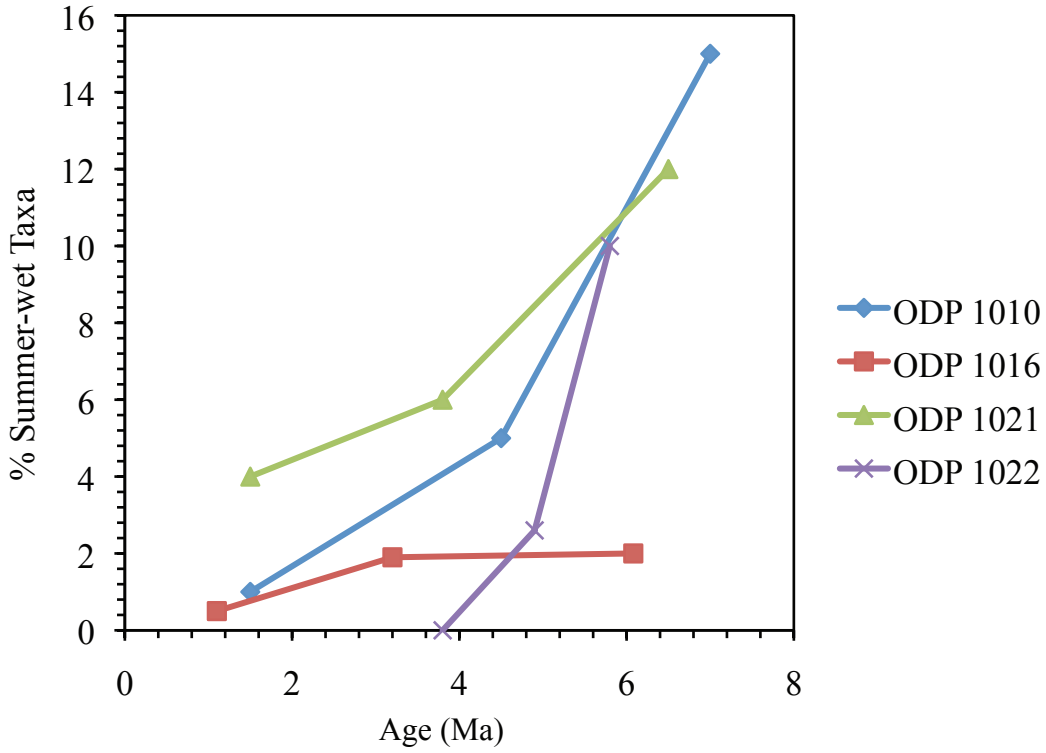

Figure 5. Pollen data from California Margin sites. All sites show a decline in the percentage of pollen indicative of summer-wet conditions since the latest Miocene. Pollen data from Heusser [*unpublished*].

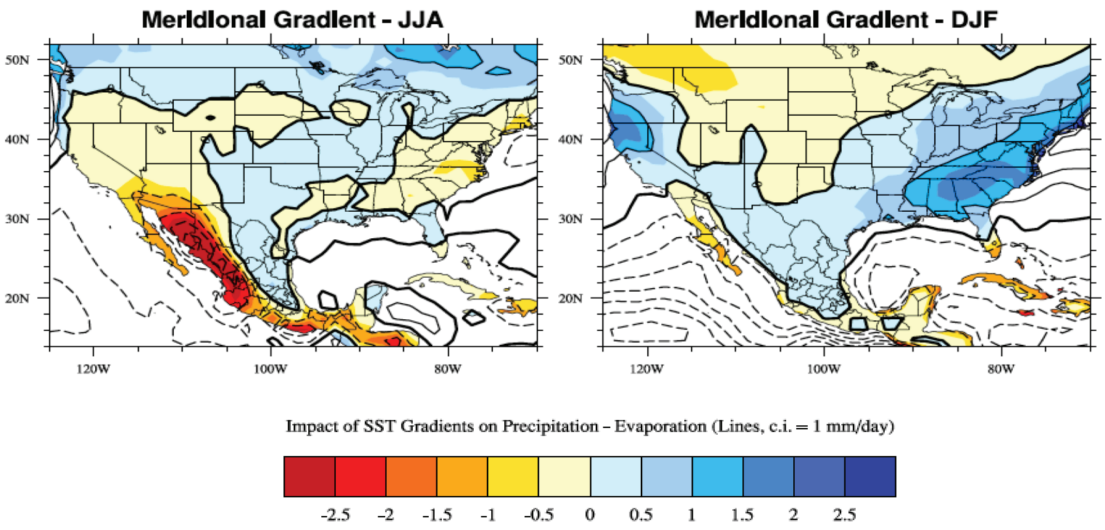

Figure 6. Model prediction of the response of P-E to increases in the tropical-subtropical (30°N – 30°S) SST meridional gradient (courtesy of Chris Brierley, based on experiments described in *Brierley and Fedorov* (2010)). Anomaly is the change in P-E that occurs when SST gradients are enhanced, as observed for the Miocene – present trend. The summer monsoon (left panel) is severely diminished, and the winter mid-latitude storms are enhanced (right panel), as global climate cools, SST gradients increase, and Hadley circulation intensifies since the late Miocene.

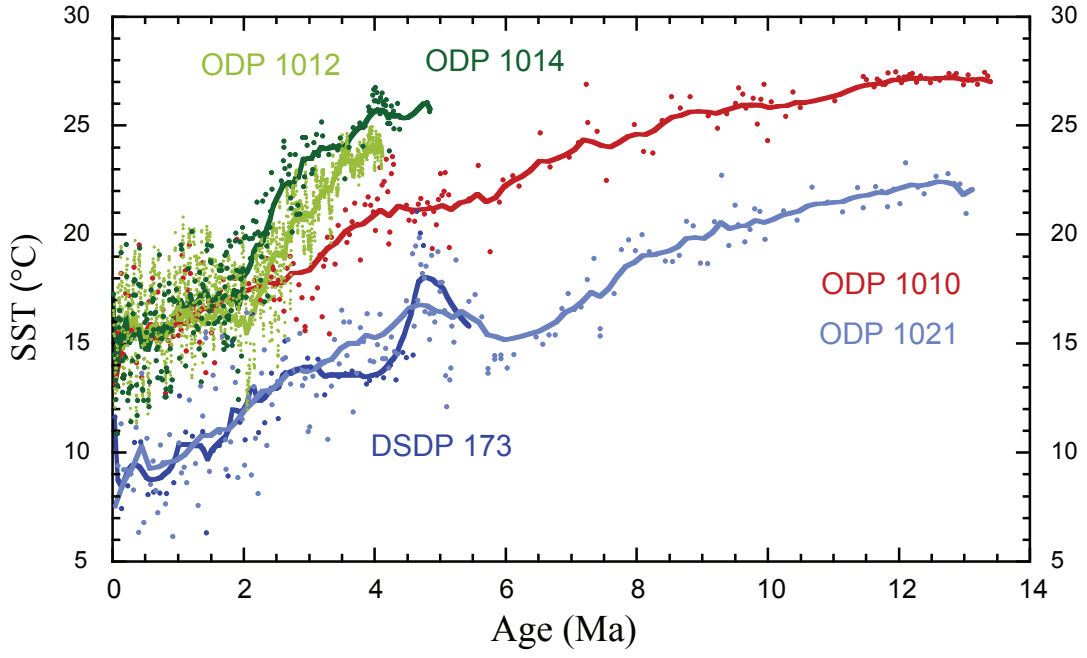

Figure 7. Alkenone based SST estimates. DSDP 173 and ODP 1021 are located in the northern California Current. ODP Sites 1012 and 1014 are located in the California Borderlands region of the southern California Current. ODP Site 1010 is located in the southern California Current. Alkenone SST estimates from Site 173 from Talmage [*UCSC senior thesis*, 2009]. SST records of Site 1012 from *Brierley et al.* [2009], Site 1014 from *Dekens et al.* [2007] Sites 1010 and 1021 from *LaRiviere et al.* [2012].

Table 1. Vegetation, precipitation amount, and isotopic composition of precipitation in sediment source regions

Map ID	Sediment source region	Maximum monthly $\delta D_{precipitation}$ (‰)[1]	Minimum monthly $\delta D_{precipitation}$ (‰)[1]	Mean annual $\delta D_{precipitation}$ (‰)[1]	Mean annual rainfall (inches)[2]	Major vegetation types[3]
1	North central Baja	-43.7	-79.3	-62.9	N/A	N/A
2	North Baja	-46.5	-82.1	-68.6	N/A	N/A
3	LA/San Diego	-45.9	-79.4	-68.6	17.4	southern oak forest coastal sagebrush chaparral
4	Santa Barbara	-47.5	-79.4	-71.0	19.7	coastal sagebrush southern oak forest chaparral mixed hardwood forest (minor)
5	Lompoc	-49.4	-81.2	-73.8	19.5	southern oak forest chaparral coastal sagebrush valley oak savanna Blue Oak-Digger Pine forest (minor)
6	Big Sur/Central Coast	-50.0	-79.5	-72.8	18.3	southern oak forest Blue Oak-Digger Pine forest California Prairie mixed hardwood forest mixed hardwood and redwood forest (minor) coastal sagebrush
7	Penninsula/North Monterey Bay	-52.6	-80.4	-74.2	30.6	redwood forest coastal prairie-scrub mosaic mixed hardwood forest (minor)
8	Russian River	-58.1	-85.4	-79.3	44.8	redwood forest coastal prairie-scrub mosaic mixed hardwood forest Blue Oak-Digger Pine forest valley oak savanna
9	North Coast	-70.6	-102.7	-93.9	58.9	redwood forest mixed evergreen forest w/ rhododendron Klamath montane forest with douglas fir mixed evergreen forest with chinquapin Klamath montane forest with yellow pine
10	Central Valley	-61.2	-93.1	-85.6	25.6	sagebrush steppe yellow pine shrub forest Sierran montane forest upper montane-subalpine forest Sierran yellow pine forest Blue Oak-Digger Pine forest California prairie Tule marsh

[1] data from *Bowen* [2012], *Bowen and Revenaugh* [2003], and *Bowen et al.* [2005]
[2] data from *CDF-FRAP* [2010]
[3] data from *Kulcher* [1990]

Table 2. Site information

Map ID	Site/Core	Core-top interval (cm)	Latitude (°N)	Longitude (°W)	late Holocene confirmation	Proximal sediment source
1	Y7302003P	9.5-11.5	29.2	117.0		North central Baja
2	ODP Site 1010		30.0	118.1		North central Baja
3	EW9504-02pc	5-7	31.3	117.6		Northern Baja
4	EW9504-03pc	5-7	32.1	117.4	*Stott et al.*, 2000	Northern Baja/LA San Diego
5	EW9504-04pc	5-7	32.3	118.4	*Stott et al.*, 2000	LA San Diego
6	EW9504-05pc	5-7	32.5	118.1	*Stott et al.*, 2000	LA San Diego
7	EW9504-08pc	5-7	32.8	118.8	*Stott et al.*, 2000	LA San Diego
8	EW9504-09pc	5-8	32.9	120.0	*Stott et al.*, 2000	Offshore California Bight- LA San Diego/Santa Barbara/Lompoc
9	EW9504-10mc08	4-5	32.9	120.0		Offshore California Bight- LA San Diego/Santa Barbara/Lompoc
10	F2-92-P29	sec 1, 17-19	32.9	122.3	*Gardner et al.*, 1997	Offshore California Bight- LA San Diego/Santa Barbara/Lompoc
11	0-2-99-SC 508 P1	12-14	33.5	117.9		LA San Diego
12	EW9504-06mc	sec 2, 5-7	33.6	118.8		Santa Barbara
13	EW9504-07pc	5-7	33.6	118.8		Santa Barbara
14	V1-81-G15	sec 1, 15-17	33.7	120.5	*Gardner et al.*, 1997	Offshore California Bight- LA San Diego/Santa Barbara/Lompoc
15	A-1-03-SC HEIN2-P1	10-14	33.9	122.3	*Normark et al.,* 2009	Offshore Lompoc
16	A-1-03 SC SMB2-P1	20-22	33.9	122.3	*Normark et al.,* 2009	Offshore Lompoc
17	A-1-03-SC SMB1-P1	9-11	33.9	122.3	*Normark et al.,* 2009	Offshore Lompoc
18	EW9504-11pc	5-7	34.5	122.3		Offshore Lompoc
19	ODP Site 1016		34.5	122.3		Offshore Lompoc
20	EW9504-12pc	5-7	34.5	121.1		Lompoc
21	F2-92-P34	sec 1, 8-10	35.0	122.3	*Gardner et al.*, 1997	Offshore Big Sur/Central Coast
22	F2-92-SC P40	sec 1, 22-26	35.4	121.4		Big Sur Central Coast
23	F2-92-SC P3	14-16	35.6	121.6	*Gardner et al.*, 1997	Big Sur Central Coast
24	ODP Site 1018		37.0	123.3		Penninsula/North Monterey Bay
25	EW9504-13pc	5-7	37.0	123.3		Penninsula/North Monterey Bay
26	F-8-90NC G21	10-12	37.2	123.2	*Gardner et al.*, 1997	Mouth of SF Bay/Penninsula/North Monterey Bay
27	V1-80-G1	2-6	38.4	123.9	*Gardner et al.*, 1997	Russian River
28	ODP Site 1021		39.1	127.8		Offshore North Coast
29	EW9504-14pc	5-7	39.4	133.1		Far offshore North Coast
30	TT141-06pc	5-7	39.5	127.8		Offshore North Coast
31	EW9504-15pc	5-7	40.1	125.4		North Coast
32	T-1-96NC (TN062)	68-70	40.9	124.6	*Stott et al.*, 2000	nearshore North Coast
33	EW9504-18pc	5-7	41.0	126.4		North Coast
34	EW9504-16pc	5-7	41.7	124.8		North Coast
35	EW9504-17pc	7-9	42.2	125.9	*Pisias et al.*, 2000	North Coast

Table 3. δD of *n*-alkanes

					δD of *n*-alkanes (‰)								
Map ID	Site/Core	Core-top interval (cm)	Latitude (°N)	Longitude (°W)	C_{27}[1]	C_{27} Std. error[2]	C_{29}	C_{29} Std. error	C_{31}	C_{31} Std. error	Number of replicates	CPI2	ACL
CORE-TOPS													
1	Y7302003P	9.5-11.5	29.2	117.0	-154.18	2.71	-153.96	0.61	-152.82	1.23	4	>10	29.57
3	EW9504-02pc	5-7	31.3	117.6	-160.36	0.88	-158.67	0.53	-157.25	0.69	3	8.91	29.68
4	EW9504-03pc	5-7	32.1	117.4	-158.1	0.64	-150.91	0.58	-152.09	0.4	5	8.20	29.81
5	EW9504-04pc	5-7	32.3	118.4	-158.14	0.1	-153.57	1.22	-154.88	1.94	4	6.48	29.95
6	EW9504-05pc	5-7	32.5	118.1	-153.46	2.69	-150.91	1.06	-153.23	1.52	5	10.71	29.72
7	EW9504-08pc	5-7	32.8	118.8	N/A	N/A	N/A	N/A	N/A	N/A	N/A	N/A	N/A
8	EW9504-09pc	5-8	32.9	120.0	-157.69	0.86	-156.32	0.56	-158.34	0.39	3	5.99	29.60
9	EW9504-10mc08	4-5	32.9	120.0	-159.06	1.04	-157.58	0.59	-162.41	0.6	3	8.89	29.66
10	F2-92-P29	sec 1, 17-19	32.9	122.3	-156.75	1.92	-158.25	0.58	-160.32	2.69	3	6.81	29.66
11	0-2-99-SC 508 P1	12-14	33.5	117.9	-162.97	2.43	-159.33	0.39	-160.37	0.27	3	10.12	29.92
12	EW9504-06mc	sec 2, 5-7	33.6	118.8	-163.46	3.96	-151.57	2.34	-156.38	3.16	3	>10	29.46
13	EW9504-07pc	5-7	33.6	118.8	-160.81	1.4	-156.57	0.35	-158.3	0.83	3	9.45	29.79
14	V1-81-G15	sec 1, 15-17	33.7	120.5	-165.74	0.08	-157.14	1.01	-159.69	2.2	4	8.99	29.73
15	A-1-03-SC HEIN2-P1	10-14	33.9	122.3	-162.84	1.77	-155.33	1.95	-157.02	2.38	4	9.26	29.84
16	A-1-03 SC SMB2-P1	20-22	33.9	122.3	-157.03	2.79	-155.67	1.06	-153.62	2.06	4	7.96	29.75
17	A-1-03-SC SMB1-P1	9-11	33.9	122.3	-168.1	2.16	-151.16	3.1	-153.64	3.57	3	9.46	29.98
18	EW9504-11pc	5-7	34.5	122.3	-156.34	0.1	-154.54	1.46	-155.77	0.19	3	6.94	29.51
20	EW9504-12pc	5-7	34.5	121.1	-167.89	0.91	-167.53	0.09	-155.04	0.31	3	6.44	28.77
21	F2-92-P34	sec 1, 8-10	35.0	122.3	-161.98	0.04	-156.37	0.88	-156.4	1.2	5	7.94	29.67
22	F2-92-SC P40	sec 1, 22-26	35.4	121.4	-155.3	3.2	-155.79	0.33	-155.97	2.31	3	7.72	29.60
23	F2-92-SC P3	14-16	35.6	121.6	-157.24	2.51	-154.09	0.45	-153.07	1.89	5	8.14	29.64
25	EW9504-13pc	5-7	37.0	123.3	N/A	N/A	N/A	N/A	N/A	N/A	N/A	N/A	N/A
26	F-8-90NC G21	10-12	37.2	123.2	-165.27	1.43	-165.09	0.85	-167.48	2.59	3	6.20	29.46
27	V1-80-G1	2-6	38.4	123.9	-170.61	2.51	-167.6	1.12	-166.05	1.92	5	5.93	29.22
29	EW9504-14pc	5-7	39.4	133.1	-157.8	1.72	-168.55	0.13	-163.73	2.33	3	4.26	29.06
30	TT141-06pc	5-7	39.5	127.8	-152.43	2.5	-155.55	0.3	-160.64	0.84	3	2.58	29.40
31	EW9504-15pc	5-7	40.1	125.4	-149.83	3.25	-159.39	2.43	-161.73	2.04	3	2.97	29.11
32	T-1-96NC (TN062)	68-70	40.9	124.6	-147.04	3.41	-160.17	1.17	-149.45	1.77	5	3.22	28.59
33	EW9504-18pc	5-7	41.0	126.4	-149.01	3.54	-156.62	1.25	-159.59	0.89	3	>10	28.36
34	EW9504-16pc	5-7	41.7	124.8	-147.86	1.03	-157.55	1.01	-154.6	0.92	3	2.63	28.63
35	EW9504-17pc	7-9	42.2	125.9	-148.39		-156.64		-155.24			2.50	28.82
Early Pleistocene transect													
2	ODP Site 1010	~1.5Ma	30.0	118.1	-150.27	1.31	-155.3	0.69	-153.54	1.93	4		
19	ODP Site 1016	~1.5Ma	34.5	122.3	-152.3	0.19	-158.66	0.65	-158.24	2.51	3		
24	ODP Site 1018	~1.5Ma	37.0	123.3	-167.82	1.08	-167.97	0.59	-169.1	0.54	3		
24	ODP Site 1018	~1.5Ma	37.0	123.3	-170.55	1.14	-167.39	0.99	-164.7	0.78	3		
28	ODP Site 1021	~1.5Ma	39.1	127.8	-155.16	0.72	-166.96	0.94	-168.39	0.74	3		
ODP 1010 down-core													
2	ODP Site 1010	~0.5Ma	30.0	118.1	-150.84	2.2	-158.06	0.81	-159.93	2.32	4		
2	ODP Site 1010	~4Ma	30.0	118.1	-151.48	1.77	-152.17	0.6	-153.78	0.8	8		
2	ODP Site 1010	~7Ma	30.0	118.1	-146.21	1.15	-151.13	0.96	-157.39	0.74	3		
2	ODP Site 1010	~10.5Ma	30.0	118.1	-148.34	0.51	-151.04	1.78	-154.22	0.63	2		

[1] Reported *n*-alkane values are the mean of replicate analyses.

[2] Std. error refers to the standard error of replicate analyses for each compound.

Chapter 5. Conclusions

This dissertation is comprised of three projects that aim to increase our understanding of the evolution of North Pacific climate since the late Miocene. Each of the projects used the geochemistry of marine sediments to reconstruct paleoceanographic and paleoclimate conditions during various intervals of the past ~13 myrs. These long-timescale studies enabled us to examine Earth system responses to diverse climate perturbations. The resulting work has highlighted the major role of the oceans in shaping global and regional climates.

In Chapter 2 of this dissertation, "Late Miocene decoupling of oceanic warmth and atmospheric carbon dioxide forcing," we compared new alkenone-based temperature data with published pCO_2 data to evaluate the relationship between them; we did not *a priori* assume that a relationship existed. The proxy records showed that during the late Miocene, ~12-5 Ma, SSTs from the mid-latitude North Pacific were substantially warmer-than-modern and decoupled from atmospheric pCO_2 concentrations. However, after ~5 Ma, possibly because of a tectonically forced shoaling of the global thermocline, SSTs became more sensitive to small changes in atmospheric pCO_2 and the coupling between atmospheric pCO_2 and climate increased through the Pliocene and Pleistocene epochs [*LaRiviere et al.*, 2012].

Because of the surprising findings in Chapter 2, the pCO_2 records of the late Miocene require critical examination. Currently there is less data available describing the late Miocene pCO_2 levels than is available for describing pCO_2 in the Pliocene and Pleistocene epochs; however, the balance of proxy-based evidence suggests that the pCO_2 of the late Miocene was near pre-industrial values [*LaRiviere et al.*, 2012]. This picture is consistent with two recently published multi-proxy studies that show pCO_2 values of ~300ppmv by ~13-14 Ma [*Foster et al.*, 2012; *Badger et al.*, *in* press]. However, even if the pCO_2 estimates for the late Miocene, ~12-5 Ma, are later revised to the uppermost estimates of ~400 ppmv [*LaRiviere et al.*, 2012 SI] the main premise of Chapter 2 will still hold: there would still have been a decoupling of the late Miocene SSTs (which are warmer than those of the early Pliocene) from the atmospheric pCO_2 levels (which, if revised, would be similar to those of the early Pliocene).

To better resolve the pCO_2 history of the late Miocene, multi-site/multi-proxy reconstructions are needed. However, pCO_2 reconstructions should not be the only target of paleoceanographers studying late Miocene climates—future work is needed to reconstruct the subsurface ocean circulation near changing oceanic gateways and to reconstruct the large-scale SST distributions of each ocean basin.

Chapter 3, "Basin-wide sea surface temperature distributions of the Pleistocene, Pliocene, and late Miocene," focuses on describing the spatial distribution of SSTs for

the global ocean using new and previously published data from the late Miocene, Pliocene, and Pleistocene. In Pliocene climate models, the spatial distribution of SSTs, specifically the basin-wide meridional SST gradient, has been identified as a potentially important contributor to global warmth [*Brierley et al.*, 2009; *Brierley and Fedorov*, 2010]. The increased sampling coverage in Chapter 3, compared to Chapter 2, enabled us to reconstruct the meridional SST gradient in the western Pacific from late Miocene, Pliocene, and Pleistocene time-slices and test the idea that weaker-than-modern basin-wide SST gradients were a prevalent feature of the late Miocene and early Pliocene climates. Of all the time-slices, the late Miocene showed the weakest meridional and zonal SST gradients. Heterogeneous regional cooling resulted in a long-term strengthening of basin-wide SST gradients through the more recent epochs.

To establish the SST distributions in data-poor regions, further SST reconstructions are needed, especially in the central regions of each ocean basin, the Southern Ocean, and the South Pacific. To more reliably reflect the different physical processes in each ocean basin and reduce the error associated with data gridding for each time-slice, future efforts to map the SSTs of each time-slice should aim to grid the SSTs of each ocean basin separately, mask land, and weigh available data based on the proxy-error and data quality. However, future work notwithstanding, the data in chapters 2 and 3 of this dissertation have begun to outline a transition from a relative decoupling of atmospheric pCO_2 and climate during the late Miocene, which featured relatively

weak basin-wide SST gradients, to a more coupled system in the Pliocene and Pleistocene, which featured stronger basin-wide SST gradients.

Chapter 4, "The utility of leaf-wax δD as a proxy for precipitation in coastal western North America: a core-top transect and down-core pilot study," assesses the potential of using the $\delta D_{n\text{-alkanes}}$ in California Margin sediments to reconstruct past changes in coastal western North American precipitation. A transect of California Margin core-tops showed that while northern and central California Margin sediments are not suitable for paleo-precipitation reconstructions, southern California Margin sedimentary *n*-alkanes could reliably record changes in the past precipitation of the western coast of North America. A low-resolution down-core study of southern California Margin sediments showed that $\delta D_{n\text{-alkane}}$ values are consistent with a progressive loss of summer precipitation through the late Pliocene and Pleistocene and may have resulted from the strengthening of basin-wide SST gradients during these times.

This study represents the first steps needed to test the effects of basin-wide SST distributions on a regional terrestrial climate system. Climate modeling results suggest that the strengthening of basin-wide SST gradients can affect the distribution and seasonality of precipitation in many regions around the globe [*Brierley et al.*, 2009]. This finding is especially relevant to studies of late Miocene climate because of both the prevalence of weak SST gradients and the evidence for wetter-than-

modern conditions in many regions [*Pound et al.*, 2011]. Future work, in the form of high-resolution multi-proxy precipitation reconstructions, is needed to better establish the timing of precipitation changes and to accurately indentify correlations between precipitation on land and SSTs.

Overall, the projects in this dissertation have helped outline a major change in the mean climate state that occurred during the latest Miocene/early Pliocene. They present several major questions about the Earth's climate system that are relevant not only to paleoclimatologists but also to researchers investigating and modeling modern climates. Which boundary conditions are most important for establishing the coupling between pCO_2 and ocean temperatures? How have changes in ocean basin shape affected ocean circulation and the depth of the global thermocline? How has the long-term evolution of basin-wide SST gradients affected the evolution of the hydrologic cycle on the continents? Answering each of these questions will require further study of deep-time climates that resulted from a wide range of atmospheric greenhouse gas, ocean circulation, and tectonic configurations.

References

Badger, M.P.S., C.H. Lear, R.D. Pancost, G.L. Foster, T.R. Bailey, M.J. Leng, and H.J. Abels (*in press*), CO_2 drawdown following the middle Miocene expansion of the Antarctic Ice Sheet, *Paleoceanography*.

Brierley, C. M., A. V. Fedorov, Z. H. Liu, T. D. Herbert, K. T. Lawrence, and J. P. LaRiviere (2009), Greatly expanded tropical warm pool and weakened Hadley circulation in the early Pliocene, *Science*, *323*(5922), 1714-1718.

Brierley, C. M., and A. V. Fedorov (2010), Relative importance of meridional and zonal sea surface temperature gradients for the onset of the ice ages and Pliocene-Pleistocene climate evolution, *Paleoceanography*, *25*, 16.

Foster, G.L., C.H. Lear, J.W.B Rae (2012), The evolution of pCO_2, ice volume and climate during the middle Miocene, *Earth and Planetary Science Letters*, 341-344, 243-254.

LaRiviere, J. P., A. C. Ravelo, A. Crimmins, P. S. Dekens, H. L. Ford, M. Lyle, and M. W. Wara (2012), Late Miocene decoupling of oceanic warmth and atmospheric carbon dioxide forcing, *Nature*, *486*(7401), 97-100.

Pound, M. J., A. M. Haywood, U. Salzmann, J. B. Riding, D. J. Lunt, and S. J. Hunter (2011), A Tortonian (Late Miocene, 11.61-7.25 Ma) global vegetation reconstruction, *Palaeogeography, Palaeoclimatology, Palaeoecology*, 300, 29-45.

Bibliography

Anand, P., H. Elderfield, and M. H. Conte (2003), Calibration of Mg/Ca thermometry in planktonic foraminifera from a sediment trap time series, *Paleoceanography*, *18*(2), 28-21 - 28-15.

Axelrod, D. (1977), Outline history of California vegetation, in *Terrestrial vegetation of California*, edited by M. Barbour and J. Major, pp. 139-194, John Wiley & Sons, New York.

Axelrod, D. I. (1939), *A Miocene Flora from the Western Border of the Mohave Desert*, Carnegie Institution of Washington, Washington, D. C.

Bac, M. G., K. R. Buck, F. P. Chavez, and S. C. Brassell (2003), Seasonal variation in alkenones, bulk suspended POM, plankton and temperature in Monterey Bay, California: implications for carbon cycling and climate assessment, *Organic Geochemistry*, *34*(6), 837-855.

Badger, M.P.S., C.H. Lear, R.D. Pancost, G.L. Foster, T.R. Bailey, M.J. Leng, and H.J. Abels (*in press*), CO_2 drawdown following the middle Miocene expansion of the Antarctic Ice Sheet, *Paleoceanography*.

Ballog, R. A., and R. E. Malloy (1981), Neogene palynology from the southern California continental borderland, Site 467, Deep Sea Drilling Project Leg 63, *Initial Reports of the Deep Sea Drilling Project*, *63*, 565-577.

Barker, S., I. Cacho, H. Benway, and K. Tachikawa (2005), Planktonic foraminiferal Mg/Ca as a proxy for past oceanic temperatures: a methodological overview and data compilation for the Last Glacial Maximum, *Quaternary Science Reviews*, *24*(7-9), 821-834.

Barron, J., L. Heusser, T. Herbert, and M. Lyle (2003), High-resolution climatic evolution of coastal northern California during the past 16,000 years, *Paleoceanography*, *18*, doi:1029/2002PA000768,002003.

Bartoli, G., B. Honisch, and R. E. Zeebe (2011), Atmospheric CO_2 decline during the Pliocene intensification of Northern Hemisphere glaciations, *Paleoceanography*, *26*, 14.

Beerling, D. J., and D. L. Royer (2011), Convergent Cenozoic CO_2 history, *Nature Geoscience*, *4*(7), 418-420.

Beerling, D. J., A. Fox, and C. W. Anderson (2009), Quantitative uncertainty analyses of ancient atmospheric CO_2 estimates from fossil leaves, *American Journal of Science*, *309*(9), 775-787.

Benson, L., and H. Klieforth (1989), Stable isotopes in precipitation and ground water in the Yucca Mountain region, southern Nevada: Paleoclimatic Implications, in *Aspects of Climate Variability in the Pacific and the Western Americas*, edited by D. Peterson, p. 445, American Geophysical Union, Washington, D.C.

Boccaletti, G., R. C. Pacanowski, S. G. H. Philander, and A. V. Fedorov (2004), The thermal structure of the upper ocean, *Journal of Physical Oceanography*, *34*(4), 888-902.

Bowen, G. J. (2012), Gridded maps of the isotopic composition of meteoric waters, http://www.waterisotopes.org.

Bowen, G. J., and J. Revenaugh (2003), Interpolating the isotopic composition of modern meteroic precipitation, *Water Resources Research*, *39*(10), doi:10.1029/2003WR002086.

Bowen, G. J., L. I. Wassenaar, and K. A. Hobson (2005), Global application of stable hydrogen and oxygen isotopes to wildlife forensics, *Oecologia*, *143*(3), 337-348.

Brierley, C. M., and A. V. Fedorov (2010), Relative importance of meridional and zonal sea surface temperature gradients for the onset of the ice ages and Pliocene-Pleistocene climate evolution, *Paleoceanography*, *25*, 16.

Brierley, C. M., A. V. Fedorov, Z. H. Liu, T. D. Herbert, K. T. Lawrence, and J. P. LaRiviere (2009), Greatly expanded tropical warm pool and weakened Hadley circulation in the early Pliocene, *Science*, *323*(5922), 1714-1718.

California Department of Forestry and Fire Protection, CDF-FRAP (2010), Map of average annual rainfall 1900-1960, digitized from source map of S.E. Rantz, *US Geological survey, 1972*, Sacramento, CA.

Carton, J. A., and B. S. Giese (2008), A reanalysis of ocean climate using Simple Ocean Data Assimilation (SODA), *Monthly Weather Review*, *136*(8), 2999-3017.

Chaisson, W. P., and A. C. Ravelo (2000), Pliocene development of the east-west hydrographic gradient in the equatorial Pacific, *Paleoceanography*, *15*(5), 497-505.

Chiang, J. C. H. (2009), The Tropics in Paleoclimate, in *Annual Review of Earth and Planetary Sciences*, *37*, 263-297.

Clement, A. C. (2006), The role of the ocean in the seasonal cycle of the Hadley circulation, *Journal of the Atmospheric Sciences*, *63*(12), 3351-3365.

Corbosiero, K. L., M. J. Dickinson, and L. F. Bosart (2009), The Contribution of Eastern North Pacific Tropical Cyclones to the Rainfall Climatology of the Southwest United States, *Monthly Weather Review*, *137*(8), 2415-2435.

Crowley, B. E., and P. L. Koch (2007), The isotopic history of western North American grasslands, *EOS Transaction of the American Geophysical Union, 88*(52), *Fall Meeting Supplement*.

Dawson, T. E. (1996), The use of fog precipitation by plants in coastal redwood forests, in *Proceedings of the conference on coastal redwood forest ecology and management*, edited by J. LeBlanc, pp. 90-93, University of California Cooperative Extension Forestry Publication, Humboldt State University.

Dawson, T. E. (1998), Fog in the California redwood forest: ecosystem inputs and use by plants, *Oecologia*, *117*(4), 476-485.

de Garidel-Thoron, T., Y. Rosenthal, F. Bassinot, and L. Beaufort (2005), Stable sea surface temperatures in the western Pacific warm pool over the past 1.75 million years, *Nature*, *433*(7023), 294-298.

DeConto, R. M., D. Pollard, P. A. Wilson, H. Palike, C. H. Lear, and M. Pagani (2008), Thresholds for Cenozoic bipolar glaciation, *Nature*, *455*(7213), 652-656.

Dekens, P. S., and A. C. Ravelo (*in prep*), Sea surface temperatures from site 758.

Dekens, P. S., A. C. Ravelo, and M. McCarthy (2007), Warm upwelling regions in the Pliocene warm period, *Paleoceanography, 22*(3), 12.

Dekens, P. S., D. W. Lea, D. K. Pak, and H. J. Spero (2002), Core top calibration of Mg/Ca in tropical foraminifera: Refining paleotemperature estimation, *Geochemistry Geophysics Geosystems*, *3*(4), 29.

Dekens, P. S., A. C. Ravelo, M. D. McCarthy, and C. A. Edwards (2008), A 5 million year comparison of Mg/Ca and alkenone paleothermometers, *Geochemistry Geophysics Geosystems*, *9*(10), 18.

Diefendorf, A. F., K. H. Freeman, S. L. Wing, and H. V. Graham (2011), Production of *n*-alkyl lipids in living plants and implications for the geologic past, *Geochimica Et Cosmochimica Acta*, *75*(23), 7472-7485.

Drenzek, N.J. (2007), The temporal dynamics of terrestrial organic matter transfer to the oceans: Initial assessment and application, PhD thesis, Massachusetts Institute of Technology and the Woods Hole Oceanographic Institution, Woods Hole, Massachusetts, United States.

Drenzek, N.J., K.H. Hughen, D.B. Montlucon, J.R. Southon, G.M. dos Santos, E.R.M. Druffel, L. Giosan, and T.I. Eglinton (2009), A new look at old carbon in active margin sediments, *Geology*, *37*(3), 239-242.

Eglinton, T. I., and G. Eglinton (2008), Molecular proxies for paleoclimatology, *Earth and Planetary Science Letters*, *275*(1-2), 1-16.

Ekart, D. D., T. E. Cerling, I. P. Montanez, and N. J. Tabor (1999), A 400 million year carbon isotope record of pedogenic carbonate: Implications for paleoatmospheric carbon dioxide, *American Journal of Science*, *299*(10), 805-827.

Etourneau, J., P. Martinez, T. Blanz, and R. Schneider (2009), Pliocene-Pleistocene variability of upwelling activity, productivity, and nutrient cycling in the Benguela region, *Geology*, *37*(10), 871-874.

Etourneau, J., R. Schneider, T. Blanz, and P. Martinez (2010), Intensification of the Walker and Hadley atmospheric circulations during the Pliocene-Pleistocene climate transition, *Earth and Planetary Science Letters*, *297*(1-2), 103-110.

Evans, H. F., J. E. T. Channell, and W. W. Sager (2005), Late Miocene-Holocene magnetic polarity stratigraphy and astrochronology, ODP Leg 198, Shatsky Rise, *Proceedings of the Ocean Drilling Program, Scientific Results*, *198*, 39.

Expedition 323 Scientsits (2011), Site U1340, *Proceedings of the Integrated Ocean Drilling Program*, 323, 1-81.

Expedition 18 Scientists (1973), Site 173, *Initial Reports of the Deep Sea Drilling Program,* XVII, 31-96.

Feakins, S. J. (*in press*), Pollen-corrected leaf wax D/H reconstructions of northeast African hydrological changes during the late Miocene, *Palaeogeography Palaeoclimatology Palaeoecology*.

Feakins, S. J., and A. L. Sessions (2010), Controls on the D/H ratios of plant leaf waxes in an arid ecosystem, *Geochimica et Cosmochimica Acta*, *74*(7), 2128-2141. doi:10.1016/j.gca.2010.1001.1016.

Fedorov, A., C. Brierley, and K. Emanuel (2010), Tropical cyclones and permanent El Nino in the early Pliocene epoch, *Nature*, *463*, 1066-1071.

Fedorov, A. V., P. S. Dekens, M. McCarthy, A. C. Ravelo, P. B. deMenocal, M. Barreiro, R. C. Pacanowski, and S. G. Philander (2006), The Pliocene paradox (mechanisms for a permanent El Niño), *Science*, *312*(5779), 1485-1489.

Fites-Kaufman, J., P. Rundel, N. Stephenson, and D. A. Weixelman (2007), Montane and subalpine vegetation of the Sierra Nevada and Cascade ranges, in *Terrestrial Vegetation of California, 3rd ed.*, edited by M. Barbour, p. 734, University of California Press, Berkeley.

Ford, H. L., A. C. Ravelo, and S. Hovan (2012), A deep Eastern Equatorial Pacific thermocline during the early Pliocene warm period, *Earth and Planetary Science Letters*, *355-356*, 152-161.

Foster, G., D. Lunt, and R. Parrish (2010), Mountain uplift and the glaciation of North America - a sensitivity study, *Climate of the Past, 6*, 707-717.

Foster, G. L. (2008), Seawater pH, pCO_2 and CO_3^{2-} variations in the Caribbean Sea over the last 130 kyr: A boron isotope and B/Ca study of planktic forminifera, *Earth and Planetary Science Letters*, *271*(1-4), 254-266.

Freeman, K. H., and J. M. Hayes (1992), Fractionation of carbon isotopes by phytoplankton and estimates of ancient CO_2 levels, *Global Biogeochemical Cycles*, *6*(2), 185-198.

Friedman, I., G. I. Smith, J. D. Gleason, A. Warden, and J. M. Harris (1992), Stable Isotope Composition of Waters in Southeastern California 1. Modern Precipitation, *Journal of Geophysical Research-Atmospheres*, *97*(D5), 5795-5812.

Gardner, J. V., W. E. Dean, and P. Dartnell (1997), Biogenic sedimentation beneath the California Current system for the past 30 kyr and its paleoceanographic significance, *Paleoceanography*, *12*(2), 207-225.

Goyet, C., R. J. Healy, and J. P. Ryan (2000), Global distribution of total inorganic carbon and total alkalinity below the deepest winter mixed layer depths, edited by O. R. N. L. Carbon Dioxide Information Analysis Center, U.S. Department of Energy, Oak Ridge, Tennessee, 40.

Griggs, G. B., and J. R. Hein (1980), Sources, dispersal, and clay mineral composition of fine-grained sediment off central and northern California, *Journal of Geology*, *88*(5), 541-566.

Groeneveld, J. (2005), Effect of the Pliocene closure of the Panamanian Gateway on Caribbean and East Pacific sea surface temperatures and salinities by applying combined Mg/Ca and d18O measurements (5.6–2.2 Ma), PhD thesis, University of Kiel, Kiel, Germany.

Groeneveld, J., S. Steph, R. Tiedemann, D. Garbe-Schonberg, D. Nurnberg, and A. Sturm (2006), Pliocene mixed-layer oceanogrpahy for Site 1241 using combined Mg/Ca and d18O analyses of *Globigerinoides sacculifer*, *Proceedings of the Ocean Drilling Program Scientific Results*, *202,* 27.

Hansen, J., M. Sato, P. Kharecha, D. Beerling, R. Berner, V. Masson-Delmotte, M. Pagani, M. Raymo, D. L. Royer, and J. C. Zachos (2008), Target atmospheric CO_2: Where should humanity aim?, *The Open Atmospheric Science Journal*, *2*, 217-231.

Harada, N., K. H. Shin, A. Murata, M. Uchida, and T. Nakatani (2003), Characteristics of alkenones synthesized by a bloom of Emiliania huxleyi in the Bering Sea, *Geochimica Et Cosmochimica Acta*, *67*(8), 1507-1519.

Haug, G. (1995), Zur Paläo-Ozeanographie und Sedimentationsgeschichte im Nordwest-Pazifik während der letzten 6 Millionen Jahre (ODP-Site 882), PhD thesis, Institute for Geosciences, Christian Albrechts University, Kiel, Germany.

Haug, G. H., et al. (2005), North Pacific seasonality and the glaciation of North America 2.7 million years ago, *Nature*, *433*(7028), 821-825.

Hein, J. R., J. S. Dowling, A. Schuetze, and H. J. Lee (2003), Clay-mineral suites, sources, and inferred dispersal routes: Southern California continental shelf, *Marine Environmental Research*, *56*(1-2), 79-102.

Heinrichs, D.F. (1973), Paleomagnetic studies of sediments from DSDP Site 173, *Initial Reports of the Deep Sea Drilling Program*, XVII, 843-846.

Herbert, T. D., L. C. Peterson, K. T. Lawrence, and Z. H. Liu (2010), Tropical Ocean Temperatures Over the Past 3.5 Million Years, *Science*, *328*(5985), 1530-1534.

Herbert, T. D., and J. D. Schuffert (1998), Alkenone unsaturation estimates of late Miocene through late Pliocene sea-surface temperatures at Site 958, *Proceedings of the Ocean Drilling Program, Scientific Results*, *159T*, 17-21.

Herbert, T. D., J. D. Schuffert, D. Thomas, C. Lange, A. Weinheimer, A. Peleo-Alampay, and J. C. Herguera (1998), Depth and seasonality of alkenone production along the California margin inferred from a core top transect, *Paleoceanography*, *13*(3), 263-271.

Heusser, L.E. (*unpublished*), Pollen records from ODP Sites 1010, 1016, 1021, and 1022.

Hills, S. J., and H. R. Thierstein (1989), Plio-Pleistocene calcareous plankton biochronology, *Marine Micropaleontology*, *14*(1-3), 67-96.

Hönisch, B., N. G. Hemming, D. Archer, M. Siddall, and J. F. McManus (2009), Atmospheric carbon dioxide concentration across the Mid-Pleistocene Transition, *Science*, *324*(5934), 1551-1554.

Hou, J. Z., W. J. D'Andrea, and Y. S. Huang (2008), Can sedimentary leaf waxes record D/H ratios of continental precipitation? Field, model, and experimental assessments, *Geochimica Et Cosmochimica Acta*, *72*(14), 3503-3517.

Huang, Y., S. C. Clemens, W. Liu, Y. Wang, and W. L. Prell (2007), Large-scale hydrological change drove the late Miocene C4 plant expansion in the Himalayan foreland and Arabian Peninsula, *Geology*, *35*(6), 531-534.

Indermuhle, A., E. Monnin, B. Stauffer, T. F. Stocker, and M. Wahlen (2000), Atmospheric CO_2 concentration from 60 to 20 kyr BP from the Taylor Dome ice core, Antarctica, *Geophysical Research Letters*, *27*(5), 735-738.

Jeng, W. L. (2006), Higher plant *n*-alkane average chain length as an indicator of petrogenic hydrocarbon contamination in marine sediments, *Marine Chemistry*, *102*(3-4), 242-251.

Jia, G., F. Chen, and P. A. Peng (2008a), Sea surface temperature differences between the western equatorial Pacific and northern South China Sea since the Pliocene and their paleoclimatic implications, *Geophysical Research Letters*, *35,* 1-5.

Jia, G., K. Wei, F. Chen, and P. A. Peng (2008b), Soil *n*-alkane δD vs. altitude gradients along Mount Gongga, China, *Geochimica et Cosmochimica Acta*, *72*(21), 5165.

Jia, G., Z. Li, P. Peng, and L. Zhou (2012), Aeolian *n*-alkane isotopic evidence from North Pacific for a late Miocene decline of C_4 plant in the arid Asian interior, *Earth and Planetary Science Letters*, *321-322*, 32-40.

Johnstone, J. A., and T. E. Dawson (2010), Climatic context and ecological implications of summer fog decline in the coast redwood region, *Proceedings of the National Academy of Sciences of the United States of America*, *107*(10), 4533-4538.

Kamikuri, S., I. Motoyama, H. Nishi, and M. Iwai (2009), Evolution of Eastern Pacific Warm Pool and upwelling processes since the middle Miocene based on analysis of radiolarian assemblages: Response to Indonesian and Central American Seaways, *Palaeogeography Palaeoclimatology Palaeoecology*, *280*(3-4), 469-479.

Karas, C., D. Nürnberg, R. Tiedemann, and D. Garbe-Schonberg (2011a), Pliocene climate change of the Southwest Pacific and the impact of ocean gateways, *Earth and Planetary Science Letters*, *301*(1-2), 117-124.

Karas, C., D. Nürnberg, R. Tiedemann, and D. Garbe-Schonberg (2011b), Pliocene Indonesian Throughflow and Leeuwin Current dynamics: Implications for Indian Ocean polar heat flux, *Paleoceanography*, *26,* 1-9.

Karas, C., D. Nürnberg, A. K. Gupta, R. Tiedemann, K. Mohan, and T. Bickert (2009), Mid-Pliocene climate change amplified by a switch in Indonesian subsurface throughflow, *Nature Geoscience*, *2*(6), 433-437.

Keller, G. (1985), Depth Stratification of planktonic foraminifers in the Miocene ocean, *Geological Society of America Memoirs*, *163*, 177-195.

Kennett, J. P., G. Keller, and M. S. Srinivasan (1985), Miocene planktonic foraminiferal biogeography and paleoceanographic development of the Indo-Pacific region, *Geological Society of America Memoirs*, *163*, 197-236.

Key, R. M., A. Kozyr, C. L. Sabine, K. Lee, R. Wanninkhof, J. L. Bullister, R. A. Feely, F. J. Millero, C. Mordy, and T. H. Peng (2004), A global ocean carbon climatology: Results from Global Data Analysis Project (GLODAP), *Global Biogeochemical Cycles*, *18*(4), 1-23.

Knorr, G., M. Butzin, A. Micheels, and G. Lohmann (2011), A warm Miocene climate at low atmospheric CO_2 levels, *Geophysical Research Letters*, *38*.

Krivoruchko, K. (2011), *Spatial Statistical Data Analysis for GIS Users*, Esri Press, Redlands, California, 928.

Kulcher, A. W. (1990), Natural vegetation of California (Map), in *Terrestrial vegetation of California*, edited by M. G. Barbour and J. Major, Native Plant Society, Special Publication Number 9, p.1020, Davis, CA.

Kürschner, W. M., J. vanderBurgh, H. Visscher, and D. L. Dilcher (1996), Oak leaves as biosensors of late Neogene and early Pleistocene paleoatmospheric CO_2 concentrations, *Marine Micropaleontology*, *27*(1-4), 299-312.

Kürschner, W. M., and Z. Kvacek (2009), Oligocene-Miocene CO_2 fluctuations, climatic and palaeofloristic trends inferred from fossil plant assemblages in central Europe, *Bulletin of Geosciences*, *84*(2), 189-202.

LaRiviere, J. P., A. C. Ravelo, H. Ford, and M. Aung (*in prep.*), Basin-wide sea surface temperature distributions of the Pleistocene, Pliocene, and late Miocene.

LaRiviere, J. P., A. C. Ravelo, A. Crimmins, P. S. Dekens, H. L. Ford, M. Lyle, and M. W. Wara (2012), Late Miocene decoupling of oceanic warmth and atmospheric carbon dioxide forcing, *Nature*, *486*(7401), 97-100.

Lawrence, K. T., and T. D. Herbert (2005), Late quaternary sea-surface temperatures in the western Coral Sea: Implications for the growth of the Australian Great Barrier Reef, *Geology*, *33*(8), 677-680.

Lawrence, K. T., Z. H. Liu, and T. D. Herbert (2006), Evolution of the eastern tropical Pacific through Plio-Pleistocene glaciation, *Science*, *312*(5770), 79-83.

Lawrence, K. T., T. D. Herbert, P. S. Dekens, and A. C. Ravelo (2007), The application of the alkenone organic proxy to the study of Plio-Pleistocene climate, in *Deep-Time Perspectives on Climate Change: Marrying the Signal from Computer Models and Biological Proxies*, edited by M. Williams, A. M. Haywood, F. J. Gregory and D. N. Schmidt, pp. 539-562, The Geological Society, London.

Lawrence, K. T., S. Sosdian, H. E. White, and Y. Rosenthal (2010), North Atlantic climate evolution through the Plio-Pleistocene climate transitions, *Earth and Planetary Science Letters*, *300*(3-4), 329-342.

Lawrence, K. T., T. Herbert, C. Brown, M. Raymo, and A. Haywood (2009), High-amplitude variations in North Atlantic sea surface temperature during the early Pliocene warm period, *Paleoceanography*, *24*, 1-15.

Lear, C. H., Y. Rosenthal, and J. D. Wright (2003), The closing of a seaway: ocean water masses and global climate change, *Earth and Planetary Science Letters*, *210*(3-4), 425-436.

Li, C., A. L. Sessions, F. S. Kinnaman, and D. L. Valentine (2009), Hydrogen-isotopic variability in lipids from Santa Barbara Basin sediments, *Geochimica et Cosmochimica Acta*, *73*(16), 4803-4823.

Li, L., Q. Y. Li, J. Tian, P. X. Wang, H. Wang, and Z. H. Liu (2011), A 4-Ma record of thermal evolution in the tropical western Pacific and its implications on climate change, *Earth and Planetary Science Letters*, *309*(1-2), 10-20.

Lisiecki, L. E., and M. E. Raymo (2005), A Pliocene-Pleistocene stack of 57 globally distributed benthic $\delta^{18}O$ records, *Paleoceanography*, *20*(1), 17.

Liu, W., and H. Yang (2008), Multiple controls for the variability of hydrogen isotopic compositions in higher plant *n*-alkanes from modern ecosystems, *Global Change Biology*, *14*(9), 2166-2177.

Locarnini, R. A., A. V. Mishonov, J. I. Antonov, T. P. Boyer, and H. E. Garcia (2006), Temperature, in *World Ocean Atlas 2005, NOAA Atlas NESDIS 61*, edited by S. Levitus, p. 182, U.S. Government Printing Office, Washington, D.C.

Locarnini, R. A., A. V. Mishonov, J. I. Antonov, T. P. Boyer, H. E. Garcia, O. K. Baranova, M. M. Zweng, and D. R. Johnson (2010), World Ocean Atlas 2009 Volume 1: Temperature, edited by S. Levitus, *NOAA Atlas NESDIS 68*, U.S. Government Printing Office, Washington, D.C.

Lunt, D., G. Foster, A. Haywood, and E. Stone (2008), Late Pliocene Greenland glaciation controlled by a decline in atmospheric CO_2 levels, *Nature, 454,* 1102-1105.

Lunt, D. J., P. J. Valdes, A. Haywood, and I. C. Rutt (2007), Closure of the Panama Seaway during the Pliocene: implications for climate and Northern Hemisphere glaciation, *Climate Dynamics*, *30*(1), 1-18.

Luthi, D., et al. (2008), High-resolution carbon dioxide concentration record 650,000-800,000 years before present, *Nature*, *453*(7193), 379-382.

Lyle, M. (1997), Reconstructed geographic positions and water depths for Leg 167 drill sites, *Proceedings of the Ocean Drilling Program, Initial Reports*, *167*, 41-46.

Lyle, M., I. Koizumi, C. Richter, and Leg 167 Shipboard Scientific Party (1997), *Proceedings of the Ocean Drilling Program, Initial Reports*, *167*.

Lyle, M., J. Barron, T. J. Bralower, M. Huber, A. Olivarez-Lyle, A. C. Ravelo, D. K. Rea, and P. A. Wilson (2008), Pacific Ocean and Cenozoic evolution of climate, *Reviews of Geophysics*, *46*, 47.

Marlow, J. R., C. B. Lange, G. Wefer, and A. Rosell-Mele (2000), Upwelling intensification as part of the Pliocene-Pleistocene climate transition, *Science*, *290*(5500), 2288-2291.

Martínez-Garcia, A., A. Rosell-Melé, E. L. McClymont, R. Gersonde, and G. H. Haug (2010), Subpolar Link to the Emergence of the Modern Equatorial Pacific Cold Tongue, *Science*, *328*(5985), 1550-1553.

Marzi, R., B. E. Torkelson, and R. K. Olson (1993), A revised carbon preference index, *Organic Geochemistry*, *20*(8), 1303-1306.

Mashiotta, T. A., D. W. Lea, and H. J. Spero (1999), Glacial-interglacial changes in Subantarctic sea surface temperature and δ^{18}O-water using foraminiferal Mg, *Earth and Planetary Science Letters*, *170*(4), 417-432.

Mayer, A.L., E. Jansen, J. Backman, and T. Takayama (1993), Climatic cyclicity at site 806: the GRAPE record, *Proceedings of the Ocean Drilling Program, Scientific Results* 130, 623-639.

McClymont, E. L., and A. Rosell-Melé (2005), Links between the onset of modern Walker circulation and the mid-Pleistocene climate transition, *Geology*, *33*(5), 389-392.

McClymont, E. L., A. Rosell-Mele, J. Giraudeau, C. Pierre, and J. M. Lloyd (2005), Alkenone and coccolith records of the mid-Pleistocene in the south-east Atlantic: Implications for the $U^{k'}_{37}$ index and South African climate, *Quaternary Science Reviews*, *24*(14-15), 1559-1572.

Minnich, R. A. (2007), California climate, paleoclimate and paleovegetation, in *Terrestrial Vegetation of California, 3rd ed.*, edited by M. Barbour, p.734, University of California Press, Berkeley.

Monnin, E., A. Indermuhle, A. Dallenbach, J. Fluckiger, B. Stauffer, T. F. Stocker, D. Raynaud, and J. M. Barnola (2001), Atmospheric CO_2 concentrations over the last glacial termination, *Science*, *291*(5501), 112-114.

Mosbrugger, V., and T. Utescher (1997), The coexistence approach - a method for quantitative reconstructions of Tertiary terrestrial palaeoclimate data using plant fossils, *Palaeogeography Palaeoclimatology Palaeoecology*, *134*(1-4), 61-86.

Müller, P. J., G. Kirst, G. Ruhland, I. von Storch, and A. Rosell-Mele (1998), Calibration of the alkenone paleotemperature index $U^{k'}_{37}$ based on core-tops from the eastern South Atlantic and the global ocean (60°N-60° S), *Geochimica Et Cosmochimica Acta*, *62*(10), 1757-1772.

Naafs, B. D. A., R. Stein, J. Hefter, N. Khelifi, S. De Schepper, and G. H. Haug (2010), Late Pliocene changes in the North Atlantic Current, *Earth and Planetary Science Letters*, *298*(3-4), 434-442.

Nathan, S. A., and R. M. Leckie (2009), Early history of the Western Pacific Warm Pool during the middle to late Miocene (~13.2-5.8 Ma): Role of sea-level change and implications for equatorial circulation, *Palaeogeography Palaeoclimatology Palaeoecology*, *274*(3-4), 140-159.

Normark, W. R., M. McGann, and R. W. Sliter (2009), Late Quaternary sediment-accumulation rates within the inner basins of the California Continental Borderland in support of geologic hazard evaluation, in *Earth science in the urban ocean: the Southern California continental borderland*, edited by H. J. Lee and W. R. Normark, p.481, Geological Society of America, Boulder, Colorado.

Nürnberg, D., and J. Groeneveld (2006), Pleistocene variability of the Subtropical Convergence at East Tasman Plateau: Evidence from planktonic foraminiferal Mg/Ca (ODP Site 1172A), *Geochemistry Geophysics Geosystems*, *7*(4), 1-18.

Oros, D. R. (1999), Application of biomarker compounds as tracers for sources and fates of natural and anthropogenic organic matter in the environment, PhD thesis, Oregon State University, Corvallis, Oregon.

Pagani, M., K. H. Freeman, and M. A. Arthur (1999), Late Miocene atmospheric CO_2 concentrations and the expansion of C4 Grasses, *Science*, *285*, 876-879.

Pagani, M., M. A. Arthur, and K. H. Freeman (1999), Miocene evolution of atmospheric carbon dioxide, *Paleoceanography*, *14*(3), 273-292.

Pagani, M., D. Lemarchand, A. Spivack, and J. Gaillardet (2005), A critical evaluation of the boron isotope-pH proxy: The accuracy of ancient ocean pH estimates, *Geochimica Et Cosmochimica Acta*, *69*(4), 953-961.

Pagani, M., Z. H. Liu, J. LaRiviere, and A. C. Ravelo (2010), High Earth-system climate sensitivity determined from Pliocene carbon dioxide concentrations, *Nature Geoscience*, *3*(1), 27-30.

Pancost, R. D., and C.S. Boot (2004), The palaeoclimatic utility of terrestrial biomarkers in marine sediments, *Marine Chemistry*, *92*, 239-261.

Pares, J. M., and T. C. Moore (2005), New evidence for the Hawaiian hotspot plume motion since the Eocene, *Earth and Planetary Science Letters*, *237*(3-4), 951-959.

Pearson, A., and T. I. Eglinton (2000), The origin of *n*-alkanes in Santa Monica Basin surface sediment: a model based on compound-specific $\Delta^{14}C$ and $\delta^{13}C$ data, *Organic Geochemistry*, *31*(11), 1103-1116.

Pearson, P. N., and M. R. Palmer (2000), Atmospheric carbon dioxide concentrations over the past 60 million years, *Nature*, *406*(6797), 695-699.

Pepin, L., D. Raynaud, J. M. Barnola, and M. F. Loutre (2001), Hemispheric roles of climate forcings during glacial-interglacial transitions as deduced from the Vostok record and LLN-2D model experiments, *Journal of Geophysical Research-Atmospheres*, *106*(D23), 31885-31892.

Petit, J. R., et al. (1999), Climate and atmospheric history of the past 420,000 years from the Vostok ice core, Antarctica, *Nature*, *399*(6735), 429-436.

Philander, S. G., and A. V. Fedorov (2003), Role of tropics in changing the response to Milankovich forcing some three million years ago, *Paleoceanography*, *18*(2), 1045.

Pisias, N. G., A. C. Mix, and L. Heusser (2001), Millennial scale climate variability of the northeast Pacific Ocean and northwest North America based on radiolaria and pollen, *Quaternary Science Reviews*, *20*(14), 1561-1576.

Polissar, P. J., and K. H. Freeman (2010), Effects of aridity and vegetation on plant-wax δD in modern lake sediments, *Geochimica et Cosmochimica Acta*, *74*(20), 5785-5797.

Pound, M. J., A. M. Haywood, U. Salzmann, J. B. Riding, D. J. Lunt, and S. J. Hunter (2011), A Tortonian (Late Miocene, 11.61-7.25 Ma) global vegetation reconstruction, *Palaeogeography Palaeoclimatology Palaeoecology*, *300*, 29-45.

Prahl, F. G., and S. G. Wakeham (1987), Calibration of unsaturation patterns in long-chain ketone compositions for paleotemperature assessment, *Nature*, *330*(6146), 367-369.

Prahl, F. G., L. A. Muehlhausen, and D. L. Zahnle (1988), Further evaluation of long-chain alkenones as indicators of paleoceanographic conditions, *Geochimica Et Cosmochimica Acta*, *52*(9), 2303-2310.

Rack, F. R., T. R. Janecek, E. Erba, J. Fenner, and J. S. Gee (1995), Synthesis of terrigenous accumulation rates and biostratigraphic studies at sites in the northwestern Pacific Ocean, with comparisons to adjacent regions of the Pacific Gyre, *Proceedings of the Ocean Drilling Program. Scientific results*, *144*, 691-736.

Rackebrandt, N., H. Kuhnert, J. Groeneveld, and T. Bickert (2011), Persisting maximum Agulhas leakage during MIS 14 indicated by massive Ethmodiscus oozes in the subtropical South Atlantic, *Paleoceanography*, *26*, 1-13.

Ravelo, A. C., M. Lyle, I. Koizumi, J. P. Caulet, E. Fornaciari, A. Hayashida, F. Heider, J. Hood, S. Hovan, T. Janecek, A. Janik, R. Stax, M. Yamamoto, and the ODP Leg 167 Shipboard Scientific Party (1997), Pliocene carbonate accumulation along the California margin, *Paleoceanography*, *12*(6), 729-741.

Raven, P. H., and D. I. Axelrod (1978), *Origin and Relationships of the California Flora*, University of California Press, Berkeley.

Raymo, M. E., B. Grant, M. Horowitz, and G. H. Rau (1996), Mid-Pliocene warmth: Stronger greenhouse and stronger conveyor, *Marine Micropaleontology*, *27*(1-4), 313-326.

Raynaud, D., J. M. Barnola, R. Souchez, R. Lorrain, J. R. Petit, P. Duval, and V. Y. Lipenkov (2005), Palaeoclimatology - The record for marine isotopic stage 11, *Nature*, *436*(7047), 39-40.

Regenberg, M., D. Nurnberg, S. Steph, J. Groeneveld, D. Garbe-Schonberg, R. Tiedemann, and W. C. Dullo (2006), Assessing the effect of dissolution on planktonic foraminiferal Mg/Ca ratios: Evidence from Caribbean core tops, *Geochemistry Geophysics Geosystems*, *7* (7), 1-23.

Retallack, G. J. (2009a), Greenhouse crises of the past 300 million years, *Geological Society of America Bulletin*, *121*(9-10), 1441-1455.

Retallack, G. J. (2009b), Refining a pedogenic-carbonate CO_2 paleobarometer to quantify a middle Miocene greenhouse spike, *Palaeogeography Palaeoclimatology Palaeoecology*, *281*(1-2), 57-65.

Retallack, G. J., S. Tanaka, and T. Tate (2002), Late Miocene advent of tall grassland paleosols in Oregon, *Palaeogeography Palaeoclimatology Palaeoecology*, *183*(3-4), 329-354.

Rincón-Martinez, D., F. Lamy, S. Contreras, G. Leduc, E. Bard, C. Saukel, T. Blanz, A. Mackensen, and R. Tiedemann (2010), More humid interglacials in Ecuador during the past 500 kyr linked to latitudinal shifts of the equatorial front and the Intertropical Convergence Zone in the eastern tropical Pacific, *Paleoceanography*, *25*, 1-15.

Rodrigues, T., A. H. L. Voelker, J. O. Grimalt, F. Abrantes, and F. Naughton (2011), Iberian Margin sea surface temperature during MIS 15 to 9 (580-300 ka): Glacial suborbital variability versus interglacial stability, *Paleoceanography*, *26*, 1-16.

Rommerskirchen, F., T. Condon, G. Mollenhauer, L. Dupont, and E. Schefuß (2011), Miocene to Pliocene development of surface and subsurface temperatures in the Benguela Current system, *Paleoceanography*, *26*, 1-15.

Rosenthal, Y., and G. P. Lohmann (2002), Accurate estimation of sea surface temperatures using dissolution-corrected calibrations for Mg/Ca paleothermometry, *Paleoceanography*, *17*(3), 16-1 - 16-6.

Rousselle, G., C. Beltran, M.-A. Sicre, I. Raffi, and M. De Rafelis (2013), Changes in sea-surface conditions in the Equatorial Pacific during the middle Miocene-Pliocene as inferred from coccolith geochemistry, *Earth and Planetary Science Letters*, *361*, 412-421.

Royce, E. B., and M. G. Barbour (2001), Mediterranean climate effects. II. Conifer growth phenology across a Sierra Nevada ecotone, *American Journal of Botany*, *88*(5), 919-932.

Ruddiman, W. F. (2010), A Paleoclimatic Enigma?, *Science*, *328*(5980), 838-839.

Russon, T., M. Elliot, A. Sadekov, G. Cabioch, T. Correge, and P. De Deckker (2010), Inter-hemispheric asymmetry in the early Pleistocene Pacific warm pool, *Geophysical Research Letters*, *37*, 1-5.

Sachse, D., J. Radke, and G. Gleixner (2004), Hydrogen isotope ratios of recent lacustrine sedimentary *n*-alkanes record modern climate variability, *Geochimica et Cosmochimica Acta*, *68*(23), 4877-4889.

Sachse, D., J. Radke, and G. Gleixner (2006), δD values of individual *n*-alkanes from terrestrial plants along a climatic gradient - Implications for the sedimentary biomarker record, *Organic Geochemistry*, *37*(4), 469-483.

Sachse, D., et al. (2012), Molecular Paleohydrology: Interpreting the hydrogen-isotopic composition of lipid biomarkers from photosynthesizing organisms, *Annual Review of Earth and Planetary Sciences, 40*(40), 221-249.

Sage, R. F., D. A. Wedin, and L. Meirong (1999), The biogeography of C4 photosynthesis: patterns and controlling factors, in *C4 Plant Biology*, edited by R. F. Sage and R. K. Monson, p. 596, Academic Press, San Diego.

Sauer, P. E., T. I. Eglinton, J. M. Hayes, A. Schimmelmann, and A. L. Sessions (2001), Compound specific D/H ratios of lipid biomarkers from sediments as a proxy for environmental and climatic conditions, *Geochimica et Cosmochimica Acta*, *65*(2), 213-222.

Sawyer, J.O. (2007), Forests of northwestern California, in *Terrestrial Vegetation of California, 3rd ed.*, edited by M. Barbour, p. 734, University of California Press, Berkeley.

Schafer-Neth, C., A. Paul, and S. Mulitza (2005), Perspectives on mapping the MARGO reconstructions by variogram analysis/kriging and objective analysis, *Quaternary Science Reviews*, *24*(7-9), 1083-1093.

Schefuß, E., J. S. S. Damste, and J. H. F. Jansen (2004), Forcing of tropical Atlantic sea surface temperatures during the mid-Pleistocene transition, *Paleoceanography*, *19*(4), 1-12.

Schefuß, E., V. Ratmeyer, J. B. W. Stuut, and J. H. F. Jansen (2003), Isotope analyses of *n*-alkanes in dust from the lower atmosphere over the central eastern Atlantic, *Geochimica et Cosmochimica Acta*, 67(10), 1757-1767.

Schimmelmann, A., A. L. Sessions, and M. Mastalerz (2006), Hydrogen isotope (D/H) composition of organic matter during diagenesis and thermal maturation, *Annual Review of Earth and Planetary Science*, *34*, 501-533.

Schlitzer, R. (2012), Ocean Data View, http://odv.awi.de.

Schneider, B., and A. Schmittner (2006), Simulating the impact of the Panamanian seaway closure on ocean circulation, marine productivity and nutrient cycling, *Earth and Planetary Science Letters*, *246*(3-4), 367-380.

Seki, O., G. L. Foster, D. N. Schmidt, A. Mackensen, K. Kawamura, and R. D. Pancost (2010), Alkenone and boron-based Pliocene pCO_2 records, *Earth and Planetary Science Letters*, *292*(1-2), 201-211.

Siegenthaler, U., et al. (2005), Stable carbon cycle-climate relationship during the late Pleistocene, *Science*, *310*(5752), 1313-1317.

Smith, F. A., and K. H. Freeman (2006), Influence of physiology and climate on δD of leaf wax *n*-alkanes from C3 and C4 grasses, *Geochimica et Cosmochimica Acta*, *70*(5), 1172-1187.

Spero, H. J., C. B. Brogenski, G. T. Jefferson, J. M. Harris, and T. E. Cerling (2003), Initiation of modern Pacific atmospheric circulation at the Plio-Pleistocene boundary recorded in horse teeth enamel, in *Geological Society of America Abstracts with Programs, 35*(6), 586.

Spicer, R. A. (2007), Recent and future developments of CLAMP: Building on the legacy of Jack A. Wolfe, *Courier Forschungsinstitut Senckenberg*, *258*, 109-118.

Spicer, R. A., P. J. Valdes, T. E. V. Spicer, H. J. Craggs, G. Srivastava, R. C. Mehrotra, and J. Yang (2009), New developments in CLAMP: Calibration using global gridded meteorological data, *Palaeogeography Palaeoclimatology Palaeoecology*, *283*(1-2), 91-98.

Steinke, S., J. Groeneveld, H. Johnstone, and R. Rendle-Buhring (2010), East Asian summer monsoon weakening after 7.5 Ma: Evidence from combined planktonic foraminifera Mg/Ca and $\delta^{18}O$ (ODP Site 1146; northern South China Sea), *Palaeogeography Palaeoclimatology Palaeoecology*, *289*(1-4), 33-43.

Steph, S., R. Tiedemann, M. Prange, J. Groeneveld, M. Schulz, A. Timmermann, D. Nurnberg, C. Ruhlemann, C. Saukel, and G. Haug (2010), Early Pliocene increase in thermohaline overturning: A precondition for the development of the modern equatorial Pacific cold tongue, *Paleoceanography*, *25*, 17.

Stott, L. D., M. Neumann, and D. Hammond (2000), Intermediate water ventilation on the northeastern Pacific margin during the late Pleistocene inferred from benthic foraminiferal $\delta^{13}C$, *Paleoceanography*, *15*(2), 161-169.

Stults, D. Z., F. Wagner-Cremer, and B. J. Axsmith (2011), Atmospheric paleo-CO_2 estimates based on Taxodium distichum (Cupressaceae) fossils from the Miocene and Pliocene of Eastern North America, *Palaeogeography, Palaeoclimatology, Palaeoecology*, *309*(3-4), 327-332.

Tipple, B., M. Pagani, R. Smith, and A. Anders (2007), Orographic and climatic influences on leaf wax carbon and hydrogen isotope ratios: A field survey from northern California, *EOS Transaction of the American Geophysical Union*, *88*(52), Fall Meeting Supplement.

Tipple, B. J., and M. Pagani (2010), A 35 Myr North American leaf-wax compound-specific carbon and hydrogen isotope record: Implications for C4 grasslands and hydrologic cycle dynamics, *Earth and Planetary Science Letters*, *299*(1-2), 250-262.

Tipple, B. J., and M. Pagani (*in press*), Environmental control on eastern broadleaf forest species' leaf wax distributions and D/H ratios, *Geochimica et Cosmochimica Acta*.

Tripati, A. K., C. D. Roberts, and R. A. Eagle (2009), Coupling of CO_2 and Ice Sheet Stability Over Major Climate Transitions of the Last 20 Million Years, *Science*, *326*(5958), 1394-1397.

Van Der Burgh, J., H. Visscher, D. L. Dilcher, and W. M. Kurschner (1993), Paleoatmospheric signatures in Neogene fossil leaves, *Science*, *260*, 1788-1790.

Venti, N. (2006), *Revised late Neogene mid-latitude planktic foraminiferal biostratigraphy for the northwest Pacific (Shatsky Rise), ODP leg 198,* Master of Science thesis, University of Massachusetts, Amherst.

Wakeham, S. G., and T. K. Pease (1992), Lipid analysis in marine particle and sediment samples, p.36, Skidaway Institute of Oceanography, Savannah.

Wara, M. W., A. C. Ravelo, and M. L. Delaney (2005), Permanent El Niño-like conditions during the Pliocene warm period, *Science*, *309*(5735), 758-761.

Williams, A. E., and D. P. Rodoni (1997), Regional isotope effects and application to hydrologic investigations in southwestern California, *Water Resources Research*, *33*(7), 1721-1729.

Wilson, J. S., and J. P. Pitts (2010), Illuminating the lack of consensus among descriptions of earth history data in the North American deserts: A resource for biologists, *Progress in Physical Geography*, *34*(4), 419-441.

Wolfe, J. (1979), Temperature parameters of humid to mesic forests of eastern Asia and relation for forests of other regions of the northern Hemisphere and Australasia, *U.S. Geol. Surv. Prof. Paper*, *11061106*, 1-37.

Wolfe, J. A. (1993), A method of obtaining climatic parameters from leaf assemblages, *U.S. Geological Survey Bulletins*, *2040*, 1-71.

Xu, L. K., D. D. Baldocchi, and J. W. Tang (2004), How soil moisture, rain pulses, and growth alter the response of ecosystem respiration to temperature, *Global Biogeochemical Cycles*, *18*(4), 10.

Yu, J. M., H. Elderfield, and B. Hönisch (2007), B/Ca in planktonic foraminifera as a proxy for surface seawater pH, *Paleoceanography*, *22*(2), 17.

Zachos, J., M. Pagani, L. Sloan, E. Thomas, and K. Billups (2001), Trends, rhythms, and aberrations in global climate 65 Ma to present, *Science*, *292*(5517), 686-693.

Zhang, X., et al. (2012), Changes in equatorial Pacific thermocline depth in response to Panamanian seaway closure: Insights from a multi-model study, *Earth and Planetary Science Letters*, *317*, 76-84.